Copyright Warning & Restrictions

The copyright law of the United States (Title 17, United States Code) governs the making of photocopies or other reproductions of copyrighted material.

Under certain conditions specified in the law, libraries and archives are authorized to furnish a photocopy or other reproduction. One of these specified conditions is that the photocopy or reproduction is not to be "used for any purpose other than private study, scholarship, or research." If a, user makes a request for, or later uses, a photocopy or reproduction for purposes in excess of "fair use" that user may be liable for copyright infringement,

This institution reserves the right to refuse to accept a copying order if, in its judgment, fulfillment of the order would involve violation of copyright law.

Please Note: The author retains the copyright while the New Jersey Institute of Technology reserves the right to distribute this thesis or dissertation

Printing note: If you do not wish to print this page, then select "Pages from: first page # to: last page #" on the print dialog screen

ABSTRACT

KINETIC STUDY OF FREE RADICAL-RADICAL REACTIONS OF COMBUSTION IMPORTANCE AT ELEVATED PRESSURES

by
Chao Yan

Combustion mechanisms consist of hundreds elementary reactions of free radicals and stable molecules. Radical-radical elementary reactions play important roles due to the high concentration in which free radicals are accumulated in combustion systems. Radical-radical reactions are typically multi-channel. Some of the channels might be of chain propagation or even chain branching nature, while other channels might be of chain termination nature. The relative importance of different channels is pressure dependent. Compared to radical-molecule reactions, radical-radical reactions are much less studied. This is due to the difficulties of well characterized quantitative production of radical species as well as due to the multi-channel nature of the majority of such reactions. This study is focused on the kinetics and mechanism of several elementary radical-radical reactions of combustion importance.

The kinetics of several free radical-radical reactions was studied using pulsed laser photolysis coupled to transient UV-vis absorption spectroscopy over the 292 – 714 K temperature range and the 1- 100 bar pressure range. Free radicals such as CH_3, OH and Cl are generated by photodissociation of parent molecules; some other radicals such as CH_3O_2 and HO_2 are generated in secondary reactions following the initial photodissociation. Different free radicals are monitored at different wavelengths depending on their UV absorption spectra. Quantitative measurements of the concentrations of free radicals relay upon the absolute intensity of photolysis laser light

determined by well characterized *in situ* actinometry. Experimental temporal absorption profiles are fitted by numerical solutions of a system of differential equations (ODE) which correspond to the reaction mechanism.

The reactions studied are $CH_3 + CH_3 \rightarrow$ Products ($k_{CH3+CH3}$), $CH_3O_2 + OH \rightarrow$ Products ($k_{CH3O2+OH}$), $CH_3 + Cl \rightarrow CH_3Cl$ (k_{CH3+Cl}) and $CH_3 + HO_2 \rightarrow$ Products ($k_{CH3+HO2}$). The reaction of recombination of CH_3 radicals is studied over the 1 – 100 bar pressure range and the 292 – 714 K temperature range. The rate constant is determined as $k_{CH3+CH3,\,\infty} = (5.66 \pm 0.43) \times 10^{-11} (T / 298\ K)^{-0.37}$ cm^3 $molecule^{-1}$ s^{-1}. The overall rate constant of CH_3O_2 with OH is $k_{CH3O2+OH} = (8.4 \pm 0.43) \times 10^{-11} (T / 298\ K)^{-0.81}$ cm^3 $molecule^{-1}$ s^{-1} at pressure 1 bar and 292 – 526 K temperature range. The branching ratios for three major channels were measured at 298 K over the 1 – 100 bar pressure range. High-pressure limit rate constants for reaction of CH_3 radicals with Cl atoms are measured over extended temperature (296 – 558 K) and pressure (1 – 100 bar) ranges. The pressure falloff was characterized by combining the high pressure data with limited literature low pressure data for reaction $CH_3 + Cl$. The reaction $CH_3 + HO_2$ is studied over the 292 – 558 K temperature range and a single pressure (1 bar). The rate constant is $k_{CH3+HO2} = (5.10 \pm 0.95) \times 10^{-11} (T / 298\ K)^{-1.01}$ cm^3 $molecule^{-1}$ s^{-1}.

KINETIC STUDY OF FREE RADICAL-RADICAL REACTIONS OF COMBUSTION IMPORTANCE AT ELEVATED PRESSURES

by
Chao Yan

A Dissertation
Submitted to the Faculty of
New Jersey Institute of Technology
in Partial Fulfillment of the Requirements for the Degree of
Doctor of Philosophy in Chemistry

Department of Chemistry and Environmental Science

May 2018

.

APPROVAL PAGE

KINETIC STUDY OF FREE RADICAL-RADICAL REACTIONS OF COMBUSTION IMPORTANCE AT ELEVATED PRESSURES

Chao Yan

Dr. Lev N. Krasnoperov, Dissertation Advisor — Date
Professor of Chemistry and Environmental Science, NJIT

Dr. Joseph W. Bozzelli, Committee Member — Date
Distinguished Professor of Chemistry and Environmental Science, NJIT

Dr. Alexei Khalizov, Committee Member — Date
Assistant Professor of Chemistry and Environmental Science, NJIT

Dr. Yong Yan, Committee Member — Date
Assistant Professor of Chemistry and Environmental Science, NJIT

Dr. Lei Zhu, Committee Member — Date
Professor of Environmental Health Sciences, Wadsworth Center, SUNY-Albany

BIOGRAPHICAL SKETCH

Author: Chao Yan

Degree: Doctor of Philosophy

Date: May 2018

Undergraduate and Graduate Education:

- Doctor of Philosophy in Chemistry,
  New Jersey Institute of Technology, Newark, NJ, 2018

- Master of Science in Chemistry,
  New Jersey Institute of Technology, Newark, NJ, 2013

- Bachelor of Science in Chemistry,
  Shanxi Normal University, Shanxi, P. R. China, 2011

Major: Chemistry

Publications:

Yan, C., Kocevska, C., and Krasnoperov, L. N. (2016). Kinetics of the Reaction of CH_3O_2 Radicals with OH Studied over the 292-714 K Temperature and 1 – 100 bar Pressure Ranges. *J. Phys. Chem. A*, 120 (31), 6111-6121.

Sangwan, M., Yan, C., and Krasnoperov, L. N. (2015). Reaction $CH_3 + CH_3 \rightarrow C_2H_6$ Studied over the 292 – 714 K Temperature and 1 – 100 bar Pressure Ranges. *J. Phys. Chem. A*, 119 (28), 7847-7857.

Yan, C., and Krasnoperov, L. N. Reaction of CH_3 + Cl over the 292 – 558 K Temperature Range and 1 – 100 bar Pressure Range. Paper is in preparation.

Yan, C., and Krasnoperov, L. N. Kinetics of the Reaction of CH_3 Radicals with HO_2 over the 292 – 558 K Temperature Range. Paper is in preparation.

Yan, C., and Krasnoperov, L. N. HO_2 Radical and Triox Yields in the Reaction CH_3O_2 with OH over the 1-100 bar Pressure Range. Paper is in preparation.

Scientific Presentations:

Yan, C., and Krasnoperov, L. N. HO_2 Radical and Triox Yields in the Reaction CH_3O_2 with OH over the 1- 100 bar Pressure Range. 37th Regional Meeting on Kinetics and Dynamics, Boston, MA, USA, 2018.

Yan, C., and Krasnoperov, L. N. Reaction of CH_3 + Cl over the 292 – 558 K Temperature Range and 1 – 100 bar Pressure Range. Poster presentation at the 10th US National Combustion Meeting, Maryland, USA, 2017

Yan, C., and Krasnoperov, L. N. Kinetics of the Reaction of CH_3 Radicals with HO_2 over the 292 – 558 K Temperature Range. 10th US National Combustion Meeting. Maryland, USA, 2017

Yan, C., and Krasnoperov, L. N. Reaction of CH_3 + Cl over the 292 – 558 K Temperature Range and 1 – 100 bar Pressure Range. 10th International Conference on Chemical Kinetics, Chicago, USA, 2017.

Yan, C., and Krasnoperov, L. N. Kinetics of the Reaction of CH_3 Radicals with HO_2 over the 292 – 558 K Temperature Range. 10th International Conference on Chemical Kinetics, Chicago, USA, 2017.

Yan, C., and Krasnoperov, L. N. Temperature Dependence of Several Radical-Radical Reactions. 35th Regional Meeting on Kinetics and Dynamics, Newark, NJ, USA, 2017.

Yan, C., Kocevska, C., and Krasnoperov, L. N. Kinetic of the Reaction of CH_3O_2 Radicals with OH Studied over the 293 – 523 K Temperature Range. 252nd ACS National Meeting Philadelphia, Philadelphia, USA. 2016.

Yan, C., Kocevska, C., and Krasnoperov, L. N. Kinetic of the Reaction of CH_3O_2 Radicals with OH Studied over the 293 – 523 K Temperature Range. 24th International Symposium on Gas Kinetics and Related Phenomena, York, United Kingdom, 2016.

Yan, C., Kocevska, C., and Krasnoperov, L. N. Kinetic of the Reaction of CH_3O_2 Radicals with OH Studied over the 293 – 523 K Temperature Range. 34th Regional Meeting on Kinetics and Dynamics, Providence, RI, USA, 2016.

Yan, C., and Krasnoperov, L. N. Reaction $CH_3 + CH_3 \rightarrow C_2H_6$ Studied over the 292 – 714 K Temperature and 1 – 100 bar Pressure Ranges. 250th ACS National Meeting Boston, Boston, USA, 2015.

Yan, C., and Krasnoperov, L. N. Kinetics of the Reaction of CH_3 Radicals with HO_2 over the 292 – 558 K Temperature Range. 9th International Conference on Chemical Kinetics, Ghent, Belgium, 2015.

Yan, C., and Krasnoperov, L. N. Photodissociation of Methanol at 193.3 nm. Poster presentation at 9th International Conference on Chemical Kinetics, Ghent, Belgium, 2015.

Yan, C., and Krasnoperov, L. N. Photodissociation of Methanol at 193.3 nm. 33th Regional Meeting on Kinetics and Dynamics, Amherst, MA, USA, 2015.

To my wife, Lang Sun; to my lovely kids, Krystal Yan; Rachel Yan and Liam Yan; to my parents, Junmei Zhang and Xianliang Yan, who have loved me unconditionally.

ACKNOWLEDGMENT

During all my graduate career, I realize now more than ever how grateful I am for the people that helped me along the way. The professors, staffs and students in chemistry and environmental science department gave me lots of good times.

First and foremost, I would like to thank my research advisor and friend, Professor Lev N. Krasnoperov, who fosters an environment where creativity abounds because science is as much fun as it is serious. Working in Prof. Krasnoperov's lab provided me with an opportunity to pursue the projects that I am interested in and to look for collaboration opportunities which advanced a future academic career (collaborate with Princeton University and University of Science and Technology of China). Working with Prof. Krasnoperov, I not only have digged into science part but also have learnt a lot on how to inspire students and to be a good advisor.

Next, I would like to thank professors Joseph Bozzelli, Alexei Khalizov, Yong Yan and Lei Zhu for being my dissertation committee members and providing support towards the completing of my dissertation. I still remember Prof. Bozzelli showed me how to use Mopac and Chemkin to calculate the kinetic parameters for which I was having a hard time with. Drs. Yogesh Gandhi and Ping Gu always opened the gate to me for any help during my teaching assistant time. Additionally, I would like to thank Prof. Yiguang Ju from Princeton University for giving me the opportunity to be a visiting researcher in his lab and for discussions about kinetics of low temperature importance.

Outside my research, the student life would not have been the same without the support of my friends. I want to thank Qize Zhang and Zhiqian Wang who spend a lot of

time with me during my graduate life. I also want to thank my friends outside NJIT (Chuan Sun, Chang Fu, Chenming Cui, Junyu Ma, Mingxing ji, Yichun Ma, Zheng Han), for supporting me for so many years.

Last but not least, I want to thank my dearest families. I don't have words to thank enough my parents: Junmei Zhang and Xianliang Yan, who always supported me to make my academic life as the first priority and made sure I have all I need and be happy. I would like to thank my wife, Lang Sun for her love and unconditional support. She has always been a source of inspiration, love and my biggest supporter in everything I do. Without her by my side, I would not be able to complete this degree. And of course, I would also like to thank my wife for our three lovely kids (Krystal Yan, Rachel Yan and Liam Yan), who compose my biggest motivation to strive for my goals.

TABLE OF CONTENTS

TABLE OF CONTENTS
(Continued)

Chapter **Page**

TABLE OF CONTENTS
(Continued)

LIST OF TABLES

LIST OF TABLES
(Continued)

LIST OF FIGURES

LIST OF FIGURES
(Continued)

Figure **Page**

LIST OF FIGURES
(Continued)

CHAPTER 1

INTRODUCTION

1.1 Objective

The objective of this thesis is to study the elementary free radical-radical reactions of combustion importance over an extended pressure range. Combustion mechanisms consist of thousands elementary reactions of hundreds free radicals. In some types of combustion engines, such as internal combustion engines, homogeneous charge compression ignition (HCCI) engines and rocket engines, the pressures might be extremely high. Therefore, detailed kinetic mechanisms with well characterized high pressure kinetics of free radical-radical reactions are required to improve the performance of these types of engines.

In combustion, reactive short-lived radicals play crucial roles. Radical-radical reactions are involved in all stages of combustion process and controlled the important parameters of combustion (such as the ignition delay, the flame propagation speed, etc.). Emission of pollutants is also controlled by the combustion mechanism. However, quantitative kinetic studies of radical-radical reactions represent a considerable challenge due to several reasons, such as lack of clean sources of free radicals in many cases, low concentrations of free radicals and overlap the absorption spectra of stable species and free radicals. Elevated pressures in this study were up to 100 bar. The UV-vis absorption spectroscopy appears as almost the only technique capable of monitoring of the transient species at high pressures. Despite of the substantial progress in the studies of radical-radical reactions at low pressures, the kinetic data at elevated pressures is still insufficient. Experimental measurements of the rate constants are normally performed

under the low pressure conditions (up to 1 bar). The rate constants in the high pressure limit then are extrapolated based on theoretical estimates, which could add significant additional uncertainty into the combustion models.

In this study, pulsed laser photolysis combined with a high-pressure flow system and transient absorption spectroscopy technique was used for kinetic measurements. Several important reactions involving free radicals of combustion importance were studied. In addition, effect of buffer gas density on the rate constants and the branching ratios was evaluated in several cases.

1.2 Background Information

Free radicals are formed by variety of processes which put sufficient energy into the parent molecule, such as photodissociation, ionizing radiation, heat, electrical discharges and chemical reactions. Free radicals play a pivotal role in combustion, atmospheric chemistry, plasma chemistry, biochemistry and many other chemical processes. In these cases, the free radicals initialize and accelerate the whole process as a result of the highly reactive nature. The presence of unpaired valence electrons makes free radicals highly reactive and their usually fast bimolecular reactions often dominate the complex reaction mechanisms.

Combustion processes belong to chain branching reactions with participation of large amounts of free radicals. Due to high concentrations of free radicals, radical-radical reactions become important. For instance, in the combustion of hydrogen, a significant fraction of the H_2 is converted to H atoms, and H atom is the principal chain carrier. The free radicals concentrations increase exponentially through the chain branching reactions

initialized by H atoms. And the overall reaction rate increase rapidly since the overall rate depends on the radical concentrations. This is usually termed as an explosion. Under conditions of high pressure, the chain termination reactions become more important due to the third body collisions. The chain termination reaction competes with the chain branching reaction. That is how high pressure affects on ignition delay time.

H	+	O_2			→	OH	+	O	Chain branching
H	+	O_2	+	M	→	HO_2	+	M	Chain termination

HO_2 radical is the other important radical in combustion. Due to the relatively low reactivity, the reactions of formation of HO_2 are normally considered as chain termination reactions. However, the reaction of methyl radicals, CH_3 with HO_2 radicals has a large rate constant. Two active free radicals CH_3O and OH are produced in the major channel of this reaction. The free radicals produced in this reaction will accelerate the ignition process. While, some other channels of this reaction are chain termination channels. Therefore, the branching ratio of these channels is important in the combustion models.

In this thesis, several important radical-radical reactions were studied. Measurements of the rate constants as well as the branching ratios are carried out over extended temperature and pressure ranges:

CH_3	+	CH_3
CH_3O_2	+	OH

CH_3 + Cl

CH_3 + HO_2

1.2.1 CH_3 + CH_3 → Products

Self-reaction of methyl radicals (1.1a, 1.1b) is important in hydrocarbon pyrolysis and combustion mechanisms:[7; 11-20]

$$CH_3 + CH_3 \rightarrow C_2H_6 \quad (1.1a)$$

$$\rightarrow C_2H_5 + H \quad (1.1b)$$

Channel 1.1a is a chain termination step, while channel 1.1b is one of the chain propagation steps. Both the branching ratio and the rate of reaction 1 have impact on self-ignition threshold, flame propagation speed and other parameters of combustion as well. The reaction is responsible for production of C2 hydrocarbons in methane combustion. Reaction 1.1 is important for fundamental chemical kinetics and is considered as a benchmark reaction for testing and improving theories of radical - radical reactions as a simplest reaction of recombination of hydrocarbon free radicals.[19] Precise knowledge of the kinetic parameters of reaction 1.1 is nessassary in laboratory studies of other reactions involving methyl radical.[21;22] In relative kinetic studies involving methyl radicals, reaction 1.1 was frequently used as a reference reaction.

1.2.2 CH_3O_2 + OH → Products

Both CH_3O_2 and OH radicals play important roles not only in combustion mechanisms

but also in atmospheric chemistry. One of the potential important pathways for the consumption of CH_3O_2 radicals in troposphere could be the reaction with hydroxyl radical, OH (reaction 1.2).[23-26] Only very limited studies have been performed on this reaction. Recently reaction 1.2 was studied theoretically.[26] Among the exothermic channels only two were found to be of importance at near ambient conditions, channels 1.2a and 1.2b:

$$CH_3O_2 + OH \rightarrow CH_3O + HO_2 \quad (1.2a)$$

$$\rightarrow {}^3CH_2OO + H_2O \quad (1.2b)$$

Channel 1.2a is a barrierless step; according to the calculations it is exothermic by 16.8 $kJmol^{-1}$. Channel 1.2b has a barrier of 30 kJ mol^{-1}.[26] The three other channels suggested in the literature[23;24; 26]

$$CH_3O_2 + OH \rightarrow CH_3OH + O_2\ ({}^1\Delta_g, {}^3\Sigma_g^+) \quad (1.2c)$$

$$\rightarrow {}^1CH_2OO + H_2O \quad (1.2d)$$

have high activation barriers (193 and 87 kJ mol^{-1} for 1.2c, singlet and triplet oxygen molecule respectively, and 188 kJ mol^{-1} for channel 1.2d). There are two more exothermic channels which also have very large activation barriers:[26]

$$CH_3O_2 + OH \rightarrow CH_3OOOH \quad (1.2e)$$

Most recent theoretical study was published by Muller et al.[27] Detailed potential energy surfaces were calculated using suitable high-level density functional theory (DFT) and *ab initio* methodologies for the singlet and triplet intermediates. The Criegee pathway is negligible in atmospheric conditions. Channel 1.2a is expected to dominate, whereas both methanol formation (channel 1.2c) and stabilization of the methylhydrotrioxide CH_3OOOH (TRIOX) are minor channels.

1.2.3 $CH_3 + Cl \rightarrow CH_3Cl$

Chlorine atoms (Cl) have been explored as key intermediate species responsible for ozone depletion in the troposphere.[28-32]

Methane (CH_4) is an important species in the atmosphere. The concentration of methane can be as high as few parts per million (ppm).[33] In the remote stratosphere, the major pathway of Cl atom removal is through the reaction 1.3.[7] Methyl radicals (CH_3) formed in reaction 1.3 might provide an essential additional pathway to consume chlorine atoms via reaction 1.4 with a large rate constant.[34]

$$Cl + CH_4 \rightarrow HCl + CH_3 \qquad (1.3)$$

$$CH_3 + Cl \rightarrow CH_3Cl \qquad (1.4)$$

In addition, reaction 1.4 is very important in the laboratory kinetics studies based on the decay of CH_3 radicals where Cl atoms are used for generating of other free radical species.[35-37] For example, in the kinetics study of the reaction of CH_3 radicals with HO_2 radicals, the formation of HO_2 radicals is initialized by Cl atoms. The reaction of CH_3

radicals with Cl atoms contributes significantly to the total decay of CH_3 radicals. Therefore, the kinetic study of the reaction of CH_3 radicals with Cl atoms is important.

1.2.4 $CH_3 + HO_2 \rightarrow$ Products

Reaction of methyl radicals with hydroperoxy radicals (1.5) plays a very important role in hydrocarbon combustion. Relatively unreactive hydroperoxy radicals, HO_2 are formed via recombination of hydrogen atoms (which are produced in the dissociation of formyl radicals (HCO) or other hydrocarbon radicals such as C_2H_5) with oxygen molecules. In addition, HO_2 radicals are formed directly in hydrogen atoms abstraction by oxygen molecules. However, the subsequent reaction of HO_2 with CH_3 radicals might lead to efficient chain propagation via the reaction channel 1.5a:[2]

CH_3	+	HO_2	→	CH_3O	+	OH	(1.5a)
			→	CH_2O	+	H_2O	(1.5b)
			→	CH_3OOH			(1.5c)
			→	CH_4	+	$^3O_2$	(1.5d)
			→	CH_4	+	$^1O_2$	(1.5e)

This reaction is exothermic and proceeds through several energetically allowed channels. Channel 1.5a is considered to be the major channel in the methane oxidation process, whereas channel 1.5d is a chain termination step. Two free radicals (CH_3O and OH) are formed in channel 1.5a. The branching ratio of channels 1.5a and 1.5d has impact on the ignition delay and other combustion parameters.

However, kinetic studies of CH_3 and HO_2 radicals are difficult due to the lack of direct photolysis sources of HO_2 radicals. Only very limited experimental studies are available, especially over extended (elevated) temperature range. This is the motivation to measure the rate constant as well as the branching ratios of reaction 1.5.

CHAPTER 2

EXPERIMENTAL APPARATUS

2.1 General

The experimental approach is based on the excimer laser pulsed photolysis coupled to UV-vis transient absorption spectroscopy and a high-pressure flow system (Figure 2.1). ArF excimer laser (Ex100 GAM Laser Inc., 193.3 nm) was used to photolyze the reactants and initialize the chemical reactions. Several ultraviolet (UV) light sources such as the Xe arc lamp (150 W, Oriel Instruments), the H_2O/Ar discharge lamp (home made), the Hg arc lamp (500 W, Oriel Instruments) and a low pressure radio frequency discharge Hg lamp were used to monitor free radicals and stable molecules by UV absorption. Combination of an imaging spectrograph (Acton Research Corporation SpectraPro – 300i), a photomultiplier tube (Hamamatsu R10699), a preamplifier (EMI) and a gated intensified CCD (ICCD) camera (ICCD Max, Roper Scientific) was used to measure transient intensity at such wavelengths as well as transient absorption spectra. The heatable high pressure flow reactor is made of 12.7 mm O.D. (1/2") stainless steel tubing. The reactor as well as two electrical resistance heaters were mounted in aluminum cylindrical block. A function generator (BNC, model 555 pulse generation) triggered by excimer laser was used to trigger the oscilloscope (LeCroy 9310A, Dual channel, 400 MHz, 100 Msamples/s, 50 Kpts/ch). The traces were usually averaged for 500 to 5000 pulses by the oscilloscope and transferred to a PC for processing. The SCIENTIST software (MicroMath, Inc.) was used to perform the nonlinear least squares fits by numerical solutions of the ODE system which corresponds to the reaction mechanism.

2.2 Optics

Two UV-grade quartz windows (12.7 in diameter, 9.5 mm thick) are sealed at the end of the reactor at ambient temperature outside the high-temperature zone using Viton O-rings. Two dichroic mirrors (CVI) with high reflectivity at 193 nm mounted at 45^0 are placed before the entrance and after the exit of the flow reactor to allow merging of both UV photolysis beam and the monitoring beam in a single-pass configuration. The monitoring beam is formed by two diaphragms (1/4" diameter) before and after the reactor. Two dielectric mirrors with high reflectivity at 193 nm are installed after the Xe arc lamp at 19^0 incidence angle which lead to the shift of the high reflectivity range from 193 nm (original) to 200 – 230 nm region, attenuating the visible light from the Xe arc lamp by ca. 200 times. To improve the homogeneity of the photolysis laser beam, the original laser beam was expanded using a lens system consisting of a spherical lens (f = 30 cm, the distance from the reactor 70 cm) and a cylindrical lens (f = 30 cm, the distance from the reactor 23 cm). Spherical convex lenses were used for converging light from monitoring light sources. Additional liquid filter ($4.3x10^{-2}$ M solution NaCl in water, 1 cm) was installed before entrance slit of the imaging spectrograph to provide virtually complete depression of scattered and back reflected 193 nm laser light.

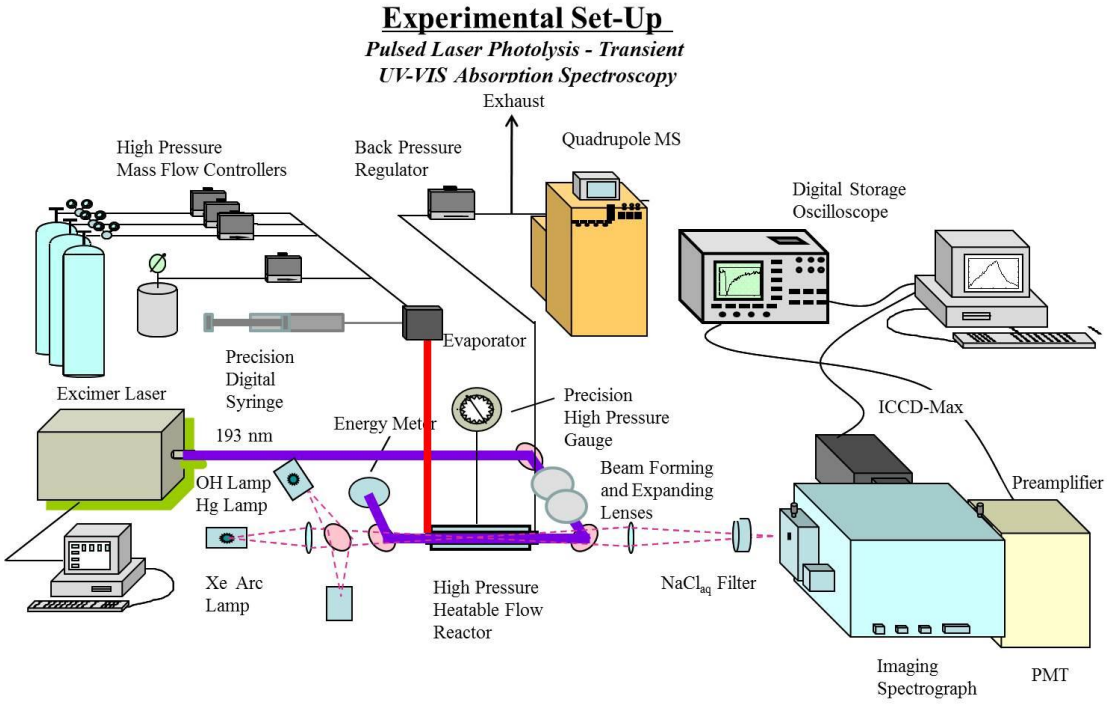

Figure 2.1 Experimental set-up. Excimer laser pulsed photolysis coupled to UV-vis transient absorption spectroscopy and a high pressure flow system.

2.3 ArF Excimer Laser (193.3 nm)

ArF excimer laser from GAM Inc. (model EX100) generates unfocused light at wavelength at 193.3 nm with a 20 ns pulse duration. The laser beam formed by the two lenses telescope previously described was reflected by a 45^0 dielectric mirror and directed along the cell axis so that it fills all the cross section of the reactor. The laser energy was measured at the exit of the reactor reflected by the dielectric mirror using the energy meter (Coherent, Max II) and a photodiode. The repetition rate of the laser was set to ensure complete replacement of the gas mixture in the reactor between the pulses (0.1−1 Hz depending upon the reactor pressure). Alignment of laser and optics cleaning were

provided periodically to keep good quality of photolysis beam. The photolysis beam fills the whole cross-section of the reactor homogeneously. The beam profile was measured by scanning with a small aperture diaphragm (ca. 0.5 mm) combined with an energy meter. The beam uniformity across the reactor cross-section is ± 7.3 % from the mean value (Figure 2.2).[38]

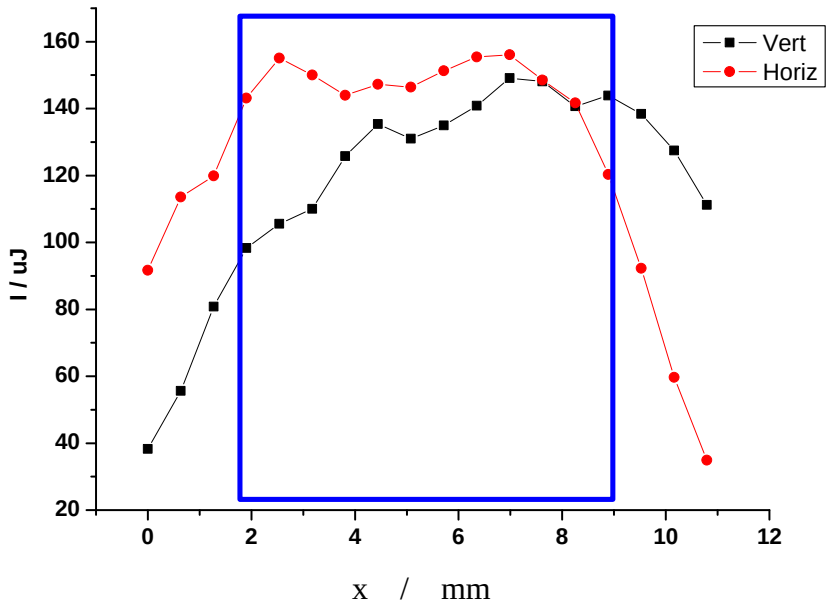

Figure 2.2 Laser intensity beam profiles of photolysis laser across the cross-section of the reactor.

2.4 Heatable High Pressure Reactor and Flow System

The heatable high pressure gas flow system consists of high pressure gas mixing vessels, high pressure precision digital syringes (Harvard Apparatus, Model PHD 4400), heatable transfer line, heatable high pressure reactor, high-pressure mass flow controllers, high-pressure precision test gauges, high pressure back pressure regulator, and the cylinders with helium, the precursors, and the reactant mixtures.

Both of the two high-pressure gas mixing vessels (Parr, high-pressure reactor, 300 mL and 700 mL) consist of a stainless steel vessels and a pressure gauge. Pressures of the reactants were measured using MKS Instruments pressure gauges for the ranges 0 – 10 Torr, 0 – 100 Torr, and 0 – 1000 Torr. The total pressure was measured by a high-pressure gauge. Several possible sources of errors were identified in the quantitative preparation of mixtures at high pressures.[3] The major error sources are the "Dead" volume effect and the temperature rise effect at elevated pressure. Efficient stirring must be provided due to the very slow diffusion at elevated pressures. A regular Teflon coated magnetic bar driven magnetically through the bottom wall (nonferromagnetic stainless steel) of the vessel was used. This provides fast and efficient mixing inside the high-pressure vessel. Loading of the vessel with helium at elevated pressures leads to a significant temperature rise. This elevated temperature dissipates quite slowly when no stirring is applied. However, cooling is efficient under stirring. The gas temperature was monitored using an internal thermocouple (supplied with the vessel). The gas mixture was cooled until the difference between the gas temperature and the ambient temperature was less than 3 K. A proper correction for the residual temperature difference was made in the mixture composition calculations. The "dead" volume is composed by the volume of tubes and pressure gauge where stirring does not reach. The diffusion requires long time when pressure is high. The following expression was derived using a model based on the assumption of perfect mixing in the bulk vessel during the mixture preparation:[3]

$$\chi_1/\chi = \chi^{\gamma} \qquad \text{(E2.1)}$$

where χ_1 is the actual mole fraction of the minor component in the bulk of the vessel, χ is the targeted mole fraction, and $\gamma = V_{dead} / (V_{total} - V_{dead})$ is the ratio of the dead volume

and the residual volume of the vessel. The larger the fraction of the dead volume and the mixture dilution is, the bigger the error is. To minimize possible errors due to the dead volume effect, the external outlets of the vessel were minimized and the gland used for the original stirrer axis sealing was removed. A conservative estimate on the dead volume is less than 5.4 cm^3, with the reactor volume of 700 cm^3. Therefore, the maximum error due to the dead volume effect for 0.1 – 0.2% mixtures was estimated to be less than 12%. Additional correction used in the calculation of the concentrations of the reactants in the flow reactor as well as in the mixture preparation is the compression Z factor. For helium, Z_{He} (100 bar, 300 K) = 1.0471 and Z_{He} (150 bar, 300 K) = 1.0707.

Liquid precursors were supplied to the flow system by a high-pressure precision digital syringe through a capillary tube via an evaporator. The evaporator temperature was kept slightly below the boiling temperature at pressure 1 bar. In the initial experiments, it was found that the concentration of the reactants was pulsing. A possible reason for this was identified as due to the process of evaporation of liquid droplets at the exit of the capillary located in the evaporator. The process of evaporation was not steady, but rather a periodic evaporation of overheated droplets. A "cap" made of a porous glass was installed on the end of the capillary. In this arrangement, liquid would penetrate through multiple channels to the surface of the cap, so that no droplets are formed, providing steady evaporation. It was observed that this approach produces steady and stable flows of liquid reactants mixtures over the pressure range 1−100 bar.

The liquid solutions were carefully degassed through a freeze-pump-thaw degassing procedure before loading in the stainless steel syringe. Either liquid nitrogen or dry ice were used to freeze liquid solutions. The freeze-pump-thaw process was typically

repeated for at least three times to remove dissolved air.

The heated transfer line was installed between the evaporator and the reactor. Temperature of heated transfer line was increased up to ca. 140 °C, when required. This was necessary to provide high concentration of water at elevated temperatures in some experiments.

Three types of high pressure reactors were used. "Old" heatable high pressure flow reactor,[1; 22; 39-43] "new" heatable high pressure flow reactor (Figure 2.3 (A)) and a room temperature high pressure flow reactor (Figure 2.3 (B)).[3]

The "new" Heatable high pressure reactor was made of 12.7 mm O.D. (1/2") stainless steel tubing (20 cm). An aluminum cylinder block that covers the central part of the tube serves as a heat distributor. Two electrical resistance heaters were located within the aluminum block parallel to the reactor. The third one was installed in the preheating unit (red dash block in Figure 2.3 (A)). Two thermocouples (K-type, Omega) are located in the preheating unit and the center of the aluminum block, respectively. The reactants were supplied through the stainless steel tube located in the middle of the reactor with adequate pre-heating. The length of the pre-heating unit is 15 cm which ensures complete preheating of helium at the flow rates used in the experiments. The preheated reactant mixtures enter the reactor in the center and leave through the two outlets located on the two sides 5 cm away from the center within the uniform temperature zone. Additional buffer gas flows enters the reactor near the external windows to flush gas from the windows towards the outlets. Two additional thick (9.5 mm) magnesium fluoride (MgF_2) windows separated by a stainless steel insert were placed without sealing inside the reactor near the reactor outlets. The active length of the reactor is precisely determined by

the length of the insert (10.0 cm). The reactant mixture was flowing towards the inside windows and the external flush flow was flowing from the other direction. This configuration prevented penetration of the reactants out of the active observation zone which provided precise definition of the observation zone within the uniform temperature region and allowed avoiding of windows sealing at elevated temperatures.

The axial temperature profiles were measured in 1 cm steps along the reactor length for each set of experimental conditions which is up to 834 K and 100 bar pressure. One of the windows was replaced by a movable coaxial 1.6 mm O.D. K-type thermocouple sealed by an adapter.[39] In active observation zone, the measured temperature profiles indicated that the uniformity of temperature is within ± 5 K (Figure 2.4).[39] Average temperature in the reactant zone was taken as the reactor temperature.

The other simplified room temperature high-pressure flow reactor was used in kinetics measurement at ambient temperature only (Figure 2.3 (B)).[3] No heating element was installed in this reactor and no aluminum block was installed. Instead of the four window configuration this reactor used two windows sealed by Viton O-rings. The reactants gas mixture was injected at one side of the observation zone and left at the other side. For all reactors used, flush gas (N_2) was used to purge outside area of the reactor.

High pressure mass flow controllers (Brooks, 5850 TR series) were used to control the gas flow rates. The mass flow controllers were periodically calibrated using the soap film method. In order to have small flow rate, a modified mass flow controller was used in which the main gas pathway was blocked and the flow rate as low as 0.1 sccm could be controlled. Calibrations plots of the mass flow controllers are in the Appendix.

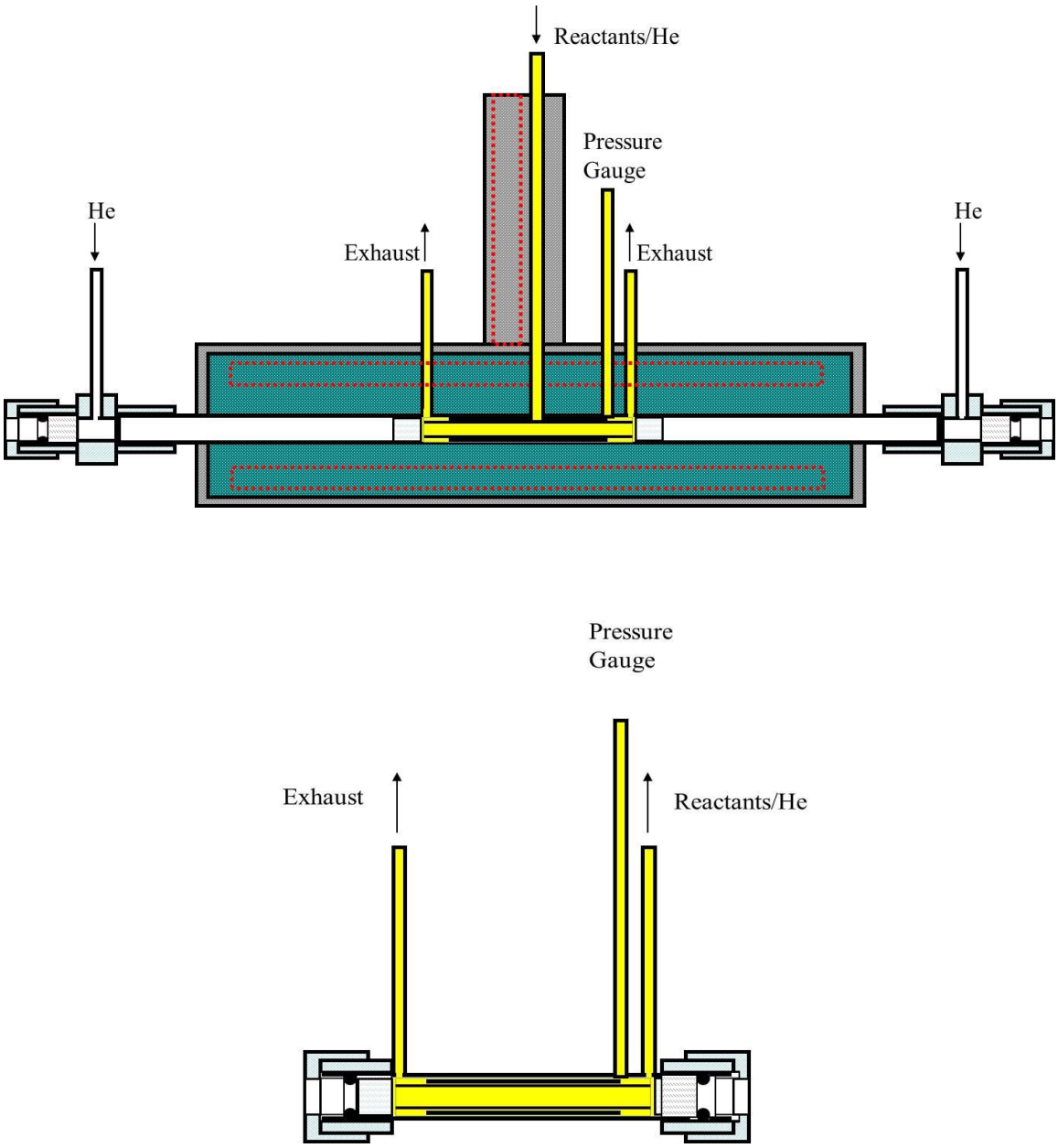

Figure 2.3 Detailed sketch as of the "new" heatable high-pressure flow reactor (A), and ambient temperature high-pressure flow reactor (B).[3]

Two high pressure precision gauges were used to measure the pressure in the flow reactor (Matheson model 63 – 5633M, up to 250 bar pressure, model 63 – 5622 M, up to

14 bar, accuracy 0.25 %). Reactor pressure was also measured by the internal calibrated pressure sensor of the electronic upstream pressure controller.

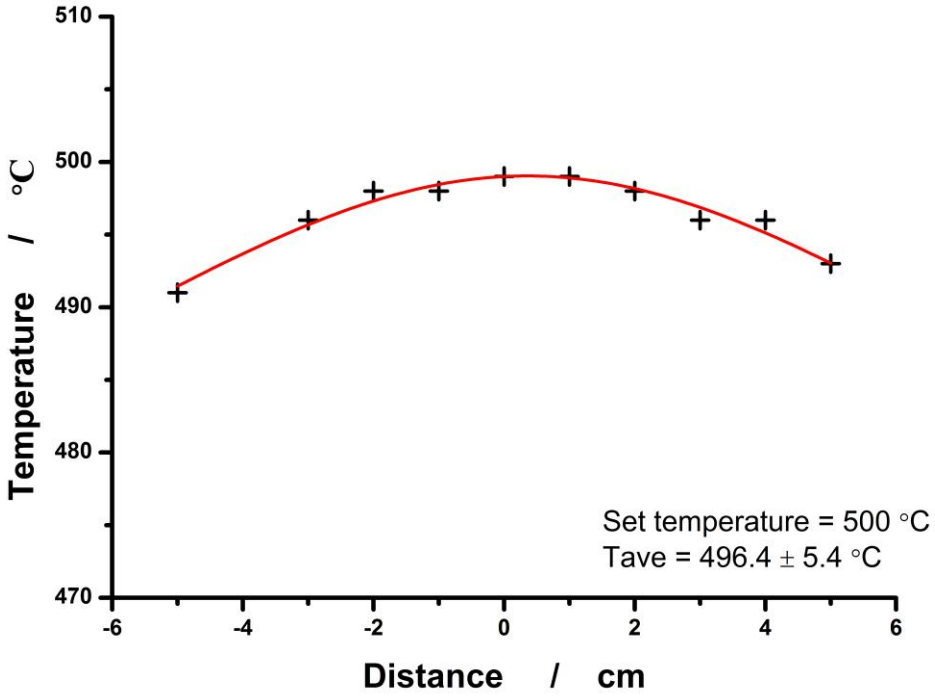

Figure 2.4 Temperature profiles of the heatable high-pressure flow reactor. The temperature vs. the distance from the center of the reactor.[31]

2.5 Generation of Free Radicals

2.5.1 Generation of CH_3 Radicals

Methyl (CH_3) radicals were generated either by excimer laser pulse photolysis of acetone

$$(CH_3)_2CO + h\nu\ (193\ nm) \rightarrow 2CH_3 + CO \quad (2.1a)$$

$$\rightarrow CH_2COCH_3 + H \quad (2.1b)$$

$$\rightarrow CH_4 + CH_2CO \quad (2.1c)$$

or N_2O in the presence of methane at 193.3 nm (ArF excimer laser):

$$N_2O + h\nu\ (193\ nm) \rightarrow O(^1D) + N_2 \quad (2.2a)$$

$$\rightarrow N(^4S) + NO(^2\Pi) \quad (2.2b)$$

$$O(^1D) + CH_4 \rightarrow OH + CH_3 \quad (2.3)$$

$$OH + CH_4 \rightarrow H_2O + CH_3 \quad (2.4)$$

In the photolysis of acetone at 193.3 nm, in addition to the major channel 2.1a resulting in two methyl radicals, there are two other possible channels 2.1b and 2.1c. The quantum yields of channels 2.1a-c at 193 nm were measured by Lightfoot et al.[44] as $\phi_{2.1a}$= 0.95, $\phi_{2.1b}$ = 0.03, and $\phi_{2.1c}$ = 0.02 at 300 K with a negligible temperature dependence (over the 300 – 600 K temperature range).

2.5.2 Generation of CH_3O_2 Radical

CH_3O_2 radicals were generated by excimer laser pulse photolysis of acetone in the presence of oxygen:

$$(CH_3)_2CO + h\nu(193\ nm) \rightarrow 2CH_3 + CO \quad (2.1a)$$

$$\rightarrow CH_2COCH_3 + H \quad (2.1b)$$

$$\rightarrow CH_4 + CH_2CO \quad (2.1c)$$

$$CH_3 + O_2 \rightarrow CH_3O_2 \quad (2.5)$$

CH_3 radicals were produced in photoissociation of acetone. When O_2 molecule was

given, the fast secondary reaction (2.5)[45] converts virtually all CH_3 radicals into CH_3O_2 radicals in a few microseconds.

2.5.3 Generation of OH Radical

OH radicals were generated by excimer laser pulse photolysis of N_2O in the presence of H_2O at 193 nm:

N_2O	+	hν(193 nm)	→	$O(^1D)$	+	N_2	(2.2a)
			→	$N(^4S)$	+	$NO(^2\Pi)$	(2.2b)
$O(^1D)$	+	H_2O	→	2OH(v = 0, 1)			(2.6a)
			→	H_2	+	O_2	(2.6b)
			→	$O(^3P)$	+	H_2O	(2.6c)

The quantum yield of the major channel 2.2a is unity within 1%, the minor channel 2.2b is less than 0.8%.[46] The fraction of vibrationally excited hydroxyl radicals OH(v=1) formed in the reaction 2.6a is 22 – 30%.[47-49] According to more recent data the yield is 22 – 24%.[47-50]

Additional OH radicals are formed in the photo-dissociation of H_2O and reactions of atomic oxygen atom with hydrocarbons such as acetone. Fraction of $O(^1D)$ formed in photolysis of N_2O that reacts with N_2O, O_2 and acetone is also taken into account:

H_2O	+	hν	(193 nm) →	H	+	OH	(2.7)
O_2	+	hν	(193 nm) →	2 $O(^3P)$			(2.8)

$O(^1D) + (CH_3)_2CO \rightarrow OH + CH_3COCH_2$ (2.9)

$O(^3P) + (CH_3)_2CO \rightarrow OH + CH_3COCH_2$ (2.10)

$O(^1D) + N_2O \rightarrow NO + NO$ (2.11)

$\rightarrow O_2 + N_2$ (2.11b)

$\rightarrow O(^3P) + N_2O$ (2.11c)

$O(^1D) + O_2 \rightarrow O(^3P) + O_2$ (2.12)

The absorption cross sections of acetone and N_2O at 193.3 nm were taken from previous studies.[39;40] The absorption cross sections of H_2O (1.51×10^{-21} $cm^2 molecule^{-1}$) and O_2 (ca. 3×10^{-22} $cm^2 molecule^{-1}$) at 193.3 nm are measured.[43]

2.5.4 Generation of Cl Atoms

Chlorine atoms (Cl) were produced either directly in photolysis of methylchloride CH_3Cl at 193.3 nm or in photolysis of oxalyl chloride $(COCl)_2$, a clean photolysis source of Cl atom.

$CH_3Cl + h\nu(193.3\ nm) \rightarrow CH_3 + Cl$ (2.13)

$(COCl)_2 + h\nu(193.3\ nm) \rightarrow 2\ Cl + 2\ CO$ (2.14)

Oxalyl chloride $(COCl)_2$ has been characterized as a clean photolytic source of chlorine atoms for kinetics studies. The UV absorption spectrum of oxalyl chloride as well as the photodissociation yield of chlorine atoms in the photodissociation of oxalyl chloride at 193 nm in helium as a bath gas at pressure 1, 10 and 100 bar is also described.[51] The

yield of chlorine atoms (the number of Cl atom appeared per one dissociated oxalyl chloride molecule) is independent of helium pressure over the pressure range 1 – 100 bar. The yields of chlorine atoms at 298 K are 2.01 ± 0.08 and 1.97 ± 0.12 at 10 bar and 100 bar, respectively.[51]

2.5.5 Generation of HO_2 Radical

Hydroperoxy radicals (HO_2) are produced in a sequence of very fast reactions initiated by chlorine atoms, produced in photolysis of oxalyl chloride:

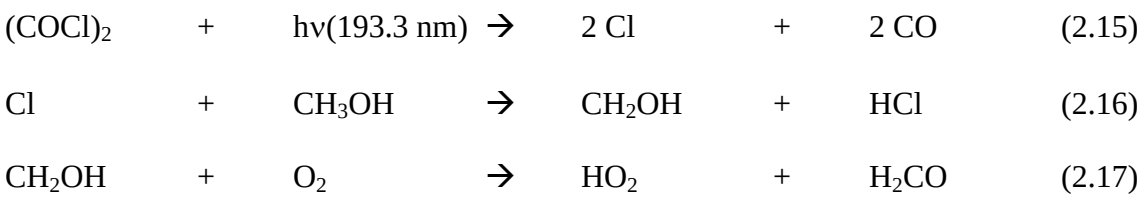

$(COCl)_2$	+	hν(193.3 nm)	→	2 Cl	+	2 CO	(2.15)
Cl	+	CH_3OH	→	CH_2OH	+	HCl	(2.16)
CH_2OH	+	O_2	→	HO_2	+	H_2CO	(2.17)

In the beginning, HO_2 radicals were produced through the reaction of $O(^1D)$ with H_2O_2 formed in photodissociation of N_2O. However, H_2O_2 has a weak oxygen-oxygen bond that is easily broken at elevated temperatures. Therefore, much more stable precursor oxalyl chloride, $(COCl)_2$, was used to initialize the reaction.

2.6 Thermal Stability of Reactants

Noticeable depletion of the radical precursors (acetone and oxalyl chloride) was observed abve 558 K, most probably due to heterogeneous reactions of these species on the wall of the preheating tubing. These experiments are illustrated in Figure 2.5. Acetone is stable up to the highest temperature used (834 K). Sharp drop concentration of $(COCl)_2$ is

observed when temperature increased. However, when acetone and oxalyl chloride gas mixture goes through the reactor, the depletion was observed at temperatures above 558 K. This limited the temperature range of the experiments.

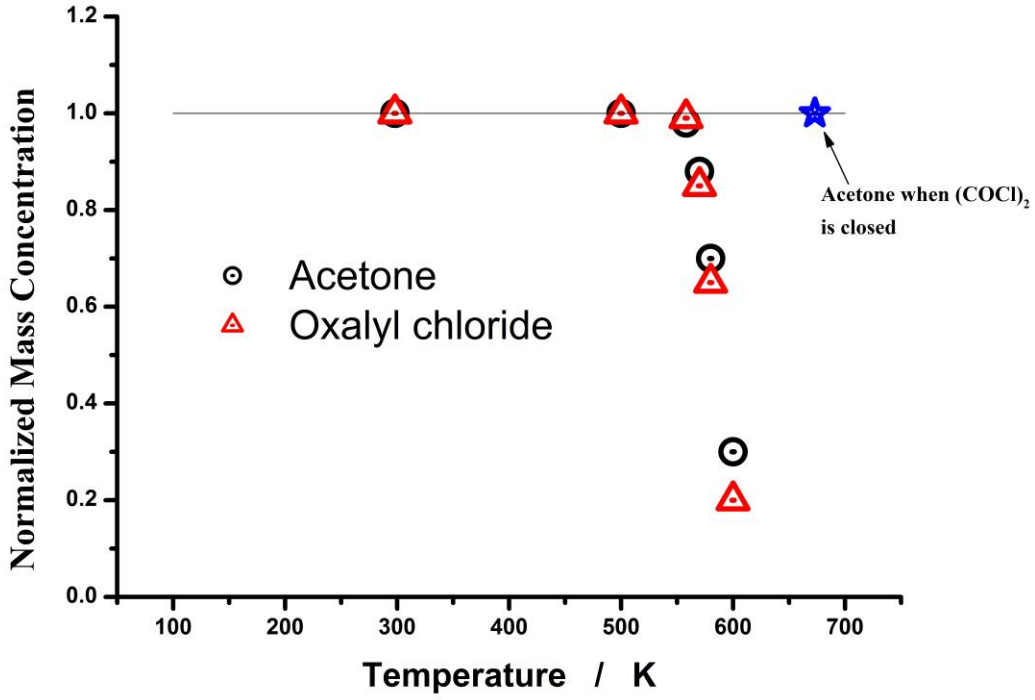

Figure 2.5 Thermal stability of the precursors (acetone and oxalyl chloride). "New" reactor was used.

2.7 UV Absorption Spectroscopy

The monitoring light sources such as Xe arc lamp (150 W, Oriel Instruments), H_2O/Ar discharge lamp (homemade), Hg arc lamp (500 W, Oriel Instruments) and low pressure RF discharge Hg lamp were used in the measurements of transient absorption at single wavelength as well as in the measurements of transient absorption spectra.

The imaging spectrograph (Acton Research Corporation SpectraPro – 300i) was equipped with a PMT (Hamamatsu R10699) with a preamplifier (EMI) and a gated intensified CCD (ICCD) camera (ICCD Max, Roper Scientific). The photomultiplier tube mounted on the exit slit operates on a reduced number of dynodes (6) with a voltage divider current of 2.7 mA, which ensures good linearity and lower noise at high photon fluxes. The residual light from the excimer laser pulse was removed using a NaCl aqueous solution ($4.3x10^{-2}$ M solution NaCl in water, 1 cm). The liquid filter provides depression of 193 nm light of 10^{12} times while attenuating the monitoring light (216.4 nm) only by 17 %. The PMT signal is preamplified, then digitized and stored using a digital storage oscilloscope (LeCroy 9310A, Dual channel, 400MHz, 100 Msamples/s, 50 Kpts/ch). The time resolution is determined by the preamplifier setting which can be 30 ns, 0.3 us, 3us, or 30 us. Normally, free radicals' lifetime in this study was shorter than 1 ms, therefore 0.3 us time constant was used. The signal, usually averaged as 500 – 5000 pulses, was transferred to PC for further processing and fitting.

In all measurements, monitoring light intensity traces were also accumulated in the absence of the precursor molecules (i.e., acetone or $(COCl)_2$). Subsequently, these traces were subtracted from the traces acquired in the presence of the precursors. This was done to exclude the effect of the monitoring light intensity change upon the exposure of the multilayer mirrors to the laser pulse (hereafter dubbed as "zero shift"). Such a change is caused by the partial release of water from the porous layers of multilayer coating as well as a small temperature change of the mirror coatings. These factors lead to small change in the indexes of refraction of the coating layers materials, and, subsequently, to the modulation of the mirrors reflectivity. The "zero shift" could be

negative or positive depending on the spectral separation of the monitoring wavelength from the wavelength of the maximum reflectivity of the mirrors, and was observed in all experiments where the same approach of merging of the photolysis and monitoring beams was used.[40;52-56] In this study, typical scale of the "zero shift" was ca. $4x10^{-4}$. In addition, subtraction of the "zero shift" trace did eliminate a minute distortion after the large spike caused by the reactor windows luminescence (of a similar scale, $(2 – 4)\times10^{-4}$).

2.7.1 Absorption Spectra of the Radicals

The absorption spectra of the free radicals discussed in this thesis are summarized in Figure 2.6. The absorption spectrum of CH_3 was measured in the previous work.[22] The absorption spectrum of OH was simulated using LIFBASE software.[57] The absorption spectra of HO_2,[9] CH_3O_2[9] and CH_2OO[6] are well studied.

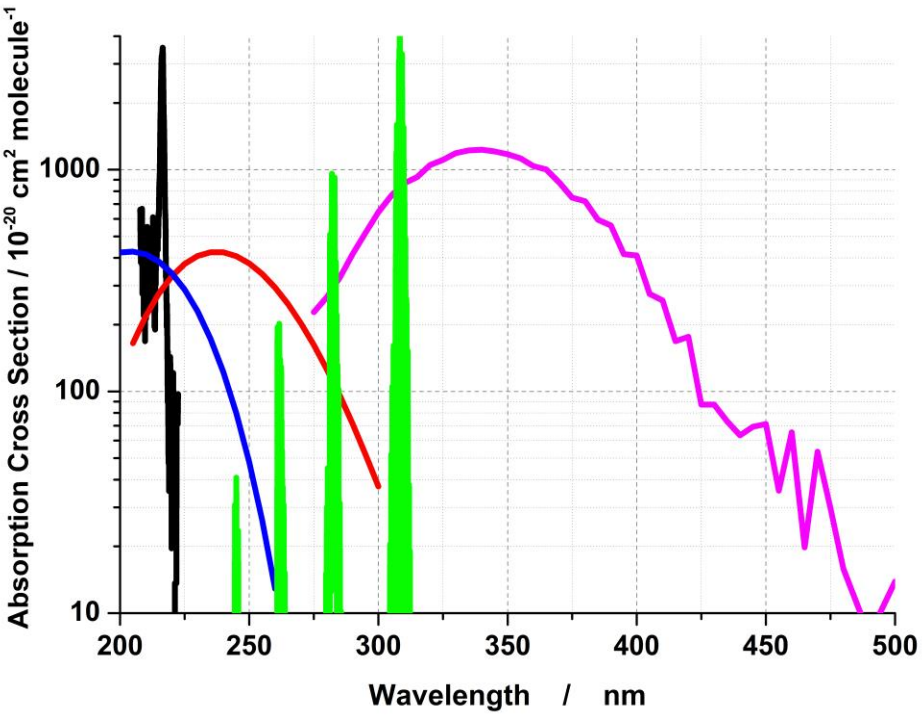

Figure 2.6 Absorption spectra of OH, CH_3, CH_3O_2, HO_2, and CH_2OO radicals. Green line – simulated OH absorption spectrum using LIFBASE;[51] black line – CH_3 absorption spectrum;[13] magenta line – CH_2OO absorption spectrum;[6] red line – CH_3O_2 absorption spectrum;[9] blue line – HO_2 absorption spectrum.[9]

2.7.2 Radicals Monitoring

The decay of methyl radicals was monitored by absorption at 216.36 nm and 216.56 nm (1200 groove/mm grating, 300 mm focal distance, both slits 0.25 mm, triangle slit function, FWHM = 0.64 nm) using 150 W (Oriel) short arc xenon lamp combined with an imaging spectrometer (Acton 300i). In some experiments, the lamp intensity was increased (ca. 100 times at 216 nm) by current boosting to 50 A using Photon Technology International MCP2010 pulser.

The kinetics of hydroxyl radicals decay curves (OH) were monitored by absorption in the UV (multiline at ca. 308 nm). A DC driven low pressure resonance hydroxyl lamp was employed.[39] The absorption cross sections of hydroxyl depend upon the lamp parameters, which are mainly the gas temperature and pressure in the lamp. Argon flow is saturated with water vapor at ambient temperature (296 ± 3 K) and 1.28 atm (4.0 psig) pressure. For purposes of the data interpolation and evaluation of the "curve of growth", a spectroscopic model was built in the previous study.[39] The decays of hydroxyl radicals (OH) were monitored by absorption at 308 nm (150 groove/mm grating, 300 mm focal length, both slits 0.5 mm, triangle slit function, FWHM = 10.7 nm) using a DC discharge H2O/Ar low-pressure resonance lamp combined with an imaging spectrometer (Acton 300i).

The decays of hydrogen peroxy radicals (HO_2) were monitored by absorption at 224 nm (1200 groove/mm grating, 300 mm focal length, both slits 0.25 mm, triangle slit function, FWHM = 0.64 nm) or 210 nm (1200 groove/mm grating, 300 mm focal length, both slits 0.75 mm, triangle slit function, FWHM = 1.96 nm) using 150 W (Oriel) short arc xenon lamp combined with an imaging spectrometer (Acton 300i).

The decays of methyl peroxy radicals (CH_3O_2) were monitored by absorption at 253.7 nm using a low-pressure radio frequency discharge mercury lamp (1200 groove/mm grating, 300 mm focal distance, both slits 0.50 mm, triangle slits function, FWHM = 1.27 nm).

The attempt to detect the Criegee intermediate (CH_2OO) was made by absorption at 340 nm (150 groove/mm grating, 300 focal distance, both slits 1.00 mm, triangle slits

function, FWHM = 21.3 nm) using 150 W (Oriel) short arc xenon lamp combined with an imaging spectrometer (Acton 300i).

2.8 *In Situ* Actinometry

Reliable determination of the absolute concentrations of free radicals is one of the most important requirements in the studying of radical-radical reactions. The photon fluence was determined using the *in situ* actinometry based on the measurements of the ozone formed in the photolysis of $N_2O/O_2/N_2$ mixtures.

In our measurements, gas mixture of 2.5% N_2O in He diluted with 8.0% O_2 in the N_2 mixture is pumped through the reactor at ambient (measured) pressure and photolyzed at 193.3 nm. Excited oxygen atoms $O(^1D)$, formed in the photolysis, undergo relaxation in collisions with nitrogen ($k_{q,N2} = 2.6x10^{-11}$)[20] and oxygen ($k_{q,O2}$ = 4.0x10-11)[20] or react with N_2O ($k = 1.35x10^{-10}$) $cm^3molecule^{-1}s^{-1}$. The concentration of oxygen-nitrogen mixture ($2.43x10^{19}$ molecule cm^{-3}) is much higher than the concentration of N_2O used in this experiment ($7.4x10^{16}$ molecule cm^{-3}) which provided almost complete (98.5%) relaxation of $O(^1D)$ to the ground state oxygen atoms $O(^3P)$ and subsequent conversion to ozone in fast (ca. 56 μsec) reaction with molecular oxygen.

N_2O	+	hν(193)	→	N_2	+	$O(^1D)$	(2.2a)
$O(^1D)$	+	M	→	$O(^3P)$	+	M	(2.18)
$O(^3P)$	+	O_2	→	O_3			(2.19)

Formation of O_3 is monitored using low pressure RF discharge mercury lamp at 253.7 nm.

The absolute concentrations of radicals are determined based on the photon flux inside the reactor, the absorption cross-section of N_2O at 193.3 nm, and the efficiency of conversion of $O(^1D)$ atoms produced in the photolysis of N_2O to these radicals. The absorption cross-section of N_2O is accurately known at 298 and 1 bar. Specifically, ozone formation, monitored at 253.7 nm, in the photolysis of $N_2O/O_2/N_2$ mixtures at 1 bar and 298 K is used. Essentially, this is a modification of the technique where ozone depletion in photolysis at 248 nm is used (Ravishankara et al.)[58] to determine in situ photon flux from a KrF laser.

The difference in the absorbance (with reactant and without the reactant) is used to calculate the concentration of ozone formed. (Only the initial parts of the traces are shown to resolve the build-up stage. In the measurements, a longer time domain (ca. 5 ms) is used).

Sample ozone formation traces are shown in Figure 2.7 with the mixture $N_2O/O_2/N_2$ (N2O = 2.42 Torr, 8.0% O_2/N_2 mixture, total pressure 1 bar) in the reactor (between the two internal windows). Without the reactants (the "blank" experiment), the flow of N_2O/He is turned off. Only O_2/N_2 mixture is pumped through the reactor. The residual absorbance is due to the photolysis of molecular oxygen inside the reactor and between the external and internal windows flushed with the O_2/N_2 mixture.

The difference in the absorbance, ΔAbs, is used to calculate the concentration of ozone formed due to the photolysis of N_2O. The photon fluence, F (photons cm^{-2}) is then calculated as:[39]

$$F = \frac{\Delta A}{\sigma_{O3} \cdot l \cdot 0.985 \cdot \sigma_{N2O}[N_2O]}$$

where $\sigma_{O3} = (1.148 \pm 0.034) \times 10^{-17}$ cm^2 molecule^{-1} is the ozone absorption cross section at 253.7 nm;[59] l = 10.00 cm is the length of the reactor (the distance between the two internal windows), and $\sigma_{N2O} = (8.77 \pm 0.44) \times 10^{-20}$ cm^2 molecule^{-1} is the N_2O absorption cross section at 193.3 nm (all at 298 K and 1 bar).[59] Two such determinations are performed – before and after a series of measurements.

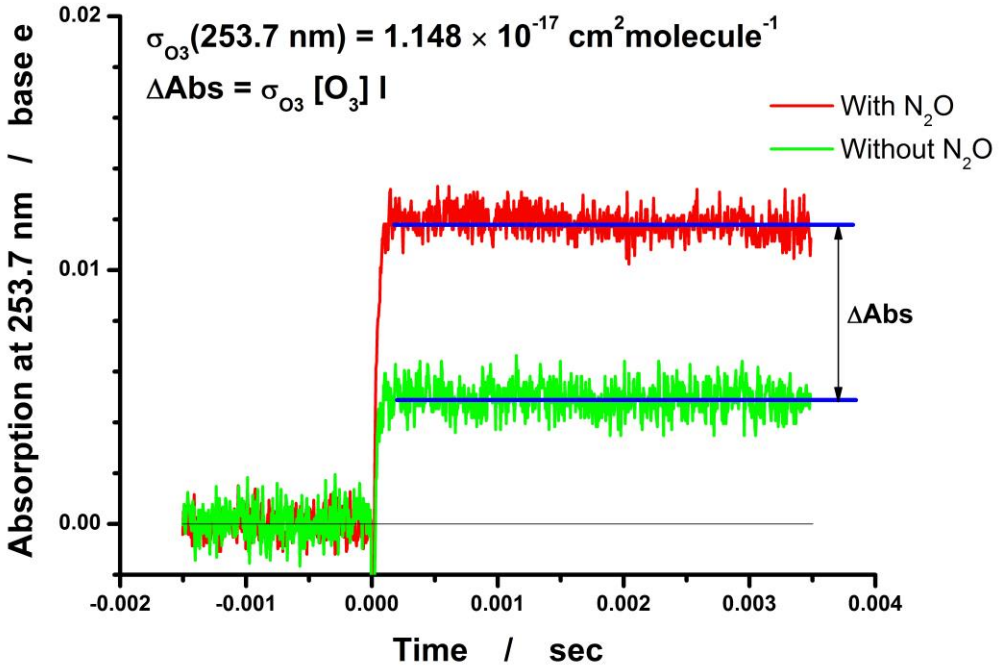

Figure 2.7 *In situ* actinometry based on the ozone formation.

CHAPTER 3

$CH_3 + CH_3 \rightarrow$ PRODUCTS

3.1 Introduction

Self-reaction of methyl radicals (1a, 1b) is important in hydrocarbon pyrolysis and combustion mechanisms:[11-20]

$$CH_3 + CH_3 \rightarrow C_2H_6 \quad (1a)$$

$$\rightarrow C_2H_5 + H \quad (1b)$$

Channel 1a is a chain termination step, while channel 1b is one of the chain propagation steps. Both the branching ratio and the rate of reaction 1 have impact on the self-ignition threshold, flame propagation speed, as well as other parameters of combustion. The reaction plays a critical role for production of C2 hydrocarbons in methane combustion. The disproportionation channel 1b has an appreciable activation energy (56.5 kJ mol^{-1} and becomes important at temperatures significantly exceeding the highest temperature of the current study (k_{1b}(714 K) = 3.6×10^{-15} $cm^3 molecule^{-1} s^{-1}$,[20]) therefore can be completely neglected over the temperature range of this study.

Reaction 1 is important for fundamental chemical kinetics is considered as a benchmark reaction for testing and improving theories of radical - radical reactions as a simplest reaction of recombination of hydrocarbon free radicals. In relative kinetic studies involving methyl radicals, reaction 1 was frequently used as a reference reaction.

Accurate knowledge of the kinetic parameters of reaction 1 is nessassary in laboratory studies of other reactions involving methyl radical.[39;55]

Reaction 1 was extensively studied both experimentally and theoretically due to the importance to the combustion field. There are numerous publications associated with the kinetics of reaction 1. For detailed bibliography the readers are referred to the NIST database[20] as well as to the bibliography in several recent publications and reviews[10;19]. Hippler et al.[60] studied reaction 1 over the pressure range 1 – 210 bar at ambient temperature in two bath gases, argon and nitrogen. The high pressure limit was reached at ca. 10 bar of Ar (within the experimental uncertainty), the determined recombination rate constant in the high pressure limit is $k_{1a,\infty} = 5.8 \times 10^{-11}$ $cm^3 molecule^{-1} s^{-1}$.

Reaction 1 has been studied across a wide temperature range, while more reliable determination of the rate constant in the high pressure limit are still required. In this work, reaction 1 was studied at elevated temperatures (293 – 714 K) and in the conditions of only minor deviations from the high pressure limit.

Kinetics of reaction 1 was partially studied previously at NJIT (Ph.D these of Manuvesh Sangwan, Ref.[38]). To resolve several issues associated with the absorption cross-section of methyl radicals, the additional kinetics measurements have been produced at a different central wavelength by the author of this thesis.

3.2 Experimental Approach

The approach is based on the excimer laser photolysis coupled to UV-Vis transient absorption spectroscopy and to a high-pressure flow system. Helium was used as a bath gas in all experiments. The measurements were performed over the 1 – 100 bar pressure

and 19 – 441 ℃ (292 – 714 K) temperature ranges. “Old” heatable reactor was used in this study.

Acetone - water mixtures were degassed using three freeze-pump-thaw cycles before loading in the stainless steel syringe. The mole fraction of acetone in water was varied from 0.02 to 0.04. The flow rate of acetone-water mixtures was varied in the range of 0.5 – 10 μL/min depending upon the reactor pressure and temperature. The concentrations of the precursors used: $(1.64 – 5.69) \times 10^{17}$ molecule cm^{-3} for CH_4, $(0.1 – 1.0) \times 10^{17}$ molecule cm^{-3} for N_2O, $(0.87 – 6.76) \times 10^{15}$ for CH_3COCH_3 and $(1.4 – 7.0) \times 10^{17}$ for H_2O. The laser photon fluence inside the reactor was varied in the range $(2.4 – 15) \times 10^{15}$ photons cm^{-2} $pulse^{-1}$. The initial concentrations of methyl radicals were in the range $(5 - 46) \times 10^{13}$ molecule cm^{-3}. The experimental conditions and concentrations of reactants are given in Tables 3.1 and 3.2.

CH_3 radicals were generated either by excimer laser pulse photolysis of acetone or of N_2O in the presence of methane at 193.3 nm (ArF excimer laser). Detailed description of generation and monitoring CH_3 radicals is given in Chapter 2.

It was indicated that methyl radical might be further photolysied by the laser light during the laser pulse.[5]

$$CH_3 + h\nu(193.3\ nm) \rightarrow CH_2 + H \qquad (E3.1)$$

The estimated fraction of methyl radicals photolyzed at the fluence of 35 mJ cm^{-2} is less than 2%.[5] The fraction of methyl radical photolyzed by the same laser pulse (α) can be estimated using equation E3.2:

$$\alpha = \phi\, \sigma_{193}(CH_3)/2 \qquad (E3.2)$$

where ϕ is the laser fluence (in photon cm^{-2}) and $\sigma_{193}(CH_3)$ is the absorption cross-section of CH_3 radicals at the laser wavelength 193.3 nm. Expression E3.2 is valid irrespective of the laser pulse shape and duration, provided that the pulse is much shorter than the decay time of CH_3 radicals, the absorption cross-section does not change during the pulse (e.g., due to the vibrational relaxation of CH_3 radical), and the fraction α is small. According to the spectrum simulations,[10] the absorption cross-section of CH_3 at 193.3 nm increases with the internal energy of methyl radicals. At 1500 K, the cross-section at 193.3 nm is smaller than 1×10^{-18} $cm^2 molecule^{-1}$.[10] At the fluence of 10 mJ cm^{-2} (ca. 10^{16}photons cm^{-2}) equation E3.2 results in $\alpha < 0.5\%$. This is in accord with the estimate made in Ref.[5] Therefore, for the laser fluences (< 10 mJ cm^{-2}) used in this study, the secondary photolysis of methyl radicals during the same laser pulse could be neglected.

Table 3.1 Experimental Conditions and Results. Photolysis of Acetone at 193.3 nm as a Source of CH_3 Radicals. Monitoring Wavelength 216.36 nm

p / bar	T / K	Number density $/10^{19}$ molecule cm^{-3}	$[(CH_3)_2CO] / 10^{15}$ molecule cm^{-3}	$[CH_3] / 10^{14}$ molecule cm^{-3}	$k_1 / 10^{-11}$ $cm^3 molecule^{-1} s^{-1}$
1.01	292	2.50	3.92	2.15	5.81
1.01	354	2.07	3.21	2.02	5.28
1.01	414	1.77	2.74	1.94	5.11
1.01	558	1.31	2.05	1.71	4.27
1.01	626	1.17	1.82	1.52	4.10
1.02	714	1.03	1.43	0.818	4.27
2.90	294	7.13	4.47	1.97	5.04
2.90	354	5.93	3.71	1.76	4.95
2.90	414	5.07	3.17	1.73	4.67
2.90	555	3.78	2.37	1.50	4.27
2.90	626	3.35	2.10	1.37	4.00
2.90	714	2.94	1.84	1.16	3.87
9.77	294	24.0	4.71	2.27	5.52
9.77	357	19.7	3.91	2.05	5.61
9.77	414	17.0	3.34	1.93	5.33

Table 3.1 Experimental Conditions and Results. Photolysis of Acetone at 193.3 nm as a Source of CH_3 Radicals. Monitoring Wavelength 216.36 nm (Continued)

p / bar	T / K	Number density /10^{19} molecule cm^{-3}	$[(CH_3)_2CO]$ / 10^{15} molecule cm^{-3}	$[CH_3]$ / 10^{14} molecule cm^{-3}	k_1 / 10^{-11} $cm^3 molecule^{-1} s^{-1}$
9.77	555	12.7	2.50	1.68	4.42
9.77	626	11.3	2.22	1.56	4.57
9.77	714	9.89	1.94	1.32	4.10
30.32	294	73.6	2.02	2.17	6.06
30.32	354	61.3	1.68	1.85	5.43
30.32	414	52.5	1.44	1.56	5.66
30.32	555	39.3	2.17	2.45	4.62
30.32	626	34.8	1.92	2.29	4.29
30.32	714	30.6	1.69	1.95	4.29
100.3	296	234	1.63	2.45	5.88
100.3	354	197	1.36	1.91	5.34
100.3	414	170	1.41	2.13	4.64
100.3	555	128	1.24	1.85	3.76
100.3	626	113	1.26	1.76	4.32
100.3	714	99.8	1.38	1.83	3.87

Table 3.2 Experimental Conditions and Results. Reactions $O(^1D)$ and, Subsequently, OH with CH_4 as a Source of CH_3 Radicals (Photolysis of N_2O/CH_4/He Mixtures at 193.3 nm). Monitoring Wavelength 216.56 nm

p / bar	T / K	Number density /10^{19} molecule cm^{-3}	$[N_2O]$/ 10^{16} molecule cm^{-3}	$[CH_4]$ / 10^{19} molecule cm^{-3}	$[CH_3]$ / 10^{14} molecule cm^{-3}	k_1 / sigmaCH_3 10^6 cm s^{-1}	k_1 / 10^{-11} $cm^3 molecule^{-1} s^{-1}$
100.4	293	237	1.84	5.69	2.53	3.99	5.63
100.4	293	237	3.63	5.67	4.60	4.31	5.26
100.4	294	235	9.16	5.66	0.978	3.64	5.31
100.4	294	235	9.16	5.66	1.07	3.24	4.21
100.4	294	235	3.60	5.63	3.62	3.63	4.76
100.4	294	235	5.50	5.67	0.574	3.41	4.50
100.8	714	99.7	6.86	2.07	3.09	2.95	3.59
100.8	714	99.7	3.46	2.07	1.60	3.31	3.42
100.8	714	99.7	2.77	2.07	1.26	3.85	3.48
100.8	714	99.7	3.47	1.64	1.50	2.68	2.84

3.3 CH_3 Radicals Absorption Cross Section

Temperature and pressure dependent absorption spectrum of CH_3 radicals is important to this work. Detailed analysis of the absorption spectrum for the $\tilde{B}^2A_1' \leftarrow \tilde{X}^2A_2''$ in the vicinity of 216 nm as well as a review of previous experimental measurements and modeling are given in a recent paper of Blitz et al.[14] The electronic transition $\tilde{B}^2A_1' \leftarrow \tilde{X}^2A_2''$ as well as the associated absorption spectrum of methyl radical have been extensively studied both experimentally and theoretically.[10;61-64]

The combination of a current boosted 75 W Xe short arc lamp, a gated ICCD camera and spectrophotometer was used to understand the changes in the apparent cross-section of methyl radical. The absorption band at 216 nm was recorded with finite spectral slit widths and with the highest resolution achievable in the current experimental set-up (1200 groove/mm, focal distance 300 mm, slit width 10 um, camera pixel size of 30 um). A 75 W Xe short arc lamp was boosted up to 50 A for 7 ms. The spectra were taken 0.9 μsec after the laser pulse (delayed by ca. 6 ms after the beginning of the boosting pulse) with the time gate of 2 μsec. The results are shown in Figure. 3.1 for the extremal combinations of temperature and pressure.

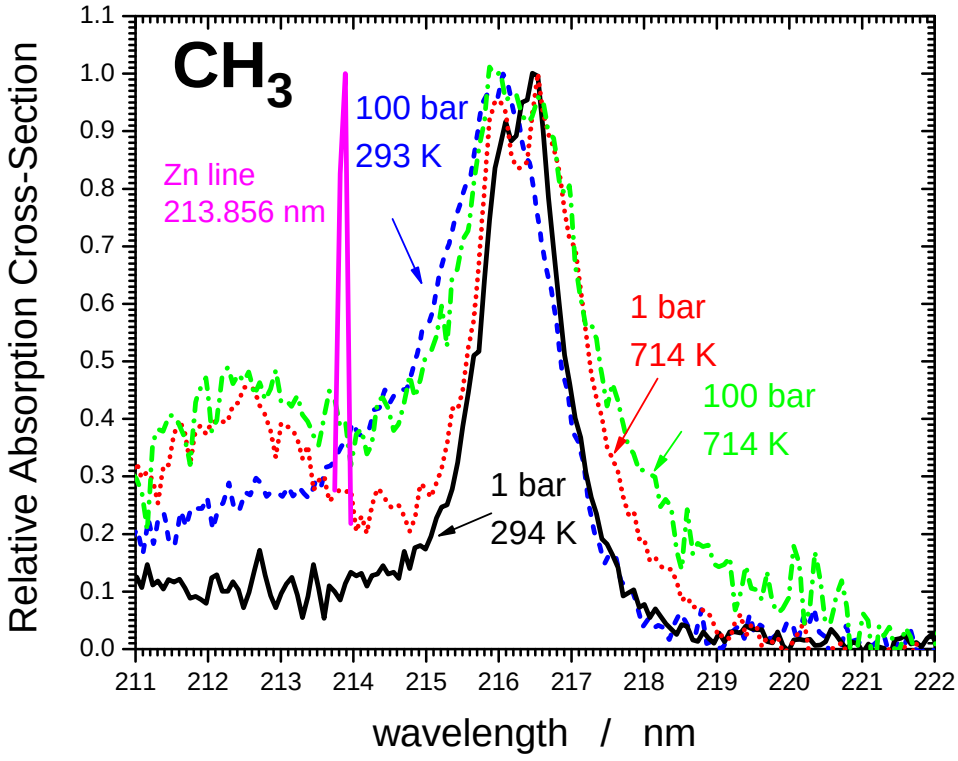

Figure 3.1 Absorption spectra of CH_3 radical near 216 nm at different experimental conditions. Solid line – 294 K, 1 bar; dotted line – 714 K, 1 bar; dashed line – 293 K, 100 bar; dash-dotted line – 714 K, 100 bar. Narrow feature – Zn resonance emission line (213.856 nm). The spectra were obtained using gated ICCD camera (ICCD Max, Princeton Instruments), the delay after the laser pulse 0.9 μsec, gate 2 μsec. Light source – current boosted 75 W Xe arc lamp (current pulse 50 A).

Blue shift of the maximum (ca. 0.22 nm at 100 bar) and a substantial broadening of the spectrum were observed when pressure increase to 100 bar.[60] The main peak at 216.36 nm is mainly due to the vibrational ground to vibrational ground transition between the ground and excited electronic states, $\tilde{B}^2A_1'(0,0,0,0) \leftarrow \tilde{X}^2A_2''(0,0,0,0)$ (the Frank-Condon factor of 0.764).[10;62] There is a "hot" transition at ca. 212.7 nm, the intensity of this peak increases with temperature (Figure. 3.1). The peak was identified as hot $\tilde{B}^2A_1'(0,1,0,0) \leftarrow \tilde{X}^2A_2''(0,1,0,0)$ transition.[65] The "shoulder" on the blue side of the

main peak observed at low temperatures is due to the contributions of these three transitions.

In the kinetic measurements, wider slits (0.25 mm) were employed. This corresponds to the triangular spectral slit function with the FWHM = 0.64 nm. Convolution of the spectra obtained with 10 um slit and ICCD detection with the triangular FWHM = 0.64 nm slit function shows almost no impact on the widths of the spectra with some reduction of the maximum apparent cross-section. It is most pronounced at 1 bar and ambient temperature, where the maximum cross-section of the convoluted spectrum drops by 12 $\pm$ 3%. The wavelength of the maximum of the apparent cross-section shifts with temperature and pressure.

In the beginning of this work by previous student (Dr. Sangwan Manuvesh), the central wavelength of 216.56 nm was used. This wavelength (216.56 nm) was also used in our previous work on the kinetics of the CH_3+OH reaction. This is the wavelength that corresponds to the maximum of the Q+P peak in the double-peaked absorption spectrum of methyl radical at room temperature. Although this wavelength provides the maximum absorption cross-section at ambient temperature and pressure for narrow line light sources, for the linewidth of 0.64 nm employed in this work the maximum apparent cross-section is for the central wavelength that corresponds to the small hole in the spectrum between the R and Q+P peaks, 216.36 nm. This wavelength (216.36 nm) was used in all projects listed in this thesis.

The central wavelength 216.36 nm corresponds to the small hole in the main peak and the maximum apparent cross-section at ambient temperature and pressure. When taken with the resolution of 0.64 nm, the cross-sections reported here (at 216.36 nm) are

slightly larger than the cross-sections reported previously at wavelength 216.56 nm (Ref.[39], Supplemental Material). The apparent cross-sections at wavelength 216.36 nm measured at different temperatures and pressures are summarized in Tables 3.3.

Table 3.3 The Product of the Apparent Absorption Cross-Section of Methyl Radical and the Half of the Quantum Yield of Methyl Radicals in Photolysis of Acetone at 193.3 nm ($\sigma_{CH3} \times (\phi_{CH3}/2)$ / 10^{-17} $cm^2 molecule^{-1}$) at Different Temperatures and Pressures. Central Wavelength 216.36 nm. The Errors are ca. ±4% at 1 bar and ca. ±7% at 100 bar

p/bar	1 bar	3 bar	10 bar	30 bar	100 bar
T/K					
298	3.86	3.23	3.15	3.27	2.15
355	3.51	3.30	3.22	3.04	2.24
414	3.22	2.93	2.97	3.00	2.23
555	2.55	2.45	2.01	2.43	1.85
626	2.33	2.15	2.08	2.10	1.88
714	2.34	1.90	1.57	1.99	1.47

The absorption cross-section measurements of Macpherson et al.[61] were made at lower pressures (< 0.53 bar) and with slightly better resolution (0.6 nm). Current results at p = 1 bar are in good agreement with the measurements of Macpherson et al.[61] However, due to the pressure induced blue shift of the absorption line, neither central wavelength 216.36 nm nor 216.56 nm provides the maximum absorbance at the conditions different from 1 bar and 298 K, especially at high pressures (Figure. 3.1).

3.4 Results and Discussion

Recombination of methyl radicals 1a would be the only major elementary reaction responsible for the decay of methyl radicals when water is not supplied. In such a case,

the second order kinetics is described by

$$Abs(t) = Abs_0/(1+2\ k_1 B\ Abs_0\ t) \qquad (E3.3)$$

when attenuation of the laser radiation resulting from the precursor's absorption is relatively small (< (5–10) %). Abs(t) is the absorbance (base e), defined via the monitoring light intensity I(t) and the light intensity before the laser pulse, I_0:

$$Abs(t) = \ln(I_0/I(t)) \qquad (E3.4)$$

parameter B is the ratio of the recombination rate constant k_1, the apparent absorption cross-section of methyl radical at the monitoring wavelength, 216.36 nm, and Abs_0 is the absorbance of the monitoring light (216.36 nm) right after the laser pulse, and the cell length *l*:

$$B = k_1/(\sigma_{CH3}\ l) \qquad (E3.5)$$

In case of strong absorption of the laser light (> 10%), exact expression accounting for the non-uniform axial initial concentration of methyl radicals was used:

$$Abs(t)= (2\ B\ \ln(G)\ t)^{-1}\ln\{(1+2Abs_0 G\ \ln(G)B\ t/(G-1)/(1+2Abs_0\ln(G)B\ t/(G-1)\} \qquad (E3.6)$$

where G is the parameter characterizing the attenuation of the laser light:

$$G = I_{laser}(x=0)/I_{laser}(x=l) \quad \text{(E3.7)}$$

Using E3.4 to fit the profiles simulated using E3.5 results only in 0.6% error in the signal amplitude and in 0.8% in the parameter B, when half of the laser light intensity is absorbed (G=2). Even at much higher attenuation (G=5, 20% of laser light is passing through) the errors are still reasonable: 4.3% in the signal amplitude and 3.3% in the B parameter.

Sample temporal profiles of methyl radical absorption at 216.36 nm in photolysis of acetone are shown in Figure. 3.2. The measurements were made on the sub-millisecond time scale.

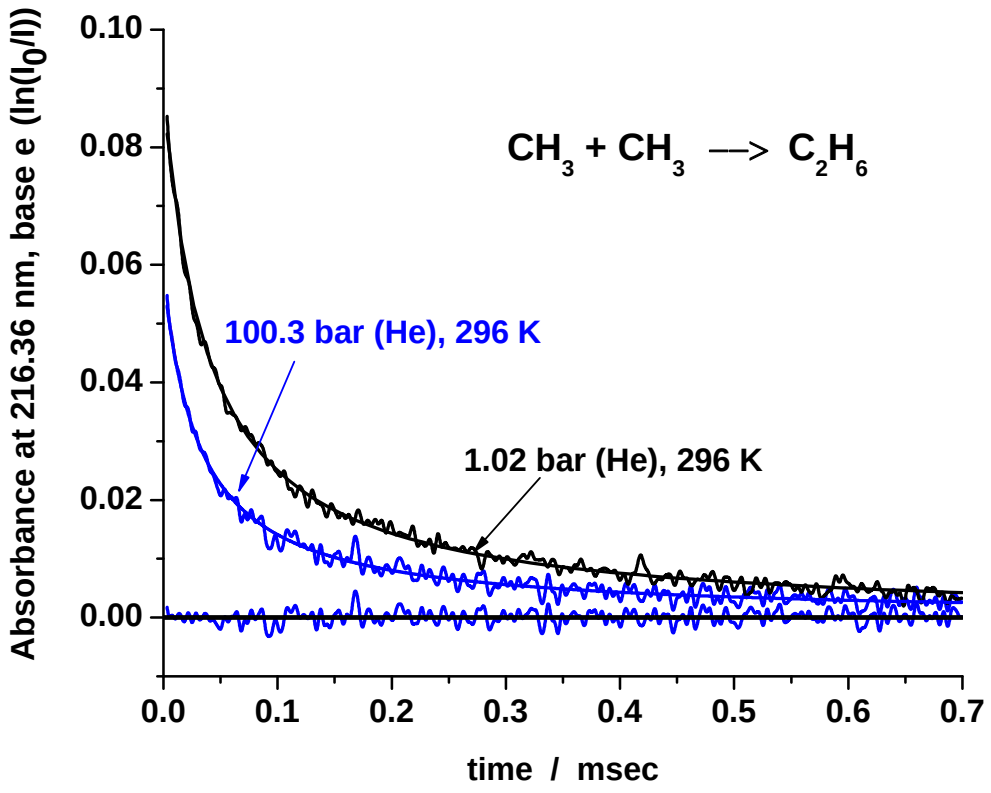

Figure 3.2 Sample temporal profiles of CH_3 decay. Temperature = 296 K, pressure = 1.02 bar (upper curve) and 100.3 bar (lower curve), bath gas He. Solid lines: fits by the reaction mechanism (see text). The residual is shown for the 100.3 bar curve. Conditions: $[(CH_3)_2CO]$ = 3.92×10^{15} and 1.63×10^{15} molecule cm^{-3}, laser fluences 8.64×10^{15} and 9.99×10^{15} photon cm^{-2} for the profiles at 1.02 bar and 100.3 bar, respectively.

Modeling with the detailed mechanism (Table 3.4) using numerical solution of the corresponding system of differential equation showed that the impact of the inclusion of water photolysis on the resulting rate constant 1 does not exceed 1.5%. The majority of the experiments were done using photolysis of acetone as a source of methyl radicals. In this photolysis system, we used solutions of acetone in water. Presence of water might potentially result in complications due to the photolysis of water molecules:

$$H_2O + h\nu(193.3\ nm) \rightarrow H + OH \quad (E3.8)$$

The experimental conditions and the results of the measurements are summarized in Tables 3.1. Additional series of measurements were carried out using photolysis of N_2O/CH_4/He mixtures. These results together with the experimental conditions are listed in Table 3.2.

Table 3.4 Reaction Mechanism Used to Simulate and Fit the Experimental Profiles of the Decay of Methyl Radicals

Reactants	Products	Rate constant[a]	Reference	Comment
$OH+CH_3$	$H_2O+{}^1CH_2$		Ref.[40]	
	CH_3OH			
$O(^1D)+H_2O$	2 OH	$1.7\times10^{-10}\exp(36/T)$	Ref.[66]	
	H_2+O_2	2.2×10^{-12}	Ref.[67]	
	$O(^3P)+H_2O$	$<0.003\ k_{3a}$	Ref.[58]	Neglected
$O(^1D)+N_2O$	2 NO	8.37×10^{-11}	Branching ratio of 0.62 based on Ref.[67]	The total rate constant $k_2=1.35\times10^{-10}$ is the average of three studies[58; 68; 69] as discussed by Bahng and Macdonald.[70]
	N_2+O_2	5.13×10^{-11}	Branching ratio of 0.38 Ref.[67]	
	$O(^3P)+N_2O$	1.3×10^{-12}	Ref.[66]	$k_{2c}/k_2<0.01$,[66] set to 1.3×10^{-12}
$O(^1D)+CH_4$	$OH+CH_3$	1.3×10^{-10}	Ref.[71]	
OH+OH	H_2O+O	$7.1\times10^{13}\exp(210K/T)$	Ref.[72]	Literature for T<415 K, Troe fit above 414 K Ref.[73]
	H_2O_2	$k_{5b,\infty}=(2.4\pm0.6)\times10^{-11}(T/300)^{-0.5}$ $k_{5b,0}=[He]\ (9.0\pm2.2)\times10^{-31}(T/300)^{-3.5\pm0.5}$ $F_{c=0.37}$.	Ref.[73]	

Table 3.4 Reaction Mechanism Used to Simulate and Fit the Experimental Profiles of the Decay of Methyl Radicals (Continued)

Reactants	Products	Rate constant[a]	Reference	Comment
$OH+CH_4$	H_2O+CH_3	$4.16\times10^{-13}(T/298)^{2.18}\exp(-1232/T)$	Ref.[74]	
OH+O	O_2+H	$2.4\times10^{-11}\exp(110/T)$	Ref.[67]	
OH+H	H_2+O	$6.86\times10^{-14}(T/298)^{2.8}\exp(-1950/T)$	Ref.[75]	
	H_2O	[M] $1.6\times10^{-31}(T/298)^{-2.6}$	Ref.[76]	
CH_3+O	H_2CO+H	1.4×10^{-10}	Ref.[45]	
OH+NO	HONO	$k_{11,0}=6.0\times10^{-31}(T/300)^{-2.5}$ $k_{11,inf}=3.3\times10^{-11}(T/300)^{-0.3}$ $F_{11,cent}=0.60\exp(91/T)$	Ref.[77]	$F_{11,cent}$: fit of the data from Ref.[77]
CH_3+H	CH_4	$6.2\times10^{-29}(T/298)^{-1.8}$	Ref.[78]	
$OH+CH_2$	CH_2O+H	3×10^{-11}	Ref.[79]	
$OH+(CH_3)_2CO$	$CH_3CH_2CO+H_2O$	$3.15\times10^{-14}\times(T/300)^4\exp(453/T)$	Ref.[80]	
$OH+H_2O_2$	H_2O+HO_2	$2.9\times10^{-12}\exp(109/T)$	Ref.[81]	
$OH+HO_2$	H_2O+O_2	$4.8\times10^{-11}\exp(250/T)$	Ref.[82]	
HO_2+NO	$OH+NO_2$	$4\times10^{-12}\exp(223/T)$	Ref.[83]	
CH_3+NO	CH_3NO	$2.1\times10^{-30}(T/298\ K)^{-1.87}$	Ref.[84]	
$CH_3+H_2O_2$	CH_4+HO_2	$2\times10^{-14}\exp(300/T)$	Ref.[79]	

Figures. 3.3 and 3.4 show selected series of measurements. Figure 3.3 illustrates the scatter of the experimental points, the consistency of the results obtained in the photolysis of acetone and N_2O/CH_4 mixtures as well as the stability of the resulting rate constants with respect to the attenuation of the laser radiation. Initial absorbance amplitude of methyl radicals yields the absorption cross-section of the methyl radicals (Figure 3.4). Maximum scatter of the experimental data does not exceed ±16%. Both photolysis systems produce consistent results indistinguishable within the experimental scatter. Figure 3.4 shows the results of the measurements of the rate constant of reaction 1 at 714 K and 100 bar as well as the absorption cross-section in the two photolysis systems at different attenuations of the laser light.

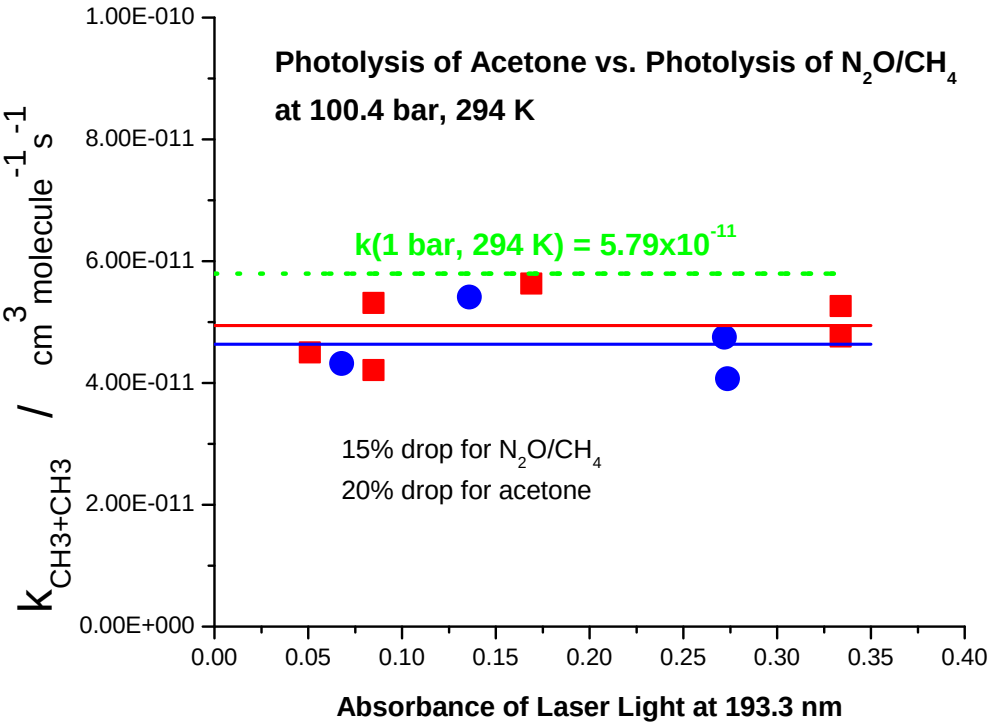

Figure 3.3 Comparison of the photolysis of acetone and N_2O/CH_4 at 193.3 nm, 100.4 bar and 294 K. Returned rate constant as a function of the attenuation of the laser light. Squares – photolysis of N_2O/CH_4, circles –photolysis of acetone. Dashed line – the results of the measurements at 1 bar, 294 K. Systematic deviation of all experimental points from the results at 1 bar is apparent. The average values are: 15% drop of the rate constant determined using N_2O/CH_4 photolysis, 20% drop using photolysis of acetone when going from 1 to 100 bar. The difference of the two measurements is within the precision, the difference with the measurements at 1 bar is outside the error limits.

Parameter B is the ratio of the recombination rate constant k_1 with the apparent absorption cross-section of methyl radical at the monitoring wavelength, 216.36 nm. Parameter B is determined directly from the decay profiles. One of the major factors contributing to the errors in the measurement is coming from the scatter of parameter B. The other major error is the accuracy of the determination of the photon fluence inside the reactor which was determined by the *in situ* actinometry.

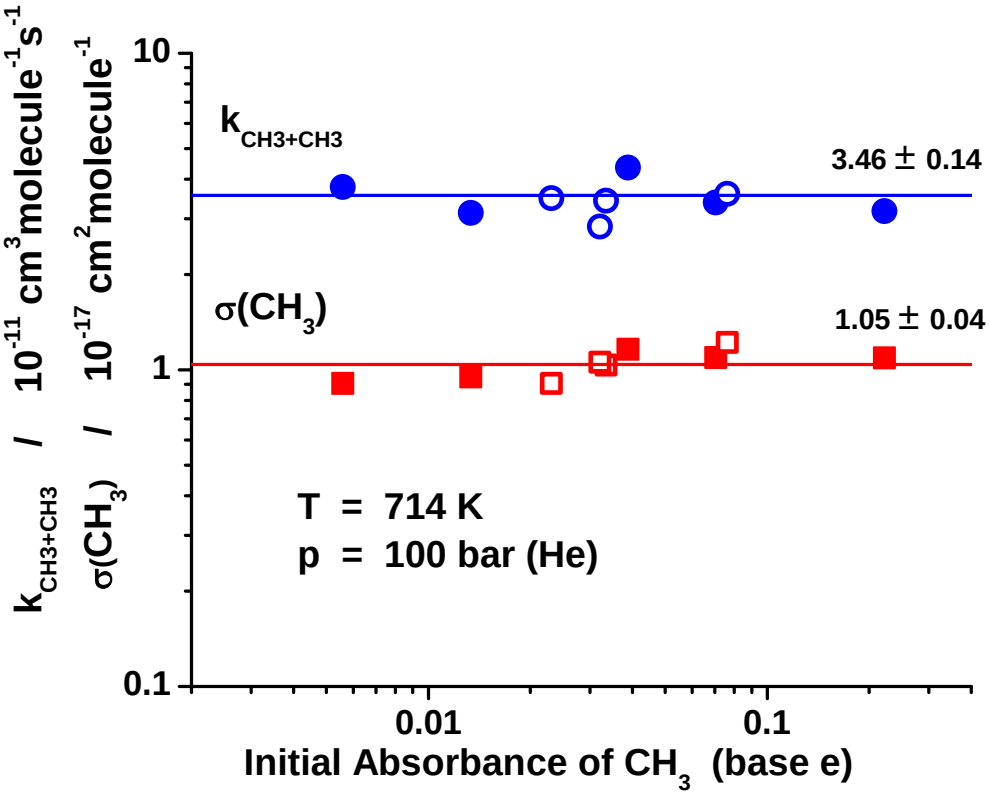

Figure 3.4 Comparison of the photolysis of acetone and N_2O/CH_4 at 193.3 nm, 100.4 bar and 714 K. Returned rate constants and the cross-sections as a function of the initial absorbance of methyl radicals. Empty symbols – photolysis of N_2O/CH_4, filled symbols - photolysis of acetone. Squares – cross-section of CH_3 radical at 216.36, circles – rate constant of reaction 1.

Figure 3.5 shows the major source of errors in this work originates from the scatter of the ratio k_1/σ_{CH3} from 44 decay profiles recorded at ambient temperature and 1 bar at different initial concentrations of methyl radicals over a period of several years. The standard deviation of the scatter is ca. 9%. The scatter is caused by the reproducibility of the central wavelength (0.05 nm as stated by the manufacturer) as well as the accuracy of the fit limited by the signal to noise ratio in the experimental decay profiles.

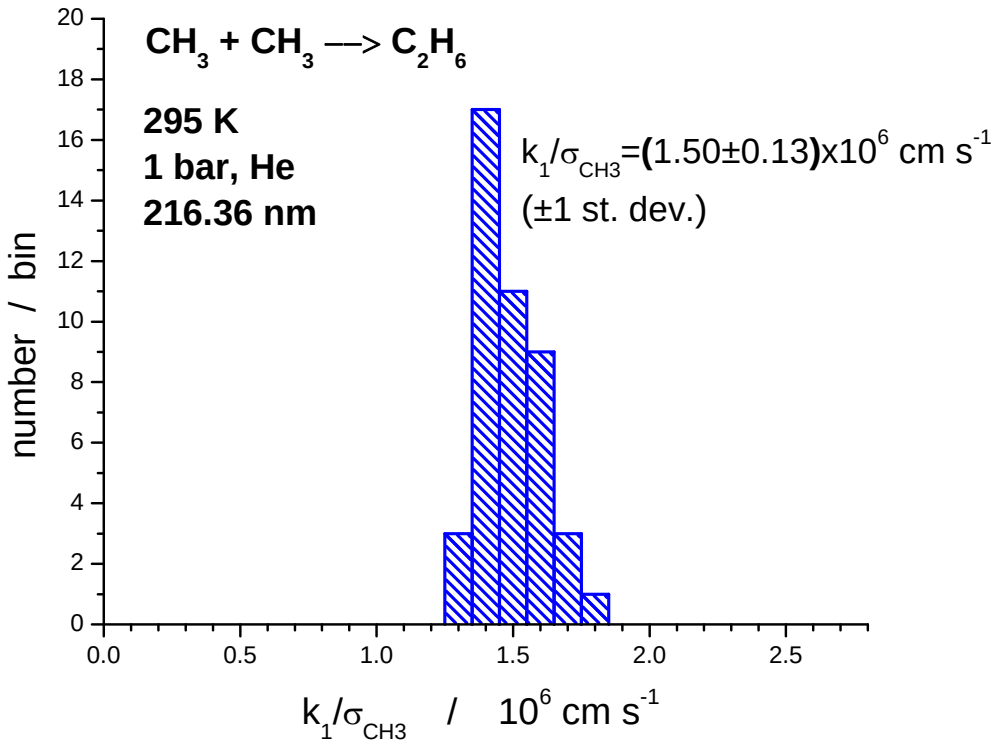

Figure 3.5 Histogram of the distribution of the rate constant – cross section ratio (k_1/σ_{CH3}) obtained at the central wavelength of the monitoring light of 216.36 nm at 1 bar (He) and 295 ± 3 K.

In this work, there is a systematic drop in the measured apparent rate constant at 100 bar pressure as compared with the measurements at 1 bar. This is shown in Figure. 3.3. Potentially, several factors might cause the drop of the rate constant with pressure. The quenching of the primary photolysis processes of $O(^1D)$ could be the problem. However, due to the large difference in the complexity of the two precursors, acetone and N_2O, such cause does not seem to be probable. The diffusion control would be the other possible reason. And finally, closely associated with the diffusion control, cage effects in

the photolysis of the precursors might be responsible for the drop of the initial concentrations of methyl radicals in the bulk, and, hence, the apparent rate constant.

Diffusion control as well as the cage effect in dense media are well established phenomena.[85-89] In application to reaction 1a, the impact of diffusion control was discussed in Ref.[15] The 15% to 20% drop at ambient temperature corresponds to the diffusion controlled rate constant of k_{diff} = (2.3-3.3)×10^{-10} $cm^3molecule^{-1}s^{-1}$. The cage effect is closely related to the diffusion control, similar estimates are applicable. Comparable effects were observed in recombination of CCl_3 radicals at comparable pressures[90] and attributable to the diffusion control. Therefore, the observed drop of the recombination rate of methyl radicals could be tentatively assigned to onset of the diffusion control. However, further investigation of the subject is necessary.

Hippler et al.[60] studied reaction 1 over the pressure range 1 – 210 bar at ambient temperature in two bath gases, argon and nitrogen, using laser photolysis coupled to transient UV absorption. The high pressure limit was reached at ca. 10 bar of Ar (within the experimental uncertainty), the determined recombination rate constant in the high pressure limit is $k_{1a,\infty}$ = 5.8×10^{-11} $cm^3molecule^{-1}s^{-1}$. A drop of the measured recombination rate constant at higher pressures (ca. 12% in Ar and ca. 3 times in N_2 at 210 bar) was also observed. The observed drop of the rate constant is smaller than that observed in He in this work (ca. 15-20% at 100 bar). Much larger drop was observed when nitrogen was used as the bath gas, ca. factor of two at 100 bar and ca. factor of three at 200 bar.[60] Neither the scale of the effects nor the relative order for different bath gases correspond to the diffusion control limited by translational diffusion of the reactants. In view of highly anisotropic interaction of methyl radicals orientation

relaxation rather than translational diffusion might be responsible for the observed decrease in the recombination rate.

The other feature is the absence within the experimental accuracy of any rise of the rate constant with pressure at 714 K over the range 1 – 100 bar, where some rise due to the pressure falloff could be expected. Estimates based on the recommended low pressure limit rate constant k_0(714 K) = 5.28×10^{-28} cm^6 $molecule^{-2}$ s^{-1} and the high pressure rate constant of 3.14×10^{-11} $cm^3molecule^{-1}s^{-1}$[114] lead at 1 bar and 714 K to the ratio $x=k_0[M]/k_{inf}$ = 171. Both the extrapolations based on the standard Troe formalism and the recent approach of Zhang and Law[91] result in the prediction of ca. 25% drop of the rate constant at 1 bar compared with the 100 bar value. Accepting more recent low pressure limit rate constant of Wang et al.[5] k_0(714 K) = 2.21×10^{-27} $cm^6molecule^{-2}s^{-1}$ leads to much higher $x=k_0[M]/k_{inf}$ = 714. Using this ratio and the Zhang and Law expressions leads to a smaller deviation of the rate constant at 1 bar from the high pressure limit of ca. 11%. However, the most recent revisions of the broadening factor in dissociation/recombination reactions by Troe and Ushakov show that the previous expressions overestimated the breadth of the transition region at high $x= k_0[M]/k_{inf}$ values (i.e., very close to the high pressure limit).[92; 93] The predicted deviation of the rate constant from the high pressure limit at 714 K and 1 bar does not exceed 5%. It should be much smaller at higher pressures taken into account in the averaging (1, 3, 10 and 30 bar). Therefore, we estimate the error associated with the fall-off effects at 714 K as not exceeding 2%. Based on these estimates, no pressure dependence of the rate constant within the experimental error is expected in accord with the experimental observations.

In view of no pressure dependence observed within the experimental error over the 1 – 30 bar pressure range and a small drop of the rate constant at 100 bar, we took average of all measurements over the range 1 -30 bar as the high pressure rate constant of reaction 1. The results are listed in Table 3.5 and shown in Figure 3.6. The results were fitted by the expression:

$$k_{1,inf} = (5.66 \pm 0.43) \times 10^{-11} (T/298\ K)^{-0.37}\ cm^3 molecule^{-1} s^{-1} \quad (292 – 714\ K). \qquad (E3.9)$$

The complete review of the literature could be found in the paper of Blitz et al.[10] Several experimental and theoretical studies are also shown in Figure. 3.6 for comparison Current experimental results are in excellent agreement with the theoretical study of Klippenstein et al.[8] over the whole temperature range of this study. There is excellent agreement at room temperature, and slight difference in the temperature dependence. The rate constant determined in this work is slightly higher (ca. 17% at 714 K) than that obtained by the data extrapolation to the high pressure limit in the most recent experimental study of Wang et al.[5]

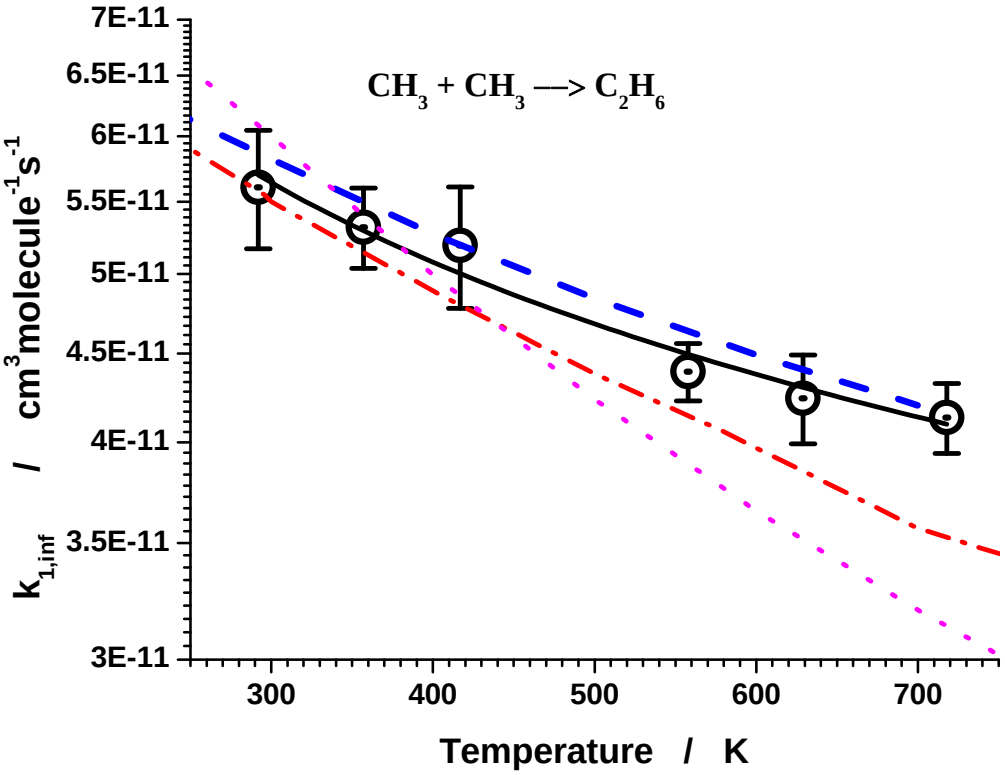

Figure 3.6 Dotted circles - rate constant k_1 in the high pressure limit over the temperature range 292 – 714 K (this work). Error bars - ± 1 St. Dev. Dash-dotted line – Wang et al.,[5] dashed line Klippenstein et al.,[8] (theory), dotted line Robertson et al.[10]

Table 3.5 Rate Constant of Reaction 1 ($CH_3 + CH_3 \rightarrow C_2H_6$) in the High Pressure Limit. Experimental Data are Averaged over the 1 – 30 bar Pressure Range. The Errors Indicated are ± 1 St. Dev

Temperature / K	(k_1 / 10^{-11} $cm^3molecule^{-1}s^{-1}$)
292	5.61 ± 0.44
354	5.32 ± 0.28
414	5.19 ± 0.42
558	4.39 ± 0.17
626	4.24 ± 0.25
714	4.13 ± 0.19

3.5 Conclusions

Reaction of recombination of methyl radicals was studied over an elevated pressure (1 – 100 bar) and temperature ranges (292 - 714 K). Slight drop of the rate constant at 100 bar is reported which requires further investigation. The rate constant in the high pressure limit exhibits negative temperature dependence, in accord with the previous studies. At elevated temperatures, these measurements are the closest to the high pressure limit. The low temperature data are in good agreement with the literature. The results at the elevated temperatures are slightly higher than those in the previous measurements, and are in excellent agreement with the theoretical calculations of Klippenstein et al.[8]

CHAPTER 4
CH_3O_2 + OH → PRODUCTS

4.1 Introduction

Methyl peroxy radical, CH_3O_2, plays an important role as a reaction intermediate in the low-temperature combustion as well as atmospheric oxidation of hydrocarbons.[94] Peroxy radicals are generated in the reactions of hydrocarbon radicals with molecular oxygen in combustion.[94] Hydroxyl radicals then might be regenerated in the further reactions of peroxy radicals in a chain reaction.

According to the recent studies, the reaction of CH_3O_2 radicals with hydroxyl radical, OH (reaction 1) might be important in the atmospheric chemistry.[24-26;95] Although substantial efforts were contributed into the studies of reaction 1, very limited information (rate constants and the branching ratios) were reported over elevated temperature range and extended pressure ranges.

$$CH_3O_2 + OH \rightarrow \text{Products} \qquad (1)$$

Bossolasco et al.[25] employed laser induced fluorescence and cw-cavity ring down spectroscopy coupled to laser photolysis to study reaction 1 at 294 K at pressures 50 and 100 Torr in helium as buffer gas. Very large rate constant was reported ($k_1 = (2.8 \pm 1.4) \times 10^{-10}$ cm^3 $molecule^{-1}$ s^{-1}). Methyl peroxy radicals, CH_3O_2, were generated in the photolysis of CH_3I at 248 nm in the presence of O_2; OH radicals were generated either in the reaction of $O(^1D)$ atoms formed in the photolysis of ozone at 248 nm with H_2O or by photodissociation of H_2O_2 at 248 nm. The rate constant of reaction 1 was obtained based

on the OH temporal profiles. Based on this relatively large rate constant of reaction 1, the conclusion of the importance of reaction 1 in atmospheric chemistry was derived.[96]

Two years after, the same group (Assaf et al.[97]) reported different rate constant (two times lower) of the reaction CH_3O_2 with OH. Same experimental set-up was used in this study. Instead of using CH_3I photolysis as a precursor, photolysis of XeF_2 at 248 nm was used to provide F atoms. In the presence of CH_4/O_2 and H_2O, CH_3O_2 and OH radicals were generated. A rate constant of $k_1 = (1.60 \pm 0.4) \times 10^{-10}$ cm^3 s^{-1} has been determined at 295 K.

Bian et al.[26] performed a theoretical study of reaction 1. Among the exothermic channels only 1a and 1b were found to be of importance at near ambient conditions:

$$CH_3O_2 + OH \rightarrow CH_3O + HO_2 \quad (1a)$$

$$\rightarrow {}^3CH_2OO + H_2O \quad (1b)$$

Channel 1a is barrierless; according to the calculations[26] it is exothermic by 16.8 kJ mol^{-1}. Channel 1b has a barrier of 30 kJ mol^{-1}. The three other channels suggested in the literature have very large activation barriers:[25;26;95]

$$CH_3O_2 + OH \rightarrow CH_3OH + O_2\ ({}^1\Delta_g, {}^3\Sigma_g^+) \quad (1c)$$

$$\rightarrow {}^1CH_2OO + H_2O \quad (1d)$$

There are two more exothermic channels which also have very large activation barriers.[26]

Both potentially important channels 1a and 1b are the chain propagation steps

forming free radical species. Channel 1a produces HO_2 and CH_3O radicals which participate in the consumption of CH_3O_2 as well as other reactions.[98] The Criegee intermediate CH_2OO, formed in channel 1b, is relatively active in the troposphere[99] where these species undergo further reactions to produce secondary organic aerosols and phytotoxic compounds.[100]

Most recent theoretical study was published by Muller et al.[27] Detailed potential energy surfaces were calculated using suitable high-level density functional theory (DFT) and *ab initio* methodologies for the singlet and triplet intermediates. The Criegee pathway is negligible in atmospheric conditions. Channel 1a is expected to dominate, whereas both methanol formation (channel 1c) and stabilization of the methylhydrotrioxide CH_3OOOH (TRIOX) are minor channels:

$$CH_3O_2 + OH \rightarrow CH_3OOOH \qquad (1e)$$

The formation of methanol can occur through the activated TRIOX intermediate decomposition. In the low-pressure conditions (less than 1 bar), the branching ratio of channel 1c is important due to the dissociation of TRIOX. However, in the high pressure conditions, the stabilization of TRIOX becomes more important. The branching ratios were reported at 298 K and 1 atm pressure ($\alpha_{1a} = 0.82$, $\alpha_{1c} = 0.069$ and $\alpha_{1e} = 0.107$).

In this work, the rate constant of reaction 1 was measured over the temperature range 292 – 526 K at pressure 1 bar. In addition, the branching ratio of channel 1b at ambient temperature and the branching ratio of 1e at pressure 1 – 100 bar were evaluated.

4.2 Experimental Approach

The technique of the excimer laser photolysis coupled to UV-Vis transient absorption spectroscopy is used. Both "new" heatable high-pressure reactor and room temperature high-pressure were used in this study. The measurements were performed over the 19 – 253 °C (292 – 526 K) temperature range and ambient pressure (1.02 ± 0.01) bar in He as a bath gas. Gas mixtures were supplied to the reactor through a heated transfer line (heated up to ca. 140 °C). This was necessary to provide high concentration of water at elevated temperatures. The flow rates of acetone-water mixtures were varied in the range of 0.5 – 30 μL/min depending on the reactor temperature.

The concentrations of the precursors used: $(0.47 – 6.90)\times10^{16}$ molecule cm^{-3} for N_2O, $(1.00 – 9.97)\times10^{17}$ for O_2, $(1.37 – 3.80)\times10^{15}$ for $(CH_3)_2CO$ and $(0.85 – 12.8)\times10^{17}$ for H_2O. The laser photon fluence inside the reactor was varied in the range $(5.2 – 10.5)\times10^{15}$ photon cm^{-2} $pulse^{-1}$. The initial concentrations of radicals were in the range of $(0.43–1.94)\times10^{14}$ molecule cm^{-3} for CH_3 radicals, $(4.85 – 109.1)\times10^{12}$ for OH radicals and $(4.01 – 55.14)\times10^{12}$ for $O(^1D)$ atoms. The measurements were performed at pressure 1 bar (He) over the 292 – 526 K temperature range. No noticeable depletion of the radical precursors (acetone and nitrous oxide) was observed at and below 526 K. At higher temperatures, depletion of the precursors was observed. Separately, these compounds are stable up to the highest temperature of the reactor of 834 K. The repetition rate of the laser was set to 1 Hz to ensure complete replacement of the gas mixture in the reactor between the pulses.

The kinetics of hydroxyl radicals (OH), methyl radicals (CH_3), hydrogen peroxy radicals (HO_2), methyl peroxy radicals (CH_3O_2) and the Criegee intermediate (CH_2OO)

were monitored by absorption in the UV at different wavelengths which are discussed in Chapter 2.

Reagents. In the experiments BIP®Helium from Airgas with 99.9999% purity with reduced oxygen content (<10 ppb) was used. Certified mixture of N_2O in He (mole fraction of 0.025, the accuracy ±2%) obtained from AirGas was used. Ultra-high purity grade (UHP) oxygen with 99.994% purity obtained from AirGas was used. Purified water (Milli-Q®) with TOC less than 5 ppb) was degassed by using three freeze-pump-thaw cycles and used as a solvent for acetone/water solutions supplied by the syringe pump (Harvard Apparatus PHD4400). Acetone used in the acetone-water mixtures was purchased from Fisher Scientific (99.7%).

4.3 Results and Discussion

4.3.1 Rate Constant $k_{CH3O2+OH}$

Transient absorption profiles of OH were measured at 1 bar over the 292 - 526 K temperature range. Sample absorption profiles at 216.36, 224, 253.7 and 308 nm are shown in Figure 4.1. Sample absorption profiles at 308 nm and 500 K where the concentration of CH_3O_2 was varied about 3 times are shown in Figure 4.2 (the corresponding experimental conditions are boldfaced in Table 4.1). The reaction mechanism (Table 4.2) was used to determine the rate constant as well as the branching ratios of the target reaction by modelling and fitting the experimental profiles. The transient absorption profiles at 253.7 nm (mainly CH_3O_2) were also fitted by the reaction mechanism.

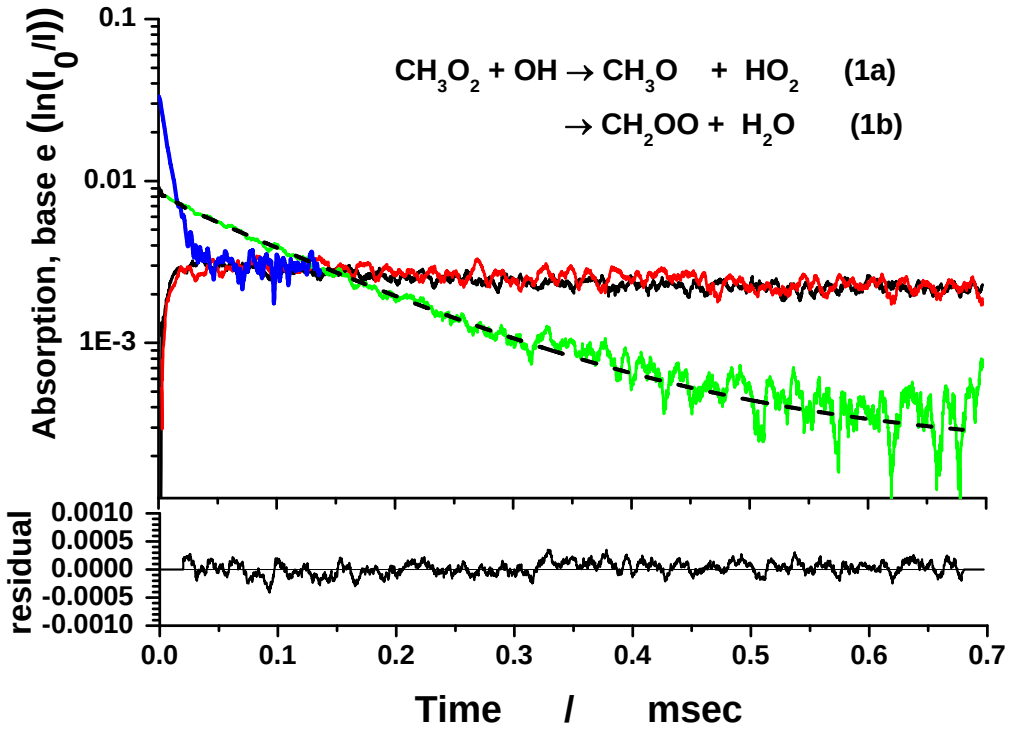

Figure 4.1 Sample temporal profiles at 216.36 nm (blue trace, mainly CH_3); 224 nm (red trace, mainly HO_2); 253.7 nm (black trace, mainly CH_3O_2) and 308 nm (green trace, mainly OH). Dashed line: fit by the reaction mechanism (see text). The residual is shown for absorption at 308 nm (note the linear scale).

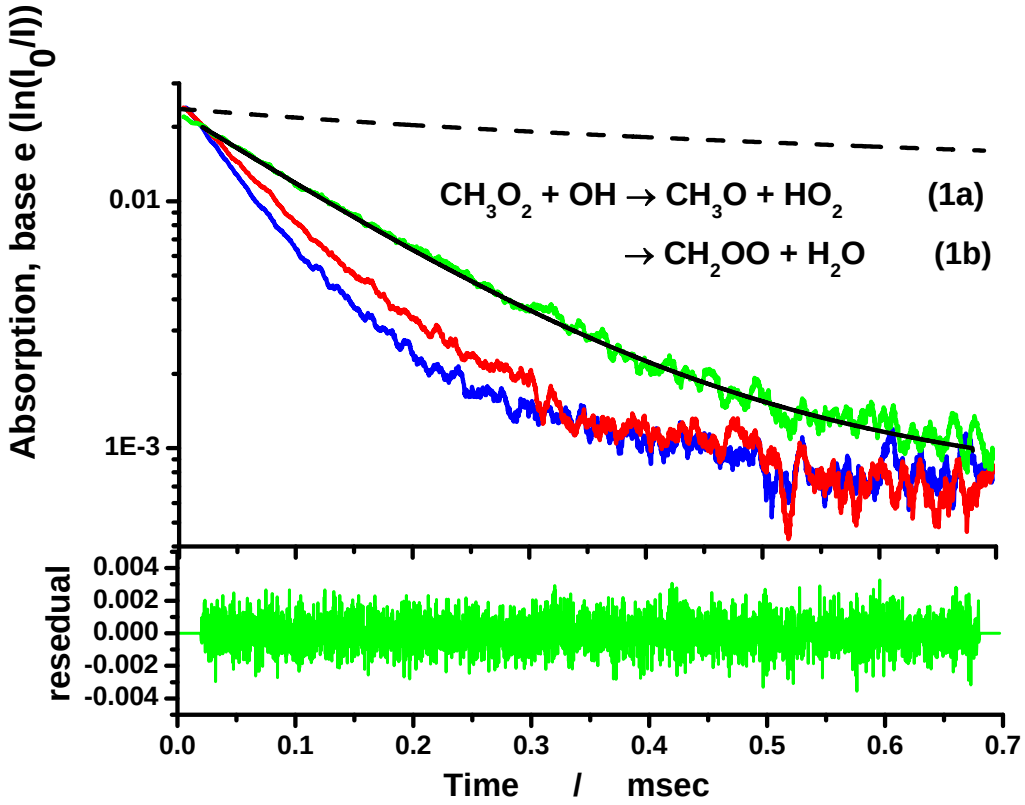

Figure 4.2 Temporal absorption profiles at 308 nm at different concentrations of CH_3O_2 radicals. Acetone concentrations varied 2.8 times from green to blue traces (low to high). Solid line: fits by the reaction mechanism (see text). Dashed line: Simulated by the reaction mechanism where initial acetone concentration equal to zero. The residual is shown for the green trace (note the linear scale). Temperature 500 K, pressure 1 bar (He). All other experimental conditions listed in Table 4.2 (bold faced lines at 500 K).

Table 4.1 Experimental Conditions and the Rate Constants of Reaction 1 at Pressure 1.02 ± 0.01 bar

T / K	$[(CH_3)_2CO]$ / 10^{15} molecule cm^{-3}	$[N_2O]$ / 10^{16} molecule cm^{-3}	$[O_2]$ / 10^{17} molecule cm^{-3}	$[H_2O]$ / 10^{16} molecule cm^{-3}	Photonfluence / 10^{15} photon cm^{-2} $pulse^{-1}$	Number density /10^{19} molecule cm^{-3}	$[OH]_0$ / 10^{12} molecule cm^{-3}	$[CH_3]_0$ / 10^{14} molecule cm^{-3}	$[O(^1D)]_0$ / 10^{12} molecule cm^{-3}	k_1 / 10^{-11} $cm^3 molecule^{-1} s^{-1}$
292	1.83	1.17	9.90	8.77	10.21	2.51	6.69	1.14	9.19	8.69
292	1.80	2.29	9.74	8.61	10.23	2.51	11.47	1.12	17.91	7.15
296	1.77	1.11	9.97	8.50	7.89	2.47	4.85	0.43	6.85	6.32
296	3.55	1.11	9.97	17.01	7.72	2.47	7.54	1.62	6.45	8.03
295	1.82	1.16	1.00	8.75	9.31	2.48	6.07	1.04	8.39	9.59
295	1.79	2.23	9.86	8.59	9.29	2.48	10.24	1.02	16.07	6.40
295	3.59	2.23	9.86	17.20	9.27	2.48	15.86	1.97	15.56	8.83
294	1.90	1.16	1.27	9.10	8.13	2.51	11.39	0.94	7.27	7.73
294	3.80	1.17	1.27	18.20	8.09	2.51	13.66	1.82	7.09	6.74
294	1.89	2.31	1.26	9.06	8.07	2.51	20.26	0.93	14.42	8.65
294	1.88	2.31	1.29	9.05	10.43	2.51	25.90	1.19	18.52	10.50
294	1.90	1.76	1.30	9.13	10.19	2.51	20.29	1.18	13.87	9.85
354	1.48	0.92	8.16	7.10	9.41	2.07	5.74	1.00	8.16	7.50
354	2.96	0.92	8.16	14.20	9.37	2.07	8.98	1.94	7.91	6.43
354	2.98	0.47	8.20	14.20	9.36	2.07	5.49	1.93	4.01	9.07
414	1.88	2.35	3.50	127.9	7.32	1.78	48.21	1.17	19.61	6.19
414	1.79	4.43	3.33	121.5	7.32	1.78	78.82	1.11	36.96	6.68
414	1.68	6.90	3.12	113.9	7.01	1.78	109.1	0.99	55.14	7.06
454	1.82	2.25	3.46	124.0	7.22	1.61	46.26	1.11	18.99	5.05
454	1.72	4.25	3.28	117.4	6.70	1.61	74.88	1.03	35.38	5.55
454	1.61	6.62	3.06	109.7	6.69	1.61	108.5	0.97	55.11	5.93
500	1.60	1.98	3.01	108.7	6.33	1.46	40.42	0.96	17.11	5.03

Table 4.1 Experimental Conditions and the Rate Constants of Reaction 1 at Pressure 1.02 ± 0.01 bar (Continued)

T / K	$[(CH_3)_2CO] / 10^{15}$ molecule cm^{-3}	$[N_2O] / 10^{16}$ molecule cm^{-3}	$[O_2] / 10^{17}$ molecule cm^{-3}	$[H_2O] / 10^{16}$ molecule cm^{-3}	Photonfluence $/ 10^{15}$ photon cm^{-2} $pulse^{-1}$	Number density $/10^{19}$ molecule cm^{-3}	$[OH]_0 / 10^{12}$ molecule cm^{-3}	$[CH_3]_0 / 10^{14}$ molecule cm^{-3}	$[O(^1D)]_0 / 10^{12}$ molecule cm^{-3}	$k_1 / 10^{-11}$ $cm^3 molecule^{-1} s^{-1}$
500	1.52	3.74	2.86	103.1	6.21	1.46	66.12	0.89	31.78	5.39
500	1.42	5.83	2.68	96.52	6.07	1.46	94.20	0.82	48.39	5.57
500	**3.39**	**2.11**	**3.25**	**115.0**	**12.8**	**1.46**	**77.52**	**3.68**	**32.96**	**4.59**
500	**2.43**	**2.16**	**3.33**	**82.51**	**12.3**	**1.46**	**73.72**	**2.60**	**33.33**	**4.55**
500	**1.24**	**2.23**	**3.42**	**42.52**	**11.8**	**1.46**	**63.32**	**1.32**	**34.20**	**4.56**
526	1.55	1.91	2.93	105.0	5.47	1.40	35.13	0.83	15.04	5.33
526	1.47	3.62	2.78	99.71	5.38	1.40	57.95	0.77	28.04	5.67
526	1.37	5.63	2.60	93.31	5.28	1.40	82.95	0.71	42.80	6.28

Table 4.2 Reaction Mechanism Used to Fit the Experimental Profiles of of the Decay of OH radicals

Reaction	Reactants	Products	Rate constant[a)]	Reference	Comment	Relative maximum rate[b)]	Sensitivity, $\delta \ln k_1 / \delta \ln k_i$
1a	CH_3O_2 + OH	CH_3O+ HO_2	to be determined			0.95	
1b		CH_2OO + H_2O	to be determined			0.05	
1e		TRIOX	to be determined				
2	CH_3 + O_2	CH_3O_2	$k_{02} = [He]\ 7\times10^{-31} (T/300K)^{-3}$, $k_{02inf} = 2.2 \times 10^{-12} (T/300K)^{0.9}$, F_{02cent} =0.33, N_{02} = 1.47	Ref.[101]		86.6	0.033
3a	$O(^1D)$ + H_2O	2OH	$1.7 \times 10^{-10} \exp(36/T)$	Ref.[102]			
3b		H_2 + O_2	2.2×10^{-12}	Ref.[67]			
3c		$O(^3P)$ + H_2O	$<0.003k_{3a}$	Ref.[58]	Neglected		

Table 4.2 Reaction Mechanism Used to Fit the Experimental Profiles of of the Decay of OH radicals (Continued)

Reaction	Reactants	Products	Rate constant[a)]	Reference	Comment	Relative maximum rate[b)]	Sensitivity, $\delta\ln k_1 / \delta\ln k_i$
4a	$O(^1D) + N_2O$	2NO	8.37×10^{-11}	branching ratio of 0.62 based on Ref[67]	The total rate constant $k_4 = 1.35 \times 10^{-10}$ is the average of three studies[58; 68; 69] as discussed in Ref[70]		
4b		$O_2 + N_2$	5.13×10^{-11}	branching ratio of 0.38[67]			
4c		$O(^3P) + N_2O$	1.3×10^{-12}		$k_{4c}/k_2 < 0.01$,[102] set to 1.3×10^{-12}		
5	$O(^1D) + O_2$	$O(^3P) + O_2$	$3.3 \times 10^{-11} \exp(55/T)$	Ref.[103]			
6	$O(^1D) + (CH_3)_2CO$	$OH + CH_3COCH_2$	$<5 \times 10^{-10}$				
7a	OH + OH	$H_2O + O$	$1.39 \times 10^{-12}(T/298)^{-0.76}$	Ref.[39]		0.0061	0.0031
7b		H_2O_2	$k_{7b,0} = [He]\ 9.0 \times 10^{-31} (T/300)^{-3.5}$, $k_{7bini} = 2.4 \times 10^{-11} (T/300)^{-0.5}$, $F_{7b,cent} = 0.37$	Ref.[41]		0.0020	0.010
8a	$CH_3 + OH$	$CH_2 + H_2O$	$k_{8a+8b} = 1.2 \times 10^{-10}(T/300)^{-0.49}$	Ref.[40]		2.51	0.15
8b		CH_3OH					
9	$CH_3 + CH_3$	C_2H_6	$k_9 = 5.66 \times 10^{-11}(T/298)^{-0.37}$	Ref.[22]		5.32	0.041
10a	$H + O_2$	$OH + O$	$1.62 \times 10^{-10} \exp(-62110/8.31447/T)$	Ref.[104]		2.2×10^{-9}	2.4×10^{-5}
10b		HO_2	$[He]\ 5.4 \times 10^{-32}(T/298)^{-1.80}$	Ref.[105]		2.02	0.020
11	$CH_3 + O$	$H_2CO + H$	1.4×10^{-10}	Ref.[45]		0.43	9.9×10^{-4}

Table 4.2 Reaction Mechanism Used to Fit the Experimental Profiles of of the Decay of OH radicals (Continued)

Reaction	Reactants	Products	Rate constant[a)]	Reference	Comment	Relative maximum rate[b)]	Sensitivity, $\delta\ln k_1 / \delta\ln k_i$
11	$O + O_2$	O_3	[He] $3.4 \times 10^{-34} (T/300)^{-1.2}$ $K_{eq} = 4.00 \times 10^{-9} (T/298)^{-1.373} \exp(14123/T)$	Ref.[106-108]	Equilibrium constant from $\Delta H_f 298(O_3)$ = 141.746 kJmol^{-1} from active thermochemical data[108] and O, O_2 fro GRI from NIST WebBook[109]	0.036	2.2×10^{-4}
12	$CH_3 + H$	CH_4	$K_{12,0}$ = [He] $6.2 \times 10^{-29} (T/298)^{-1.8}$, $k_{12,inf} = 3.5 \times 10^{-10}$, $F_{cent,11} = 0.638 \exp(-T/3231)$	Ref.[104]		0.19	8.45×10^{-4}
13	$OH + CH_2$	$CH_2O + H$	3×10^{-11}	Ref.[95]		0.010	0.0053
14	$OH + (CH_3)_2CO$	$CH_3CH_2CO + H_2O$	$3.15 \times 10^{-14} (T/300)^{-4} \exp(453/T)$	Ref.[110]		0.058	0.044
15	$OH + HO_2$	$H_2O + O_2$	$4.8 \times 10^{-11} \exp(223/T)$	Ref.[111]		0.089	0.055
16	$CH_3 + NO$	CH_3NO	$k_{16,0}$ = [He] $6.9 \times 10^{-32} \exp(1430/T)$, $k_{16,inf} = 1.5 \times 10^{-11} \exp(-60/T)$, $F_{cent,16} = 5 \exp(-T/120)$	Ref.[112]		0.016	2.4×10^{-5}
17	OH + NO	HONO	$k_{17,0}$ = [He] $3.9 \times 10^{-31} (T/298)^{-2.6}$ $k_{17,inf} = 3.3 \times 10^{-11}$, $F_{cent,17} = 1.23 \exp(-T/815)$	Ref.[113]		0.0033	7.1×10^{-4}
18	$O + HO_2$	$O_2 + OH$	$2.0 \times 10^{-14} \exp(300/T)$	Ref.[67]		0.0079	0.0046
19	OH + O	$O_2 + H$	$2.4 \times 10^{-11} \exp(109/T)$	Ref.[67]		0.023	0.0067
20a	OH + H	$H_2 + O$	$6.86 \times 10^{-14} (T/298)^{2.8} \exp(-1950/T)$	Ref.[95]		1.2×10^{-8}	2.3×10^{-5}

Table 4.2 Reaction Mechanism Used to Fit the Experimental Profiles of of the Decay of OH radicals (Continued)

Reaction	Reactants	Products	Rate constant[a)]	Reference	Comment	Relative maximum rate[b)]	Sensitivity, $\delta\ln k_1 / \delta\ln k_i$
20b		H_2O	[He] $1.6 \times 10^{-31}{}_{(T/298)}{}^{-2.6}$	Ref.[76]		1.4×10^{-4}	2.4×10^{-5}
21a	$CH_3 + HO_2$	$CH_3O + OH$	$k_{21a} = \varphi_{21a}\ 3.7 \times 10^{-11}$ $\varphi_{21a} = 0.7$	Ref.[1; 2]	According to Jasper et al., the branching ratio between 21a and 21b is $_{21a} = 0.7$ at 300 K.	0.014	0.0040
21b		$CH_4 + O_2$	$k_{21b} = (1 - \varphi_{21a})\ 3.7 \times 10^{-}$ $_{11}$	Ref.[1; 2]		0.0060	0.0013
22a	$CH_3O + CH_3$	$CH_2O + CH_4$	4×10^{-11}	Ref.[95]		0.029	5.1×10^{-4}
22b		$(CH_3)_2O$	5.5×10^{-11}	Ref.[114]		0.040	8.2×10^{-4}
23a	$CH_3O + CH_3O$	$CH_3OH + CH_2O$	3.85×10^{-11}	Ref.[114]		0.071	5.3×10^{-4}
23b	$CH_3O + CH_3O$	$(CH_3O)_2$	3×10^{-12}	Ref.[95]		0.0055	4.9×10^{-4}
24	$CH_3O + OH$	$CH_2O + H_2O$	3×10^{-12}	Ref.[95]		0.033	0.026
25	$CH_3O + O_2$	$CH_2O + HO_2$	$7.82 \times 10^{-14} \exp(-9560/8.31447/T)$	Ref.[115]		0.028	6.8×10^{-4}
26	$CH_3O_2 + CH_3$	$CH_3O + CH_3O$	4.5×10^{-11}	Ref.[116]		0.91	0.015
27	$CH_3O_2 + O$	$CH_3O + O_2$	4.3×10^{-11}	Ref.[117]		0.081	4.4×10^{-4}
28	$CH_3O_2 + H$	$CH_3O + OH$	1.6×10^{-10}	Ref.[95]		0.027	0.0061
29	$CH_3O_2 + HO_2$	$CH_3OOH + O_2$	$3.8 \times 10^{-13} \exp(6650/8.31447/T)$	Ref.[98]		0.044	0.0017
30a	$CH_3O_2 + CH_3O_2$	$CH_3O + CH_3O + O_2$	$7.4 \times 10^{-13} \exp(-4320/8.31447/T)$	Ref.[98]		0.0079	2.7×10^{-4}
30b		$CH_2O + CH_3OH + O_2$	$k_{30b} = k_{30}/(1+25 \exp(-9730/8.31447/T))$ $k_{30} = 1.0 \times 10^{-13} \exp(3030/8.31447/T)$	Ref.[98]		0.015	0.0011
30c		$(CH_3O)_2 + O_2$	3×10^{-14}	Ref.[118]		0.0018	2.5×10^{-4}

Table 4.2 Reaction Mechanism Used to Fit the Experimental Profiles of of the Decay of OH radicals (Continued)

Reaction	Reactants	Products	Rate constant[a)]	Reference	Comment	Relative maximum rate[b)]	Sensitivity, $\delta\ln k_1 / \delta\ln k_i$
31	CH_3O_2 + CH_3O	CH_3OOH + CH_2O	1.82×10^{-11}	Ref.[95]		0.17	0.0027
32	OH + H_2O_2	H_2O + HO_2	2.9×10^{-12} exp(-109/T)	Ref.[81]		2.0×10^{-5}	2.2×10^{-5}
33	HO_2 + NO	OH + NO_2	4×10^{-12} exp(223/T)	Ref.[83]		0.0021	4.11×10^{-4}
34	CH_3 + H_2O_2	CH_4 + HO_2	2×10^{-14} exp(300/T)	Ref.[95]		3.6×10^{-7}	7.3×10^{-6}
35	O + H_2O_2	OH + HO_2	1.4×10^{-12} exp(-16630/8.31447/T)	Ref.[67]		2.7×10^{-9}	2.4×10^{-5}
36a	H + HO_2	H_2 + O_2	7.11×10^{-11} exp(-5900/8.31447/T)	Ref.[119]		2.8×10^{-5}	2.4×10^{-5}
36b		OH + OH	2.81×10^{-10} exp(-3600/8.31447/T)	Ref.[119]		2.7×10^{-4}	8.0×10^{-5}
36c		H_2O + O	5.0×10^{-11} exp(-7200/8.31447/T)	Ref.[119]		1.1×10^{-5}	7.3×10^{-5}
37	OH + O_3	HO_2 + O_2	1.72×10^{-12} exp(-7820/8.31447/T)	Ref.[67]		1.6×10^{-6}	4.8×10^{-6}
38	O + O_3	O_2 + O_2	8.0×10^{-12} exp(-17130/8.31447/T)	Ref.[98]		3.1×10^{-8}	4.8×10^{-5}
39	H + O_3	OH + O_2	1.4×10^{-10} exp(-3990/8.31447/T)	Ref.[118]		2.6×10^{-6}	2.4×10^{-5}
40	HO_2 + O_3	OH + O_2 + O_2	1.97×10^{-16} $(T/298)^{4.57}$ exp(5760/8.31447/T)	Ref.[67]		1.4×10^{-7}	4.4×10^{-5}
41	HO_2 + HO_2	H_2O_2 + O_2	2.2×10^{-13} exp(4990/8.31447/T)	Ref.[67]		0.0045	2.4×10^{-5}
42	CH_3O + HO_2	CH_2O + H_2O_2	5×10^{-13}	Ref.[95]		8.0×10^{-4}	2.0×10^{-6}
43a	CH_3O + O	CH_2O + OH	1×10^{-11}	Ref.[95]		0.0018	0.0014
43b		CH_3 + O_2	2.5×10^{-11}	Ref.[120]		0.0046	7.3×10^{-5}
44	CH_3O + H	CH_2O + H	3.3×10^{-11}	Ref.[121]		1.7×10^{-4}	1.9×10^{-6}
45	CH_2OO+ CH_2OO	CH_2O + CH_2O + O_2	6×10^{-11}	Ref.[122]		1.6×10^{-4}	2.4×10^{-5}
46	CH_2OO + CH_3O_2	Products	6×10^{-11}		Estimated	9.6×10^{-3}	0.0013

[a] Rate constants and concentrations are based on molecule, cm^3, and s.
[b] Maximum reaction rate relative to the maximum (initial) total rate of reaction 1 (1a + 1b), for the experimental conditions at 294 K, 1 bar, $[CH_3]_0 = 9.42 \times 10^{13}$, $[OH]_0 = 1.15 \times 10^{13}$, $[H_2O]_0 = 9.1 \times 10^{16}$, $[O_2]_0 = 1.27 \times 10^{17}$, $[N_2O]_0 = 1.16 \times 10^{16}$, $[(CH_3)_2CO]_0 = 1.9 \times 10^{15}$ molecule cm^{-3} and the photon fluence = 8.11×10^{15} photon cm^{-2} $pulse^{-1}$. (Other conditions are listed in Table 4.1).

In the reaction mechanism, reactions of $O(^1D)$ with precursors produce the initial concentrations of radicals such as OH, NO, O and H whose subsequent reactions were taken into account in the reaction mechanism (reactions 3 – 6 listed in Table 4.2). These reactions of $O(^1D)$ are fast and the time required for these reaction completion is very short, typically ca. 10^{-8} s, compared to the lifetimes of the other transient species. The production of methyl peroxy radicals was the photolysis of acetone in the presence of large concentrations of O_2.

The concentrations of N_2O, H_2O, O_2, which were present in large excess of the transient species (100 - 9000 times), were considered to be constant during the course of the reaction. The transient species in the kinetic modeling were CH_3, OH, CH_3O_2, O, H, HO_2, H_2O_2, O_3, NO, HONO, CH_2, CH_2OO and $(CH_3)_2CO$. The experimental conditions and the results of the measurements are summarized in Table 4.1. Contributions to the initial concentrations of hydroxyl radicals and hydrogen atoms from the photolysis of water were taken into account. The wall loss of hydroxyl radicals on the stainless steel wall was discussed in the previous publications.[39-41] The wall loss of hydroxyl radicals is efficient and is diffusion controlled. This small contribution of the wall loss was also taken into account.

Sensitivity analysis for all reactions in the mechanism listed in Table 4.2 has been carried out. Among the reactions included in the mechanism, some reactions play significant roles, some reactions have only marginal importance, and some are not important at all. If a criterion (the coefficient larger than 0.003) of reaction importance was accepted, total 14 reactions labeled in Table 4.2 (reaction 2, 7, 8a, 9, 10b, 13, 14, 15, 18, 19, 21a, 24, 26 and 28) were selected as important. The most important reaction 8a

(CH_3 + OH, the sensitivity coefficient of 0.15), is well studied. In the case of the representative experimental profile, turning off all unimportant reactions results in the change of the returned rate constant k_1 not exceeding 1.3%. Among all the "important" reactions, assigned errors are of ±20% for the well-studied reactions (reaction 2, 7, 8a, 9, 14 and 21a) and ±50% for the rest of the "important" reactions. The combined error in the target reaction rate constant k_1 of ± 5.0% is then determined assuming statistical independence of their errors.

The average rate constants at different temperatures are listed in Table 4.3. The temperature dependence of k_1 was fitted by expression E4.1 (solid line in Figure 4.3). The error bars are ±1 standard deviation.

$$k_1 = (8.4 \pm 1.7) \times 10^{-11} (T/298\ K)^{-0.81}\ cm^3\ molecule^{-1}\ s^{-1} \qquad (292 - 526\ K). \qquad (E4.1)$$

The previous experimental determinations from the same group (at ambient temperature) are also shown in Figure 4.3. The rate constant measured in this work is a factor of 3.4 lower than the first one reported by Bossolasco et al[25] and about a factor of 2 lower than the next one by Assaf et al.[97]

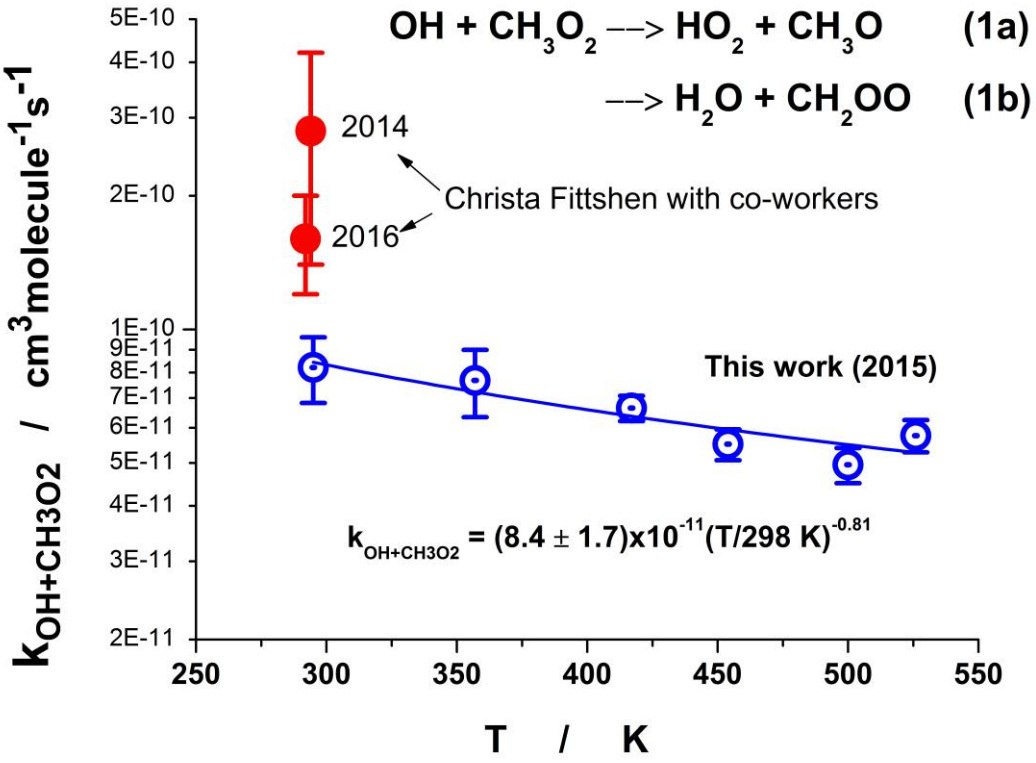

Figure 4.3 Temperature dependence of the rate constant of reaction 1. Open dotted circles – this study, solid line – fit by equation E4.1, $k_1 = (8.4 \pm 1.7)x10^{-11}(T/298\ K)^{-0.81}$. Error bars are ±1 St. Dev. Solid circle – experimental study of Christa Fittshen with co-workers.

Table 4.3 Averaged Rate Constants of Reaction 1. The Errors Indicated are ±1 St. Dev

Temperature / K	k_1 / 10^{-11} $cm^3molecule^{-1}s^{-1}$
292	8.21 ± 1.39
354	7.67 ± 1.33
414	6.64 ± 0.44
454	5.51 ± 0.44
500	4.95 ± 0.45
526	5.76 ± 0.48

In one of the selected models[96] of remote atmosphere, 25 % of the removal rate of CH_3O_2 radicals was evaluated as due to the high rate constant of reaction 1 reported by Bossolasco et al.[25] Therefore, reaction 1 is important in atmospheric chemistry as a potential sink of methyl peroxy radicals. Reduction of the rate constant of reaction 1 ca. 3.4 times (Ref.[25]) or ca. 2 times (Ref.[97]) is expected to similarly reduce the importance of this reaction in the CH_3O_2 removal.

The significant discrepancy was found between the rate constant in this work with the two previous experimental direct measurements at ambient temperature (ca. 3.4 times lower compared with the value in Ref.[25] and ca. 2 times lower compared with the value in Ref.[97]). Several factors which might contribute to the discrepancy are discussed below.

Essentially, both studies reported by Bossolasco et al.[25] and Assaf et al.[97] are not direct but rather relative kinetic studies. The concentrations of methyl peroxy radicals were determined based on the previously measured absorption cross-section of a specific vibrational line in the v_{12}-transition of the $A \leftarrow X$ band at 7489.16 cm^{-1}.[123] In turn, in the previous study where the absorption cross-section of methyl peroxy was assessed, the concentrations of the radicals were established based on the decay lifetimes of the radical, i.e., via the apparent rate constant of self-reaction of methyl peroxy radicals. It should be noted that self-reaction of methyl peroxy radicals is not a simple recombination/disproportionation reaction, but a relatively complex reaction where the initial step has at least two channels, with one of them leading to HO_2 and very reactive CH_3O radicals, and at least three additional radical-radical reactions.

Bossolasco et al.[25] and Assaf et al.[97] employed laser induced fluorescence and cw-cavity ring down spectroscopy coupled to laser photolysis to study reaction 1 at two sets

of the experimental conditions (294 K and 50, 100 Torr) and (295 K and 50 Torr), respectively. The photolysis beam and the monitoring beam were crossing at a small angle. Therefore, the intensity distribution in the cross-section of the photolysis beam is directly transferred to the intensity distribution along the monitoring beam. Out of beam diffusion was factored out from the reaction kinetic – the approach valid only for the first order reactions. Although purely second order reactions are known to be stable with respect to some radical field inhomogeneity, the impact of the intensity inhomogeneity as well as the extent of the inhomogeneity on the kinetics of a reaction consisting of bimolecular reactions superimposed on the out-of-beam diffusion were not assessed.

In these studies[25;97] all these processes were lump summed into a single second order term. However, the self-reaction of methyl peroxy radicals is a complex process, consisting of the initial bimolecular step with subsequent secondary reactions of methoxy radicals and hydroperoxy radicals. Diffusion losses were approximated by the first order decay, which is not a justifiable approximation. These approximations resulted in a kinetic equation consisting of a second order (lump sum of the self-reaction of methyl peroxy radicals) and a first order term (approximation of the out of beam diffusion). The equation has exact solution; however, further approximations of unknown nature have been involved in the derivation of the final equation (Eq. 3 of Ref.[96]) which was used in the data processing.

In addition, CH_3I was used as a source of methyl radicals in the study.[25] Photolysis of this species leads to copious production of spin-orbital excited $I(^2P_{1/2})$ atoms. Possible impact of the further reactions and relaxation of these atoms was not assessed. Finally, the cross-section of CH_3O_2 reported in Ref.[96] is ca. 3 times larger than

in the previous determinations as indicated in Ref.[96] Assuming the previous determinations of the cross-sections as correct will bring the results of the study[25] close to our determination.

4.3.2 Branching Ratios

Two channels are considered important in the theoretical study by Bian et al.[26] Channel 1a is the dominant channel while channel 1b is a minor channel. An attempt was made to evaluate the branching ratio of channel 1b, α_{1b} at ambient temperature and pressure. Criegee intermediates (CH_2OO) might be produced through channel 1b. The ultraviolet absorption spectrum of the Criegee intermediates (CH_2OO) was studied several times by different groups.[6;100;124] The upper limit for the branching ratio of channel 1b was determined using the lowest value of peak absorption cross-sections among these studies. The lowest and the most recent determination of the absorption peak cross-section is 1.23×10^{-17} cm^2 $molecule^{-1}$ at 340 nm.[6] The simulations were provided using the reaction mechanism (Table 4.2) and the branching ratio α_{1b} was varied over the range 0.01 – 0.2. The branching ratio was determined through comparing the observed experimental transient absorption profiles at 340 nm with the simulations. One potential importance of CH_2OO consumption pathway (the reaction of CH_2OO with CH_3O_2) was added into the reaction mechanism. Since there is no rate data for this reaction, a reasonable estimate for the rate constant of this reaction $6x10^{-11}$ cm^3 $molecule^{-1}$ s^{-1} was chosen. Self-reaction of CH_2OO also plays some role in the CH_2OO removal. The rate constant of the self-reaction is 6×10^{-11} $cm^3molecule^{-1}s^{-1}$.[122] The comparison of the experimental absorption trace with the modeling is shown in Figure 4.4.

The upper limit of the branching ratio of the channel leading to Criegee intermediate (channel 1b) is less than 5% at ambient temperature. This result is consistent with the theoretical study.[26] Although no assessment of the rate constants or the branching ratios was made in this theoretical study, the branching ratio for channel 1b was estimated assuming equal A-factors for channels 1a and 1b and the relatively high activation barrier of channel 1b of ca. 30 kJ mol^{-1}. The experimentally determined branching ratio for channel 1b is ca. 10^{-5} at ambient temperature.

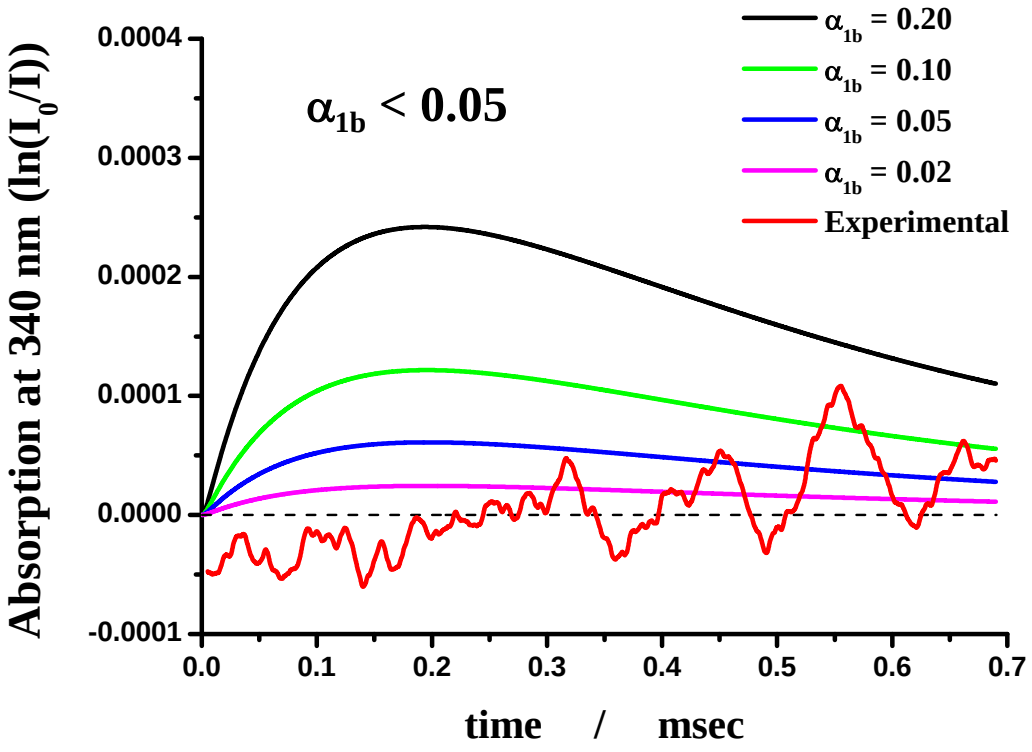

Figure 4.4. Comparison of the experimentally observed absorption profile at 340 nm with the simulated by the mechanism with different branching ratios of channel 1b. Red line – experimental profile; black line – simulation with α_{1b} = 0.20; green line – simulation with α_{1b} = 0.10; blue line – simulation with α_{1b} = 0.05; magenta line – simulation with α_{1b} = 0.02.

The most recent theoretical study is published by Muller et al.[27] The Criegee pathway (channel 1b) is negligible in the atmospheric conditions which is consistent with our result. Channel 1a is expected to dominate, and both methanol formation (channel 1c) and stabilization of the TRIOX are minor channels:

$$CH_3O_2 + OH \rightarrow TRIOX \qquad (1e)$$

The branching ratios were reported at 298 K temperature and 1 atm pressure (α_{1a} = 0.82, α_{1c} = 0.069 and α_{1e} = 0.107). Channel 1e (formation of TRIOX) is pressure dependent and becomes more important at higher pressures, whereas channel 1c becomes less important. An attempt was made to evaluate the branching ratio of channel 1e, α_{1e}, over the 1 – 100 bar pressure range and ambient temperature. The ultraviolet absorption spectrum of the TRIOX (stabilized in channel 1e) was not available in UV range at wavelength above 200 nm (the limited range of current experimental set-up). Therefore, transient absorption profiles of HO_2 (formed in channel 1a) were used to study the branching ratio of 1e, assuming that only channel 1e and channel 1a are important over the 1 – 100 bar pressure range at ambient temperature.

Transient absorption profiles were measured at wavelength 210 nm and 224 nm (mainly from the absorption of CH_3O_2 and HO_2) over the 1 - 100 bar pressure range at ambient temperature. Sample transient absorption profiles at wavelength 210 nm and 224 nm are shown in Figure 4.5 and Figure 4.6.

In the beginning of these experiments, transient profiles were recorded at 224 nm. The absorption cross-sections of CH_3O_2 and HO_2 at 224 nm are $\sigma_{CH3O2,\ 224nm} = 3.67 \times 10^{-18}$

$cm^2molecule^{-1}$ and $\sigma_{HO2,\ 224nm} = 2.99\times10^{-18}$ $cm^2molecule^{-1}$, respectively. The ratio of these two absorption cross sections (σ_{HO2} / σ_{CH3O2}) at 224 nm is 0.81. In order to improve the relative contribution of HO_2 radicals in the absorption, a larger ratio of σ_{HO2} / σ_{CH3O2} is desirable. A shorter monitoring wavelength (210 nm) was used for this purpose. In the current arrangement, there is a sharp drop in the light intensity at wavelength shorter than 210 nm. The light intensity at 208 nm drops more than a factor of 3 compared with the light intensity at 210 nm. The absorption cross-sections of CH_3O_2 and HO_2 at wavelength 210 nm are $\sigma_{CH3O2,\ 210nm} = 2.19\times10^{-18}$ $cm^2molecule^{-1}$ and $\sigma_{HO2,\ 224nm} = 4.15\times10^{-18}$ $cm^2molecule^{-1}$, respectively. The ratio of these two absorption cross sections (σ_{HO2} / σ_{CH3O2}) at 210 nm is 1.89.

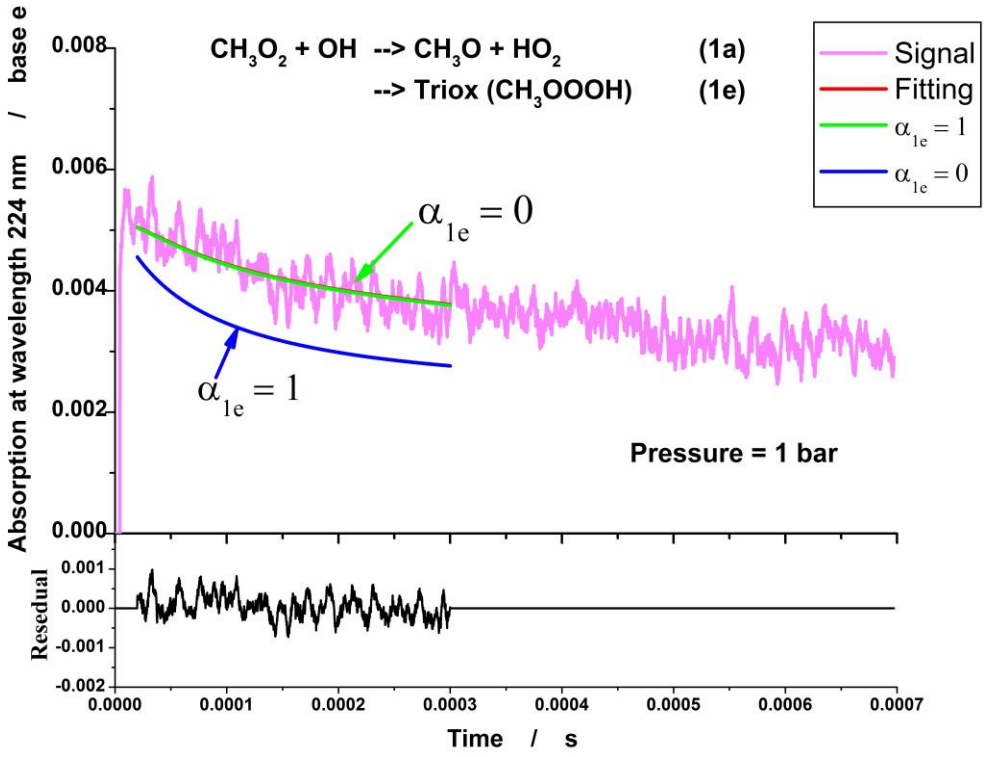

Figure 4.5 Temporal absorption profiles at 224 nm at ambient temperature and 1 bar pressure. [Acetone]=4.82×10^{15} molecules cm^{-3}. [N_2O]=4.29×10^{17} molecules cm^{-3}. [H2O]=3.11×10^{17} molecules cm^{-3}. [O_2]=1.18×10^{17} molecules cm^{-3}. Photon Fluence=6.6×10^{15} photons cm^{-2}. Red line: fitted by the reaction mechanism result as α_{1e} = 0.01 at 1 bar and 296 K. Green line: simulation with α_{1e} = 0. Blue line: simulation with α_{1e} = 1. The residual is shown for the black trace.

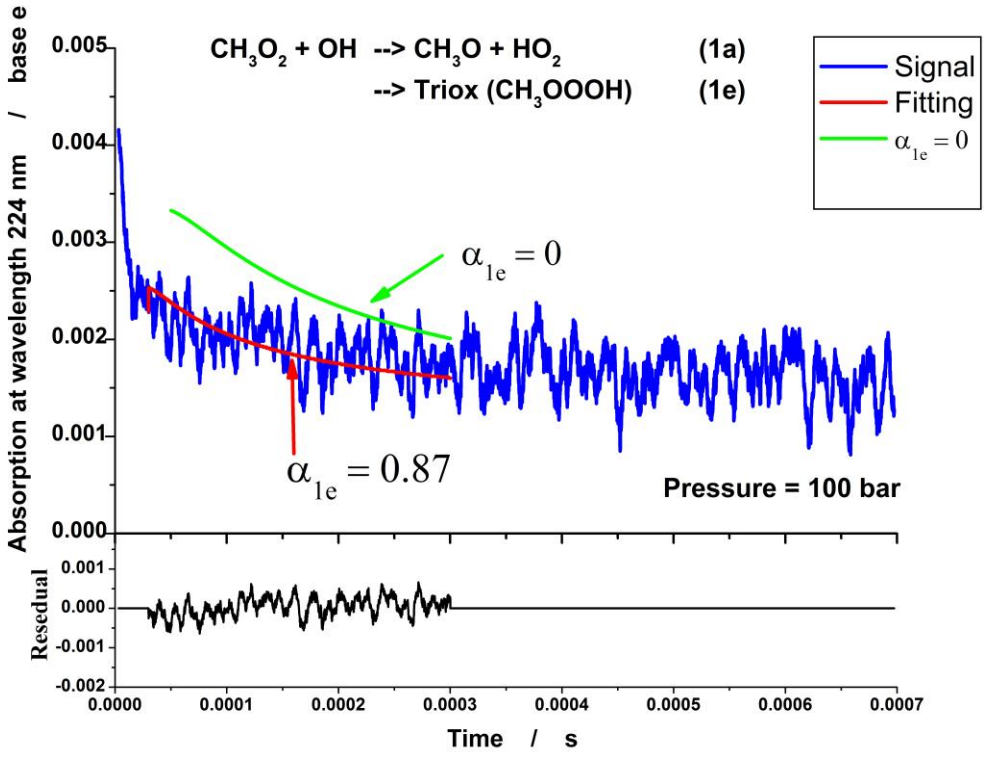

Figure 4.6 Temporal absorption profiles at 210 nm at ambient temperature and 100.2 bar pressure. [Acetone]=1.03×10^{15} molecules cm^{-3}. [N_2O]=1.52×10^{17} molecules cm^{-3}. [H_2O]=4.06×10^{17} molecules cm^{-3}. [O_2]=8.82×10^{16} molecules cm^{-3}. Photon Fluence=1.15×10^{16} photons cm^{-2}. Red line: fitted by the reaction mechanism result as α_{1e} = 0.87 at 100.2 bar and 296 K. Green line: simulation with α_{1a} = 1. The residual is shown for the black trace.

The branching ratio of the channel leading to TRIOX stabilization (channel 1e) is pressure dependent. The experimental conditions as well as the branching ratios are listed in Table 4.4 and shown in Figure 4.7. This is the first determination of the branching ratios of channel 1e (formation of TRIOX) over the pressure range 1 – 100 bar at ambient temperature. The yield of TRIOX at ambient conditions is consistent with the theoretical study.[27]

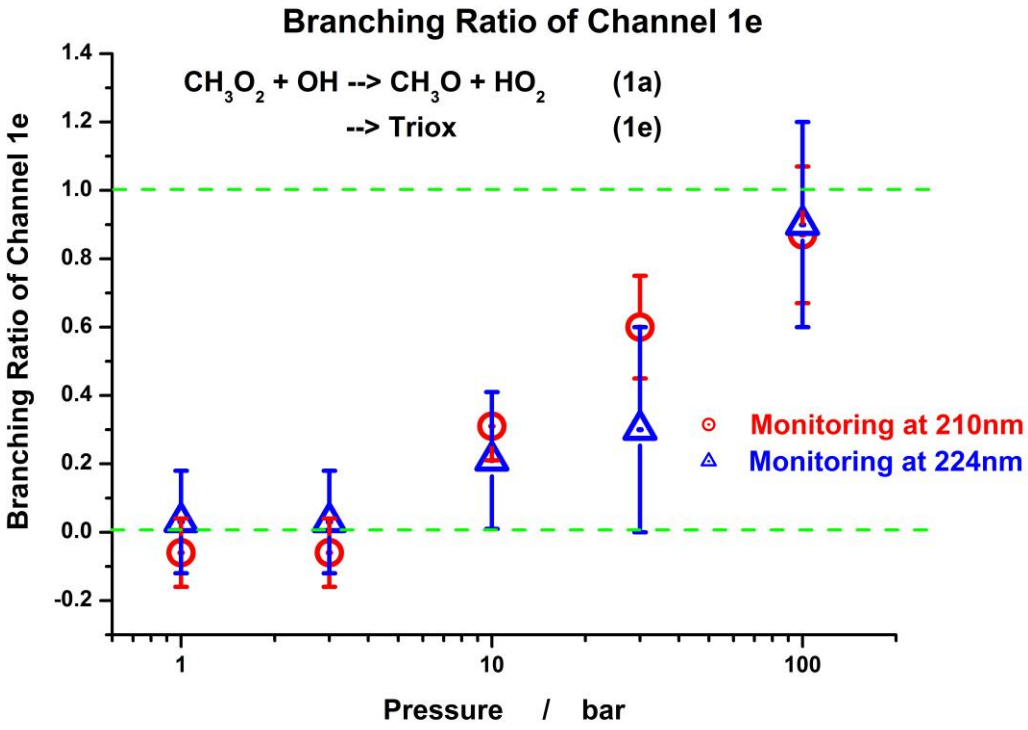

Figure 4.7 The branching ratios of channel 1e over the 1 – 100 bar pressure and ambient temperature. Red – the branching ratios were determined at wavelength 210 nm. Blue – the branching ratios were determined at wavelength 224 nm.

Table 4.4 Experimental Conditions and the Branching Ratio of Channel 1e of Reaction 1 at Pressures 1 – 100 bar and 296 K

Pressure/ bar	Temperature/K	Wavelength/nm	Acetone/10^{15} molecule cm^{-3}	$H_2O/10^{17}$ molecule cm^{-3}	$N_2O/10^{17}$ molecule cm^{-3}	$O_2/10^{16}$ molecule cm^{-3}	PhotoFluence / 10^{15} photons cm^{-2}	HO_2 Yield	Branching ratio of channel 1e
1	296	224	4.82	3.11	4.29	11.8	6.6	1.00 ±0.15	0 ±0.15
3	296	224	3.63	4.56	3.94	17.8	9.5	1.00 ±0.15	0 ±0.15
10	296	224	7.09	4.61	2.84	6.59	2.3	0.79 ±0.2	0.21 ±0.2
30	296	224	1.00	3.97	1.49	8.18	10.3	0.70 ±0.3	0.30 ±0.3
100	296	224	1.03	4.09	1.53	8.44	10.4	0.10 ±0.3	0.90 ±0.3
1	296	210	0.90	3.56	1.36	5.90	8.2	1.06 ±0.1	-0.06 ±0.1
3	296	210	0.95	3.23	0.74	7.36	12.5	1.06 ±0.1	-0.06 ±0.1
10	296	210	0.94	3.71	0.84	8.44	12.7	0.69 ±0.1	0.31 ±0.1
30	296	210	0.93	3.69	0.81	8.06	11.5	0.40 ±0.15	0.60 ±0.15
100	296	210	1.03	4.06	0.88	8.82	12.5	0.13 ±0.2	0.87 ±0.2

4.4 Conclusions

The rate constant of the reaction of OH with CH_3O_2 has been measured over the temperature range 292 – 526 K at ambient pressure. The absolute concentrations of CH_3O_2 and OH radicals were determined using UV absorption spectroscopy as well as *in situ* actinometry. Current study does not confirm the anomalously high value of the rate constant of reaction 1 reported in Ref.[25] and Ref.[97] The measured rate constant at 298 K is lower than the only literature values by a factor of 3.4 and 2, respectively. The branching channel 1b leading to the Criegee intermediate CH_2OO does not exceed 5% at 298 K in accord with the calculations.[26] The branching ratios of channel 1e (TRIOX stabilization) were measured over the pressure range of 1 – 100 bar at ambient temperature.

CHAPTER 5

$CH_3 + Cl \rightarrow CH_3Cl$

5.1 Introduction

Chlorine atom (Cl) has been explored as key intermediate species in the troposphere.[28-32] In the stratosphere, it is responsible for ozone depletion through a chlorine catalytic cycle:

CFC	+	hν (<220 nm)	→	Cl	+	CFC(minus one Cl)	(E5.1)
Cl	+	O_3	→	ClO	+	O_2	(E5.2)
ClO	+	O	→	Cl	+	O_2	(E5.3)

where short wavelength solar UV radiation is available to produce Cl atoms from dissociation of stable species such as chlorofluorocarbon (CFC) compounds.[30;125] The Cl atom produced in the reaction shown in E5.1 destroys O_3 as shown in E5.2 with the formation of the free radical chlorine oxide ClO. The active free radical, ClO, can release Cl atom through the reaction shown in E5.3 which accelerates this chlorine catalytic cycle.

The reactive Cl atom can be quickly removed by the reaction with methane CH_4:[30]

Cl	+	CH_4	→	HCl	+	CH_3	(E5.4)

Methane (CH_4) is an important species in the atmosphere, its concentration can be as high as few parts per million (ppm).[33] In the remote stratosphere, the major pathway of Cl atom removal is through the reaction shown in E5.4.[7] Methyl radicals (CH_3) formed in the reaction (E5.4) might provide an essential additional pathway to consume chlorine atoms via reaction 1 with a large rate constant.[34]

$$CH_3 + Cl \rightarrow CH_3Cl \qquad (1)$$

In addition, reaction 1 is very important in the laboratory kinetics studies based on the decay of CH_3 radicals. Especially many kinetics studies are initialized by Cl atom reactions.[35-37] For instance, in the kinetics study of the reaction CH_3 radicals with HO_2 radicals, the formation of HO_2 radicals is initialized by large amount of Cl atoms. The reaction of CH_3 radicals with Cl atoms significantly contribute to the total decay of CH_3 radicals. Therefore, the kinetics study of the reaction of CH_3 radicals with Cl atoms is important.

In the most recent direct experimental and computational study of reaction 1, Parker et al.[126] employed the discharge flow – mass spectrometry technique. The rate constant was measured over the temperature range of 202 - 298 K at 0.3 – 2.0 Torr in helium as buffer gas. The reported pressure dependent rate constants are smaller than 1.8×10^{-11} cm^3 $molecule^{-1}$ s^{-1} over this pressure range. The high-pressure limit rate constant based on the RRKM calculations is 6×10^{-11} cm^3 $molecule^{-1}$ s^{-1}.[126]

Timonen et al.[127] used discharge flash lamp photolysis of chlorine molecules at the maximum wavelength of 330 nm to generate Cl atoms, with the time-resolved

measurement by UV absorption of CH_3 radicals at 216.36 nm wavelength. The final products are measured by a gas chromatograph. The rate constant was measured over the temperature range of 298 – 423 K and 40 – 360 Torr pressure range in CO_2 as buffer gas. They reported the high-pressure limit rate constant $k_1 = (2.56 \pm 0.24) \times 10^{-10}$ cm^3 $molecule^{-1}$ s^{-1}. and zero activation energy was reported. The rate constants of reaction 1 were calculated based on either the decay of methyl radical or the final products. The mechanism was built based on literature values. The rate constants of three reactions (CH_3+Cl_2, CH_3+Cl and Cl+Cl) were calculated simultaneously through fitting with the methyl decay and final products concentrations. However, this combination of time-resolved measurements of CH_3 radicals and measurements of stable final products bring uncertainty which is hard to assess. Very large rate constant was reported compared with the later publication by Parker et al.[126]

In this work, reaction 1 was studied at near the high pressure limit conditions. The measurements were performed over the temperature range 292 – 558 K and extended pressure range 1 - 100 bar. Despite some available experimental results at low pressure and one high pressure limit value from theoretical study of reaction 1, there are still remaining uncertainty of the reaction parameters over extend pressure and elevated temperature ranges, such as the high-pressure limit rate constants, the pressure falloff central pressure p_c and the broadening factor F_c. These reasons were the motivation for the current study.

5.2 Experimental Approach

The technique of the excimer laser pulsed photolysis coupled to UV-Vis transient

absorption spectroscopy was used for this work. The "new" high-pressure heatable reactor and the high-pressure flow system are shown in Figure 2.1. The detailed experimental arrangements and signal accumulation are described in Chapter 2. Helium was used as the buffer gas in all measurements. The experiments were performed over the 19 – 285 °C (292 – 558 K) temperature range and extended pressure range (1 - 100) bar.

The gas flow rates were controlled by several high-pressure mass flow controllers (Brooks, model 5850). The total flow rates of the reactants mixtures and helium bath gas were in the range 420 - 3000 sccm. Fresh reactants gas mixtures were prepared in high-pressure vessels right before the kinetic measurement. Additional flush flows to the reactor were in the range 270 – 600 sccm.

The concentrations of the precursors used: $(0.88 – 6.05)\times10^{15}$ molecule cm^{-3} for $(COCl)_2$ and $(0.51 – 2.36)\times10^{15}$ for acetone. The laser photon fluence inside the reactor were varied in the range $(3.6 – 10.3)\times10^{15}$ photon cm^{-2} $pulse^{-1}$. The initial concentrations of radicals were in the range $(2.60 – 16.75)\times10^{13}$ molecule cm^{-3} for CH_3 radicals and $(2.32 – 29.04)\times10^{13}$ for Cl atoms. No noticeable depletion of the radical precursors (acetone and oxalyl chloride) was observed at and below 558 K. At higher temperatures, depletion of the precursors was observed. The detail of thermal stability of precursor was discussed in Chapter 2. The repetition rate of the photolysis laser was set to (0.1 – 1) Hz to ensure complete replacement of the gas mixture in the reactor between the pulses.

Cl Atom Generation. In the initial experiments, Cl atoms were produced directly by photolysis of methyl chloride CH_3Cl at 193.3 nm (ArF excimer laser). In the wavelength range 180 – 216 nm the photolysis occurs with unit quantum efficiency by

breaking the C-Cl bond to yield CH_3 + Cl:[128]

$$CH_3Cl + h\nu(193.3\ nm) \rightarrow CH_3 + Cl \quad (E5.5)$$

equal amount of CH_3 radials and Cl atoms were formed simultaneously. However, it was found that this photolysis system is not well suited for kinetic study of the reaction of CH_3 with Cl. The absorption cross section of CH_3Cl molecules at 193.3 nm is relatively small, about 7×10^{-20} cm^2 $molecule^{-1}$, therefore high concentrations of CH_3Cl molecules are required to provide sufficient concentrations of the free radicals. Even through that the rate constant of the reaction of CH_3Cl with Cl is more than 100 times slower compared with the rate constant of reaction 1, reaction of chlorine atoms with CH_3Cl molecules dominate the consumption of Cl atoms.

Therefore, oxalyl chloride $(COCl)_2$ was used to produce Cl atoms by photo dissociation at 193.3 nm (ArF excimer laser).

$$(COCl)_2 + h\nu(193.3\ nm) \rightarrow 2\ Cl + 2\ CO \quad (E5.6)$$

Oxalyl chloride $(COCl)_2$ has been characterized as a clean photolytic source of chlorine atoms for kinetics studies. The UV absorption spectrum of oxalyl chloride as well as the quantum yield of chlorine atoms resulting from photodissociation of oxalyl chloride at 193 nm have been well characterized in helium as a bath gas at pressures 1, 10 and 100 bar.[51] The quantum yield of chlorine atoms (the number of Cl atom formed per one dissociated oxalyl chloride molecule) is independent of helium pressure over the

pressure range 1 – 100 bar. The quantum yields of chlorine atoms at 298 K are 2.01 ± 0.08 and 1.97 ± 0.12 at 10 bar and 100 bar, respectively.

CH_3 Radical Generation and Monitoring. Methyl radicals were generated in pulse photolysis of acetone at 193.3 nm wavelength (ArF excimer laser). The kinetics of methyl radical decay was monitored by absorption in the UV (multiline at 216.36 nm). A xenon arc lamp was employed. The imaging spectrograph (Acton 300i) was equipped with a PMT (Hamamatsu R106) with a preamplifier (EMI) as a detector. The PMT signal was preamplified (EMI preamplifier), digitized, and stored using a digital storage oscilloscope (LeCroy 9310A 9310A, Dual channel, 400 MHz, 100 Msamples/s, 50 Kpts/ch). The time resolution is determined by the preamplifier setting. Typically, 0.3 μs time constant was used (the measured actual rise time $t_{0.1–0.9}$ was 0.46 μs). The traces were accumulated (500−5000 pulses) and transferred to a PC for processing.

***In Situ* Actinometry**. The absolute concentrations of methyl radicals and chlorine atoms were determined on the basis of the photon flux inside the reactor, the absorption cross-section of the precursors (acetone and oxalyl chloride), and the quantum yield in the photolysis processes. The photon flux was determined using the *in situ* actinometry based on the measurements of the ozone formed in the photolysis of $N_2O/O_2/N_2$ mixtures. Details of this technique as well as the accounting for the laser energy drift in the course of measurements are described in Chapter 2.

The Absorption Cross Sections. The absorption cross section of oxalyl chloride at 193.3 nm was measured as a function of temperature. The pure oxalyl chloride liquid was degassed using freeze – pump – thaw cycles before the gas mixture preparation. Oxalyl chloride was diluted by helium and mixed in the high pressure vessel. A modified

atomic absorption (AA) spectrophotometer (Perkin-Elmer model 2380) was installed at downstream of the reactor. The AA spectrophotometer was used to determine *in situ* the oxalyl chloride concentration via absorption at 193.6 nm. The gas from the exit of the reactor was transferred to the AA spectrophotometer using a Teflon tubing. The AA spectrophotometer was used as a UV absorption spectrometer with the As hollow cathode lamp (element As, current 18 mA – 20 mA) as the light source. The burner on the AA spectroscopy was removed and replaced by a flow cell. The flow cell was made of 25.4 mm O.D. (1 in.) and 16.4 cm long quartz tubing. The intensity of the light passed through the cell was measured with and without the oxalyl chloride gas mixture entering the AA spectrophotometer. This was done to ensure that no decomposition of $(COCl)_2$ in the flow reactor when the reaction occurs.

Light from an ArF excimer laser (GAM Laser) at 193.3 nm was used to measure the absorption of oxalyl chloride. The absorption cross-sections were calculated from the spectra measured in the presence and in the absence of oxalyl chloride in the reactor (Figure 5.1 and Table 5.1).

The absorption cross section of acetone as a function of temperature and pressure was studied by Sangwan et al.[40]

Table 5.1 Absorption Cross-Sections of Oxalyl Chloride ($\sigma_{193.3}$(oxalyl chloride) / $1x10^{-18}$ $cm^2molecule^{-1}$) at 193.3 nm at Different Temperatures and Ambient Pressure, Measured Using Laser Light at 193.3 nm. Errors are One Standard Deviation

T / K	292	357	417	500	558
P / bar					
1.01	3.83 ± 0.04	4.43 ± 0.05	4.46 ± 0.03	4.60 ± 0.07	4.89 ± 0.07

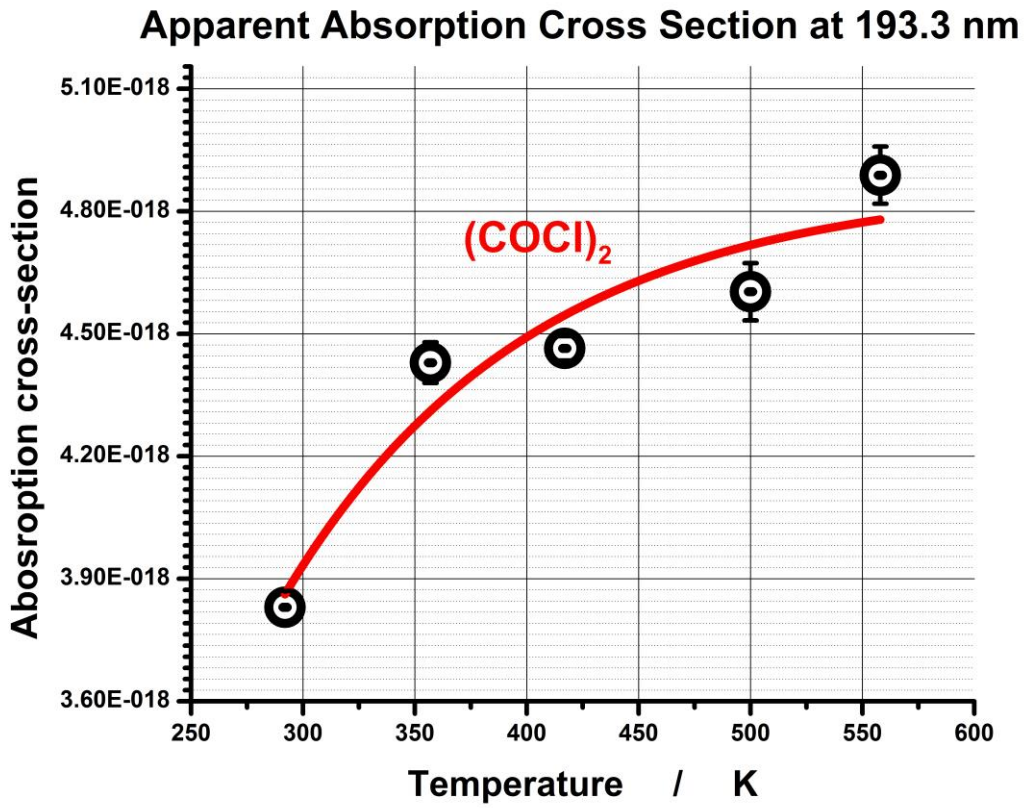

Figure 5.1 Absorption cross-sections of oxalyl chloride at 193.3 nm as a function of temperature at ambient pressure.

The kinetics of methyl radicals (CH_3) were monitored by the absorption in the UV at wavelength 216.36 nm (Chapter 2). Compared to the CH_3 radicals concentrations, the oxalyl chloride concentrations were much higher (~10 – 100 times). Therefore, the spectrum interference of oxalyl chloride depletion could not be neglected. The absorption cross-sections of oxalyl chloride were measured as a function of temperature at 216.36 nm. Light from the xenon arc lamp (150 W Oriel) was used to measure the absorbance. The measured absorption cross-sections are listed in the Table 5.2 and Figure 5.2.

Table 5.2 Absorption Cross-Sections of Oxalyl Chloride ($\sigma_{216.36}$(oxalyl chloride) / $1x10^{-18}$ $cm^2molecule^{-1}$) at 216.36 nm at Different Temperatures and Ambient Pressure, Measured Using Light at 216.36 nm. Errors are One Standard Deviation

T / K	292	357	417	500	558
P / bar					
1.01	1.30 ±0.31	1.21 ±0.20	1.18 ±0.30	1.15 ±0.40	1.04 ±0.27

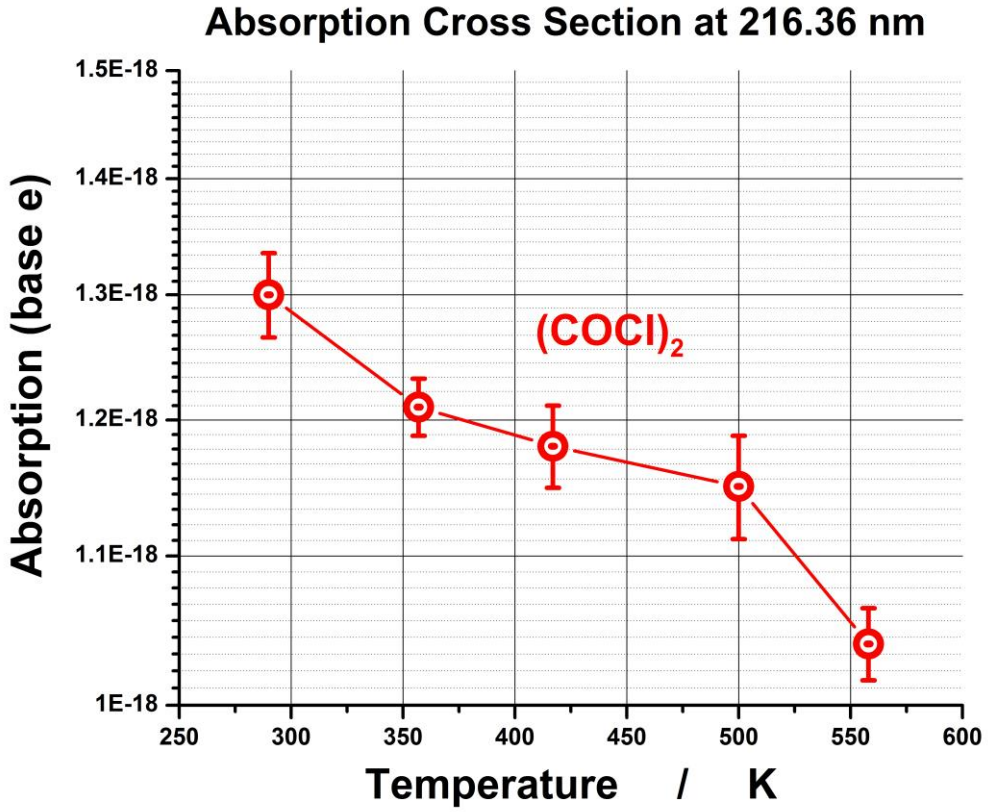

Figure 5.2 Absorption cross-sections of oxalyl chloride at 216.36 nm as a function of temperature at ambient pressure.

Reagents. In the experiments BIP®Helium from Airgas with 99.9999% purity with reduced oxygen content (<10 ppb) was used. Certified mixture of N_2O in He (mole fraction of 0.025, the accuracy ±2%) obtained from AirGas, was used for *in situ*

actinometry. Liquid reactants such as CH_3Cl (Sigma-Aldrich, >99.5%), acetone (Fisher Scientific 99.7%) and oxalyl chloride (Sigma-Aldrich, >99%) were degassed through three freeze-pump-thaw cycles. Reactant CH_3Cl were supplied either in liquid phase by the syringe pump (Harvard Apparatus PHD4400) at high pressure (10, 30 and 100 bar) or in gas phase at low pressure (1, 3 bar) Gas mixtures acetone/He and oxalyl chloride/He were prepared before the experiments in the high pressure vessels.

5.3 Results and Discussion

Transient absorption profiles of CH_3 radicals were measured at 25 combinations of temperature and pressure. Examples of measured temporal profiles of absorption at 216.36 nm are shown in Figure 5.3. To determine the rate constant of reaction 1, a reaction mechanism described below (Table 5.3) was used to model and fit the experimental profiles. The absorption profiles were fitted by a numerical solution of a system of differential equations corresponding to the reaction mechanism using MicroMath SCIENTST software.

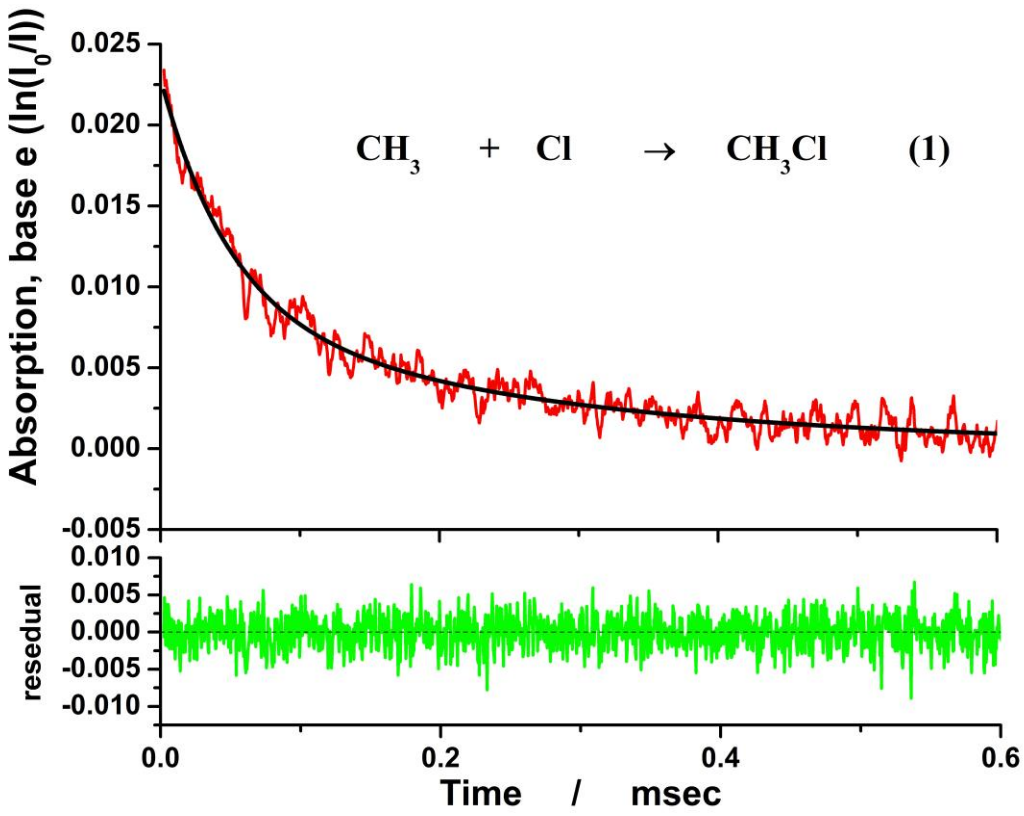

Figure 5.3 Sample temporal profiles at 216.36 nm (red trace, mainly CH_3). Solid line: fit by the reaction mechanism (see text). The residual (green trace) is shown for the 30.2 bar curve. Conditions: $[(CH_3)_2CO] = 1.74\times10^{15}$ and $[(COCl)_2] = 1.71\times10^{15}$ molecule cm^{-3}, laser fluences 7.01×10^{15} photon cm^{-2}.

Table 5.3 Reaction Mechanism Used to Simulate and Fit the Experimental Profiles

Reaction	Reactants	Products	Rate constant[a)]	Reference	Comment	Relative maximum rate[b)]	Sensitivity, $\delta\ln k_1 / \delta\ln k_j$
1a	$CH_3 + Cl$	CH_3Cl	to be determined				
1b		$HCl + CH_2$	Neglected	Ref.[129]			
2	$CH_3 + CH_3$	C_2H_6	$5.66 \times 10^{-11}(T/298)^{-0.37}$	Ref.[22]		0.13	0.16
3	$Cl + Cl$	Cl_2	[He] 4.69×10^{-33}	Ref.[130]		0.0052	0.0014
4	$CH_3Cl + Cl$	$CH_2Cl + HCl$	$1.7 \times 10^{-11}\exp(-8647/8.31447/T)$	Ref.[131]		0.0032	0.0014
5	$C_2H_6 + Cl$	$C_2H_5 + HCl$	$8.3 \times 10^{-11}\exp(-830/8.31447/T)$	Ref.[98]		0.037	0.0065
6	$CH_3 + Cl_2$	$CH_3Cl + Cl$	2.93×10^{-13} (T/298)^1.45exp (-350/8.31447/T)	Ref.[132]		8.7×10^{-7}	1.9×10^{-5}
7	$CO + Cl$	$COCl$	[He]1.33×10^{-33}	Ref.[98]		0.0015	1.7×10^{-4}
8	$COCl$	$CO + Cl$	$4.1 \times 10^{-13}\exp(-24610/8.31447/T)$	Ref.[98]		6.8×10^{-9}	5.8×10^{-5}
9	$COCl + Cl$	$CO + Cl_2$	$2.16 \times 10^{-9}\exp(-13891/8.31447/T)$	Ref.[133]		0.00069	3.8×10^{-5}
10a	$C_2H_5 + Cl$	$C_2H_4 + HCl$	3.01×10^{-10}	Ref.[134]		0.014	7.8×10^{-5}
10b		C_2H_5Cl	4.55×10^{-10}	Ref.[127]		0.020	1.3×10^{-4}
11	$C_2H_5 + CH_3$	C_3H_8	5.6×10^{-11}	Ref.[104]		0.00010	6.1×10^{-4}
12	$(COCl)_2 + CH_3$	products	$<1.67 \times 10^{-13}$	Studied in this work	The upper limit of reaction 12 was mesured at 296 K and 558 K separately.	0.025	0.025
13	$(CH_3)_2CO + Cl$	$CH_3COCH_2 + HCl$	$1.53 \times 10^{-11}\exp(-4940/8.31447/T)$	Ref.[135]		0.48	3.4×10^{-5}

[a)] Rate constants and concentrations are based on molecule, cm^3, and s.

[b)] Maximum reaction rate relative to the maximum (initial) total rate of reaction 1 (1a+1b), for the experimental conditions at 294 K, 1 bar, $[CH_3]_0 = 6.05 \times 10^{13}$, $[Cl]_0 = 2.90 \times 10^{14}$, $[(COCl)_2]_0 = 5.34 \times 10^{15}$, $[(CH_3)_2CO]_0 = 1.44 \times 10^{15}$ molecule cm^{-3} and the photon fluence = 7.46×10^{15} photon cm^{-2} $pulse^{-1}$. (Other conditions are listed in Table 5.4).

The UV absorption cross sections were either measured in the current work (e.g. absorption of $(COCl)_2$) or were taken from the literature. The reaction mechanism as well

as the kinetic parameters used in the model are listed in table 5.3. The initial radicals such as Cl, CH_3 and H were produced in photodissociation of precursors. Subsequent reactions were taken into account in the reaction mechanism. The initial concentrations of these species were calculated on the basis of the photon fluence, absorption cross sections and quantum yields of the initial photolysis processes. The rate constants listed in the reaction mechanism were taken from the literature. The transient species in the kinetics model were CH_3, Cl, C_2H_5, C_2H_6, CO, COCl and CH_3Cl. The concentrations of $(COCl)_2$ and $(CH_3)_2CO$ which were present in large excess of the transient species (10 - 50 times), were considered to be constant during the course of the reaction. The rate constants of reaction 1 were obtained from the fits of the absorption profiles at 216.36 nm (mainly CH_3 radicals). The experimental conditions and the results of the measurements are summarized in Table 5.4.

Table 5.4 Experimental Conditions and the Rate Constants of Reaction 1 at Pressure 1 – 100 bar and 296 – 558 K Temperature Range

T / K	P / bar	$[(CH_3)_2CO]$ / 10^{15} molecule cm^{-3}	$[(COCl)_2]$ / 10^{15} molecule cm^{-3}	Photonfluence / 10^{15} photon cm^{-2} $pulse^{-1}$	Number density /10^{19} molecule cm^{-3}	$[Cl]_0$ / 10^{13} molecule cm^{-3}	$[CH_3]_0$ / 10^{13} molecule cm^{-3}	k_1 / 10^{-11} cm^3molecule$^{-1}s^{-1}$
296	1.02	1.74	1.64	6.77	2.49	9.20	7.29	9.02
296	1.02	1.63	3.03	7.46	2.49	16.38	7.30	8.85
296	1.02	1.44	5.34	7.38	2.49	28.96	6.47	7.51
296	1.01	1.74	1.71	8.03	2.47	10.10	8.45	7.26
296	1.01	1.60	3.14	8.01	2.47	17.59	7.43	5.90
296	1.01	1.44	5.53	7.39	2.47	30.37	6.55	7.07
292	1.02	1.90	1.97	4.02	2.53	6.24	4.51	9.40
292	1.02	1.79	3.64	3.99	2.53	10.01	4.08	6.94
292	1.02	0.98	2.01	7.16	2.53	9.58	3.85	7.79
292	1.02	0.91	3.66	7.09	2.53	16.26	3.33	7.77
292	1.02	0.80	6.34	7.02	2.53	25.26	2.62	8.50

Table 5.4 Experimental Conditions and the Rate Constants of Reaction 1 at Pressure 1 – 100 bar and 296 – 558 K Temperature Range (Continued)

T / K	P / bar	$[(CH_3)_2CO]$ / 10^{15} molecule cm^{-3}	$[(COCl)_2]$ / 10^{15} molecule cm^{-3}	Photonfluence / 10^{15} photon cm^{-2} $pulse^{-1}$	Number density /10^{19} molecule cm^{-3}	$[Cl]_0$ / 10^{13} molecule cm^{-3}	$[CH_3]_0$ / 10^{13} molecule cm^{-3}	k_1 / 10^{-11} cm^3molecule$^{-1}s^{-1}$
354	1.01	0.80	1.65	6.41	2.07	8.23	3.48	6.30
354	1.01	0.74	3.00	6.22	2.07	13.70	2.97	6.43
354	1.01	0.65	5.20	6.03	2.07	21.05	2.30	6.53
354	1.01	1.28	5.05	5.84	2.07	19.43	4.30	5.81
414	1.01	1.43	1.50	5.60	1.77	6.70	5.96	4.60
414	1.01	1.25	2.59	5.47	1.77	11.09	5.00	4.37
414	1.01	1.10	4.44	5.35	1.77	17.60	4.07	4.59
500	1.01	1.06	2.16	5.45	1.46	9.52	4.70	3.59
500	1.01	0.92	3.70	5.32	1.46	14.90	3.73	3.59
500	1.01	0.75	6.05	5.18	1.46	21.4	2.67	4.39
558	1.02	1.52	3.12	5.38	1.32	18.6	9.60	3.35
558	1.02	1.22	5.06	5.27	1.32	26.05	6.63	2.84
558	1.02	1.70	1.76	5.19	1.32	9.42	12.06	4.52
293	2.85	1.26	2.11	4.85	7.03	7.53	5.25	6.78
293	2.85	1.01	3.58	4.72	7.03	12.60	4.30	6.73
293	2.85	0.84	5.88	4.59	7.03	22.71	3.28	7.30
354	2.89	1.76	1.12	4.33	5.90	2.32	3.40	6.92
354	2.89	1.68	2.12	4.21	5.90	4.18	3.10	5.67
354	2.89	1.54	3.88	4.18	5.90	7.22	2.67	7.03
417	2.93	1.08	0.92	7.15	5.08	4.45	5.63	4.36
417	2.93	1.02	1.74	7.01	5.08	8.05	5.00	5.18
417	2.93	0.94	3.16	6.88	5.08	14.2	4.54	6.63
500	2.87	1.33	1.23	5.11	4.15	3.64	4.24	4.69
500	2.87	1.25	2.31	5.00	4.15	6.11	3.57	4.61
500	2.87	1.12	4.15	4.88	4.15	9.61	2.79	5.57
558	2.90	0.53	0.88	9.20	3.76	7.23	5.13	5.67
558	2.90	0.54	0.55	9.00	3.76	3.89	5.01	3.51
558	2.90	0.51	1.65	8.80	3.76	12.74	4.59	4.70
293	9.77	1.25	2.64	5.50	24.04	13.90	7.66	6.87
293	9.77	1.33	1.55	5.37	24.04	8.97	7.37	7.14
293	9.77	1.25	4.89	5.24	24.04	25.71	7.21	7.07
354	9.83	2.36	1.51	3.75	20.02	4.67	7.49	7.38
354	9.83	2.32	2.93	3.69	20.02	8.49	6.93	7.27
354	9.83	2.24	5.63	3.60	20.02	13.10	6.55	7.03
417	9.91	1.39	1.19	6.28	17.13	5.95	8.01	7.99

Table 5.4 Experimental Conditions and the Rate Constants of Reaction 1 at Pressure 1 – 100 bar and 296 – 558 K Temperature Range (Continued)

T / K	P / bar	$[(CH_3)_2CO]$ / 10^{15} molecule cm^{-3}	$[(COCl)_2]$ / 10^{15} molecule cm^{-3}	Photonfluence / 10^{15} photon cm^{-2} $pulse^{-1}$	Number density /10^{19} molecule cm^{-3}	$[Cl]_0$ / 10^{13} molecule cm^{-3}	$[CH_3]_0$ / 10^{13} molecule cm^{-3}	k_1 / 10^{-11} cm^3molecule$^{-1}s^{-1}$
417	9.91	1.36	2.32	6.20	17.13	10.30	7.56	6.07
417	9.91	1.32	4.44	6.12	17.13	19.63	6.95	6.67
500	9.83	1.27	0.81	3.23	14.17	3.71	6.28	6.02
500	9.83	1.21	1.53	3.12	14.17	7.01	5.98	5.24
500	9.83	1.12	2.79	3.01	14.17	11.64	5.62	6.43
558	9.86	1.03	1.05	8.61	12.74	8.71	9.70	5.24
558	9.86	1.01	2.05	8.47	12.74	14.81	9.15	5.13
558	9.86	0.97	3.92	8.32	12.74	26.90	8.24	5.85
295	30.1	1.14	5.18	7.08	72.85	29.04	6.73	8.27
295	30.1	1.17	2.67	6.98	72.85	14.05	7.23	7.59
295	30.1	1.19	1.28	3.12	72.85	7.50	7.85	7.93
357	30.0	1.02	1.04	8.88	60.00	9.21	8.01	8.11
357	30.0	0.99	2.05	8.69	60.00	15.48	7.61	7.49
357	30.0	0.92	3.91	8.51	60.00	28.01	7.22	7.52
417	30.1	1.19	0.98	6.52	51.54	6.20	6.62	7.44
417	30.1	1.14	1.91	6.47	51.54	11.52	6.35	7.01
417	30.1	1.07	3.72	6.41	51.54	20.08	5.88	6.99
500	30.4	2.02	1.48	4.25	43.41	5.35	8.71	6.39
500	30.4	2.01	2.98	4.21	43.41	10.90	8.38	6.18
500	30.4	1.97	5.90	4.17	43.41	18.61	7.80	6.53
558	30.4	1.56	0.98	10.30	38.89	9.06	16.75	5.37
558	30.4	1.50	1.99	9.98	38.89	15.01	15.58	6.13
558	30.4	1.42	3.82	9.68	38.89	24.33	14.21	6.82
295	100.1	1.27	3.01	4.66	234.7	12.20	7.85	7.95
295	100.1	1.27	1.85	4.54	234.7	7.14	8.21	7.17

Sensitivity analysis. Sensitivity analysis has been carried out for all reactions in the mechanism listed in Table 5.3 using a representative experimental profile (see footnote b for Table 5.3). Among the reactions included in the mechanism, some have only marginal importance, and some are not important at all. Only two additional reactions were selected as important in all reactions in the mechanism if the criterion of a

reaction importance of the sensitivity coefficient exceeding 0.01 was accepted. These two reactions are reaction 2 (CH_3 + CH_3) and reaction 12 ($(COCl)_2$ + CH_3). The most important Reaction 2 (CH_3 + CH_3) the sensitivity coefficient of 0.16 is well studied.

The second important reaction 12 ($(COCl)_2$ + CH_3, the sensitivity coefficient of 0.026) is studied in this work. Since $(COCl)_2$ was present in large excess over the free radicals, the contributions of the decay of methyl radicals by reacting with oxalyl chloride were evaluated at room temperature and the highest experimental temperature. Values of $k'_{(CH3+Cl)}$ were obtained with large concentrations of $(COCl)_2$ at different photon fluences (Figures 5.4 and 5.5). The concentrations of Cl atoms were varied by changing the photon fluences with the constant $(COCl)_2$ concentration. Reaction CH_3 + $(COCl)_2$ contributes to the intercepts in Figures 5.4 and 5.5. The upper limits of the rate constants of reaction 12 ($(COCl)_2$ + CH_3) were obtained from the intercepts divided by the concentration of $(COCl)_2$. The upper limit of the rate constants of the reaction of CH_3 with $(COCl)_2$ are $k_{CH3+(COCl)2} < 2.3 \times 10^{-14}$ cm^3 $molecule^{-1}$ s^{-1} (296 K, 1 bar) and $k_{CH3+(COCl)2} < 1.5 \times 10^{-13}$ cm^3 $molecule^{-1}$ s^{-1} (558 K 1 bar).

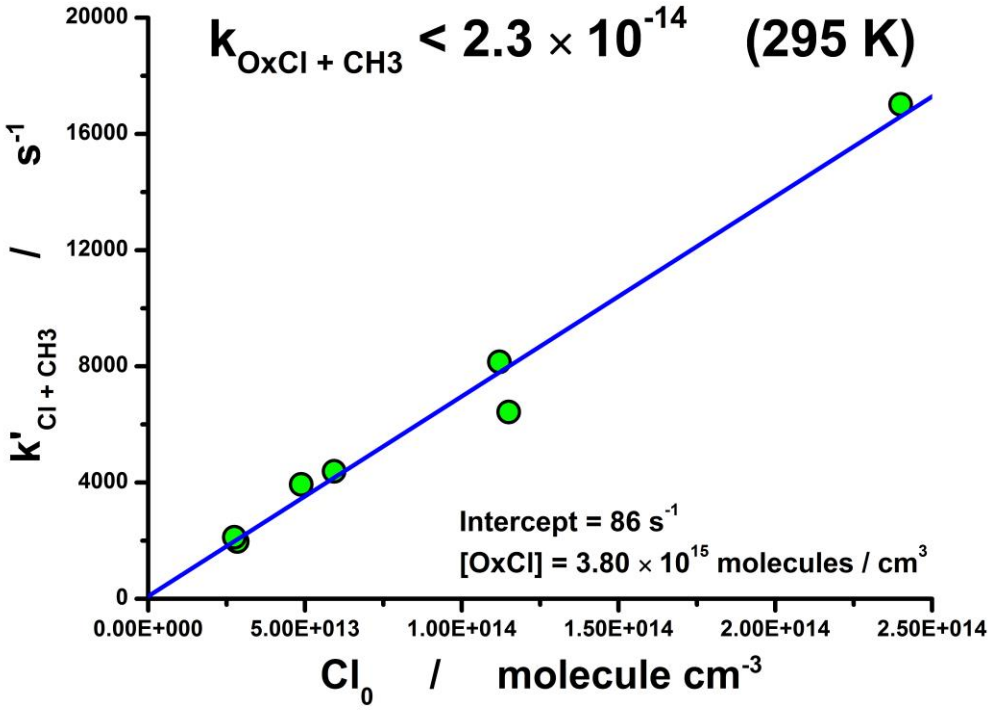

Figure 5.4 Plot of the pseudo-first-order rate constant k'_{Cl+CH3} versus $[Cl]_0$. $k_{CH3+(COCl)2} < 2.3 \times 10^{-14}$ (296 K 1 bar) cm^3 $molecule^{-1}$ s^{-1}. $[(COCl)_2] = 3.80x10^{15}$ molecule cm^{-3}.

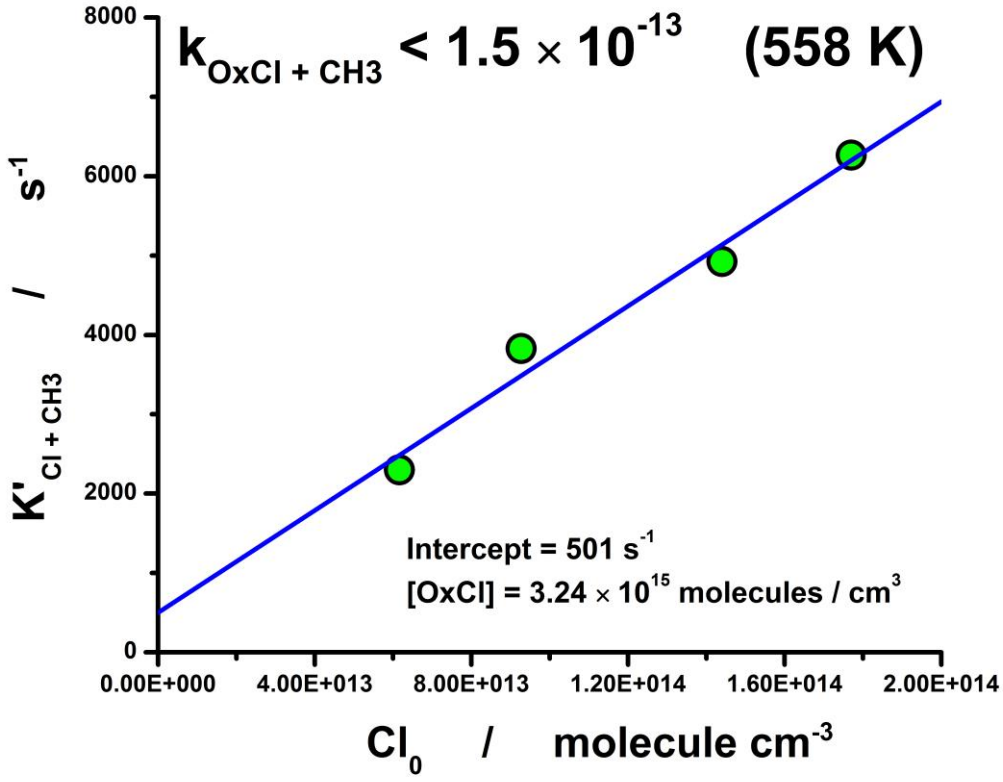

Figure 5.5 Plot of the pseudo-first-order rate constant k'_{Cl+CH3} versus $[Cl]_0$. $k_{CH3+(COCl)2} < 1.67 \times 10^{-13}$ (558 K 1 bar) cm^3 $molecule^{-1}$ s^{-1}. $[(COCl)_2] = 3.12x10^{16}$ molecule cm^{-3}.

The other radical-radical reactions and radical-molecule reactions also contribute to the decay of methyl radicals, while most of them play minor roles under current experimental conditions. For the representative experimental profile, turning off all unimportant reactions results in the change of the returned rate constant k_1 not exceeding 4.1%.

There are three sources of errors in the measured rate constants. The first one is the uncertainty of the absolute concentrations of Cl atoms. The accuracy of *in situ* actinometry ($\pm$4%) and the uncertainties of the absorption cross-section of $(COCl)_2$ at the

elevated temperatures and pressures (±12% in the worst cases at 100 bar and 558 K) contribute to the accuracy of the determination of the absolute concentrations of Cl atoms. The second one is the statistical error in the decay parameters of CH_3 radicals (±15% in the worst cases at 100 bar and 558 K). The third one are the uncertainties associated with the reaction mechanism. Assigning the error of ±20% for the well-studied reaction 2 ($CH_3 + CH_3$), and ±50% for the other important reaction 12 ($CH_3 + (COCl)_2$), and assuming statistical independence of these errors, leads to the combined error in the target reaction rate constant k_1 of $\pm 3.5\%$. The estimated uncertainty associated with the reaction mechanism is about 10% – 15%. Assuming the all these uncertainties are independent, the overall estimate the accuracy of the rate constant is $\pm 25\%$.

All these data are close to the high-pressure conditions. The experimental data of this study alone still are not sufficient to derive the reaction rate parameters, such as the low-pressure limit and the high-pressure limit rate constants as well as the pressure falloff behavior. Therefore, the following strategy in the data processing was chosen. At 298 K, the rate constant is independent of pressure within the experimental error (Figure 5.6). It was taken as the high-pressure limit rate constant at this temperature. The pressure fall off curves are close to the high-pressure limit at 30 bar pressure over the temperature range, and they can be used to determine the temperature dependence of $k_{1,inf}$.

An iterative procedure was used. In the first iteration, the experimental data at 30 bar were taken as the high-pressure limit rate constants. Based on this, pressure falloff curves were calculated. Based on the calculated pressure falloff curve, correction factors k_{exp}/k_{inf} at 30 bar was determined at all temperatures. Then the experimental data at 30 bar were corrected by these correction factors and new k_{inf} at all temperatures were

obtained. Based on this new k_{inf}, new falloff curves have been calculated as well as the new correction factors. This procedure converged in four iterations to three significant digits in the correction factors. The corrected temperature dependent high-pressure rate constants are shown in Figure 5.7. The correction factors are: 0.952 at 357 K, 0.919 at 414 K, 0.881 at 500 K and 0.843 at 558 K.

$$k_{1,inf}(T) = k_{1,inf,\,298\,K}(T/298)^{-0.19} \qquad \text{(E5.7)}$$

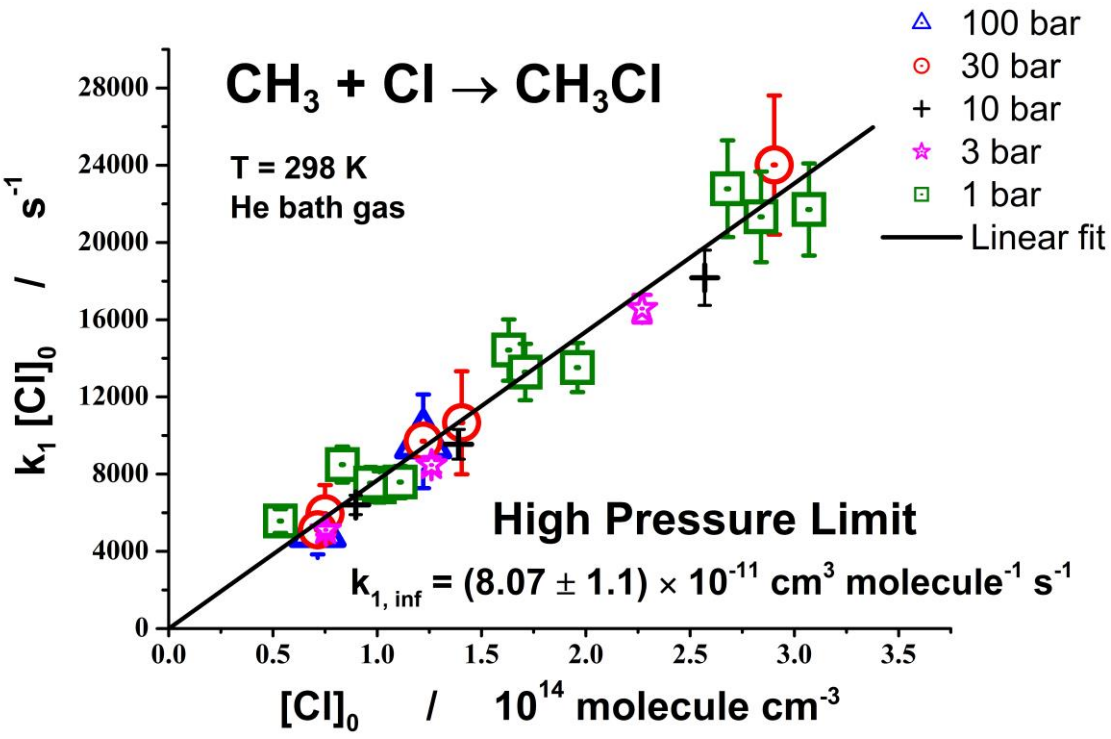

Figure 5.6 High-pressure limit rate constant of reaction 1 at ambient temperature over the 1 – 100 bar pressure range. Helium is the bath gas. High-pressure k' plotted vs initial Cl atoms concentration ($[Cl]_0$). Green square, 1 bar; magenta star, 3 bar; black cross, 10 bar; red circle, 30 bar and blue triangle, 100 bar (see also inset in the figure).

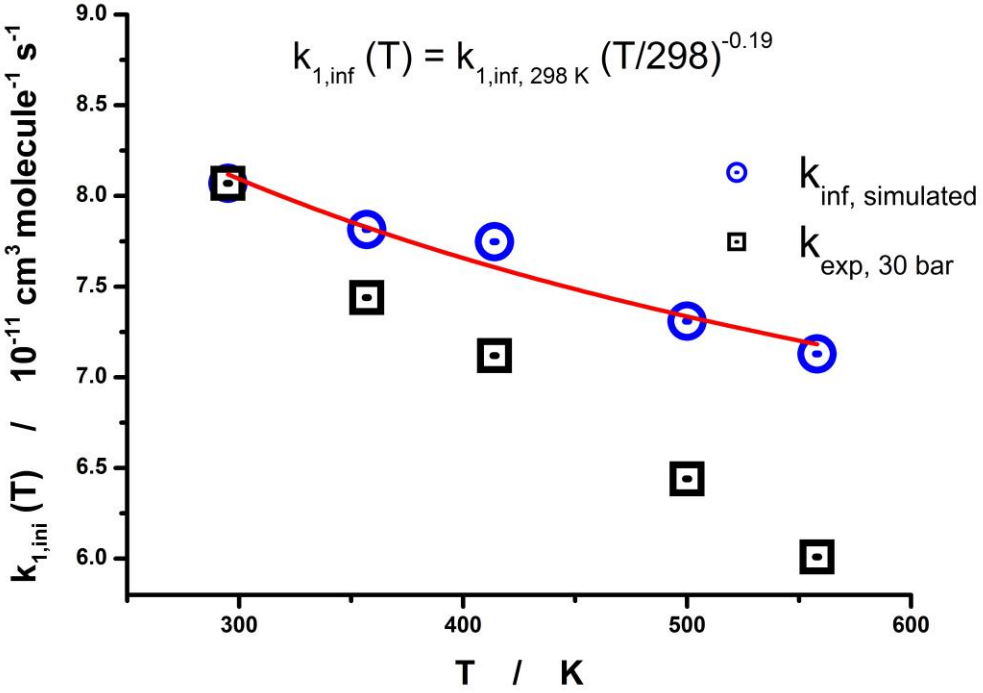

Figure 5.7 The temperature dependence of the high pressure-limit rate constant $k_{1,\ inf}$ over 296 – 558 K temperature range (see text). Blue dotted circle: the corrected temperature dependent high-pressure rate constants. Black dotted square: the experimental rate constants at 30 bar over the 296 – 558 K temperature range.

The theoretically derived temperature dependent broadening factor (F_c)[7] was accepted:

$$F_c = 0.674(T/298\ K)^{-0.414} \exp(-38.7/T) \qquad \text{(E5.8)}$$

The data were fitted using Troe expression:[136]

$$k_1 = k_{1,inf}\left(\frac{\frac{[M]}{[M]_c}}{1+\frac{[M]}{[M]_c}}\right) \times 10^{\left[\frac{\log(Fc)}{1+\left(\frac{\left[\log\left(\frac{[M]}{[M]_c}\right)\right]}{N}\right)^2}\right]} \qquad \text{(E5.9)}$$

$$[M] = pN_A / (ZRT) \quad \text{(E5.10)}$$

$$N = 0.75 - 1.27 \log(F_c) \quad \text{(E5.11)}$$

where $k_{1,inf}$ is the rate constant of reaction 1 in the high-pressure limit, [M] is the number density of the gas, $[M]_c$ is the number density in the center of the pressure falloff curve. The small non-ideality of helium (4.7% at 298 K and 100 bar) was taken into account via the compression factor Z(T,p):[22]

$$Z = 1 + 0.00047(p/bar)(298\ K/T) \quad \text{(E5.12)}$$

The literature low pressure data (298 K) reported by Parker et al.[7] together with our experimental data were used to fit the number density at central pressure as well as the high-pressure rate constants. The fits are shown in Figure 5.8 as solid lines.

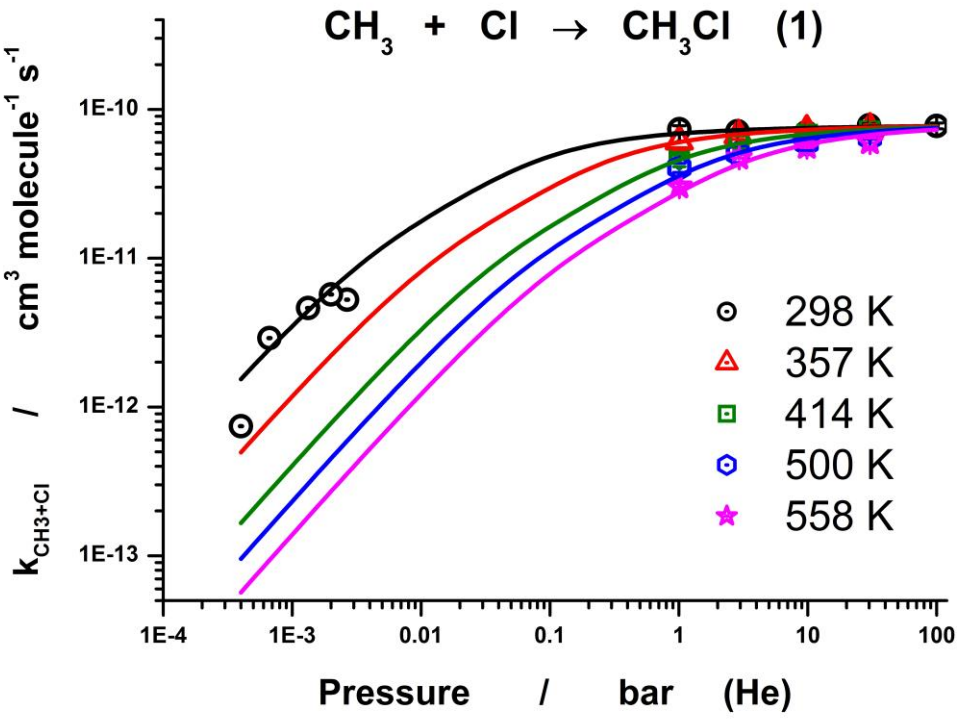

Figure 5.8 Pressure dependence of the rate constant of reaction 1 at different temperatures. Solid lines: fits using the Troe expression: black, 298 K; red, 357 K; green, 414 K, blue, 500 K; magenta, 558 K (see also inset in the figure). The data at room temperature over the pressure range 0.3 – 2 Torr was taken from the literature (Parker et al.)[7]

The center pressure of the falloff curves p_c as a function of temperature is shown in Figure 5.9. The center pressure (p_c) defined as the pressure of ideal gas at the center number density $[M]_c$.

$$p_c = [M]_c RT/ N_A \qquad \text{(E5.13)}$$

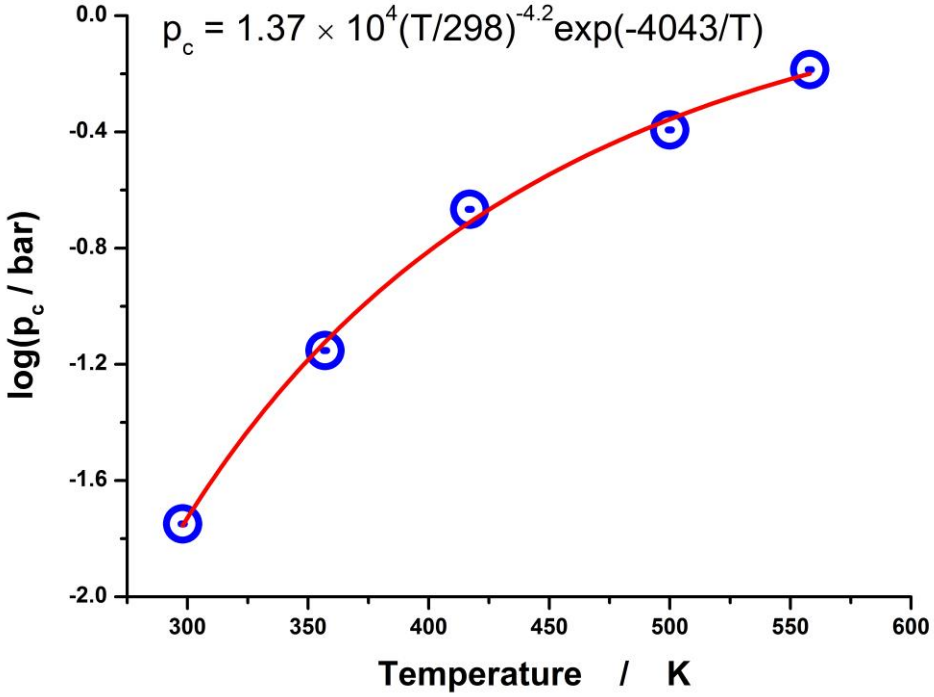

Figure 5.9 Fitting parameter p_c (the center of the falloff curves) plotted vs. temperature. Dotted circles are obtained with the recommended broadening factor (F_c) and the two other parameters ($k_{1,inf}$ (T) and n) reported in this study (see text).

The center pressure p_c as a function of temperature is shown in Figure 5. The temperature dependence determined from the regression is

$$p_c \text{ / bar} = (1.37 \pm 0.2) \times 10^4 (T/298 \text{ K})^{(-4.2 \pm 0.9)} \exp((-4043 \pm 950)/T) \qquad \text{(E5.14)}$$

Therefore, for the low-pressure limit rate constant $k_{1,0}$

$$k_{1,0} = ([He]/[M]_c) k_{1,inf}$$

$$= [He]\, k_{1,inf} RT/(p_c N_A)$$

$$= [He]\, k_{1,inf} 3.01 \times 10^{-24} (T/298)^{5.2} / \exp(-4043/T) \quad \text{(E5.15)}$$

The expression for the high-pressure rate constant $k_{1,inf}$ with the 298 K value obtained from the iterative procedure is:

$$k_{1,inf}(T) = (8.07 \pm 1.1) \times 10^{-11} (T/298)^{-0.19} \text{ cm}^3 \text{ molecule}^{-1} \text{ s}^{-1} \quad \text{(E5.16)}$$

The high-pressure limit rate constant is 35% higher than that recommended by Parker et al., 6.0×10^{-11} cm^3 molecule^{-1} s^{-1},[7] at 298 K. In contrast to the theoretical positive temperature dependence, the high-pressure limit rate constant obtained in this study has negative temperature dependence. Combining E5.15 and E5.16 leads to the low-pressure limit rate constant $k_{1,0}$:

$$k_{1,o} = (2.42 \pm 0.35) \times 10^{-34} (T/298)^{(5.0 \pm 0.9)} / \exp(-4043/T)\, [He]$$

$$\text{cm}^3 \text{ molecule}^{-1} \text{ s}^{-1} \quad \text{(E5.17)}$$

At 298 K, the equation E5.17 shows a factor of ca. 2 times lower value (low-pressure limit rate constant) compared to that recommended by Parker et al[7] and stronger negative temperature dependence. However, it fits well the majority of the experimental profiles, as shown in Figure 5.8.

Comparing to the reaction of CH_3 with Br, the lower central pressure of the falloff curves is observed. Based on the Active Thermochemical Tables (ATcT),[108] CH_3Cl has a

deeper well by 55.6 kJ mol^{-1} compared with CH_3Br. Therefore, assuming the same excess energy, the dissociation of active CH_3Br molecules is faster than CH_3Cl.

5.4 Conclusions

High-pressure limit rate constants of reaction 1 is measured over extended temperature (296 – 558 K) and pressure (1 – 100 bar) ranges. The measured high-pressure limit rate constant is in reasonable agreement with the theoretical prediction (ca. 35 % higher). The pressure falloff was characterized by combing the high-pressure measurements with limited literature low pressure data as well as the theoretical results. At 298 K, low-pressure limit rate constant shows a factor of ca. 2 times lower value compared to that recommended by Parker et al[7] and stronger negative temperature dependence. However, it fits well the majority of the experimental profiles.

CHAPTER 6

$CH_3 + HO_2 \rightarrow$ Products

6.1 Introduction

Reaction of methyl radicals with hydroperoxy radicals (1) plays a very important role in hydrocarbon combustion. Relatively unreactive hydroperoxy radicals, HO_2, are formed via recombination of hydrogen atoms with oxygen molecules. Hydrogen atoms are produced in the dissociation of formyl radicals (HCO) or other hydrocarbon radicals (such as C_2H_5). In addition, HO_2 radicals are formed directly in hydrogen atoms abstraction by oxygen molecules. However, the subsequent reaction of HO_2 with CH_3 radicals might lead to efficient chain propagation via the reaction channel 1a:[2]

CH_3	+	HO_2	→	CH_3O	+	OH	(1a)
			→	CH_2O	+	H_2O	(1b)
			→	CH_3OOH			(1c)
			→	CH_4	+	$^3O_2$	(1d)
			→	CH_4	+	$^1O_2$	(1e)

This reaction is exothermic and proceeds through several energetically allowed channels. Channels 1a and 1d are considered to be the major channels in the high pressure methane oxidation process. Channel 1a is a chain propagation step, whereas channel 1d is a chain termination step.[2] Two free radicals (CH_3O and OH) are formed in channel 1a. Channel 1d and 1e are the direct abstraction reactions forming molecular oxygen in triplet and

singlet electronic states. Among channels 1d and 1e, channel 1d is dominating in forming the triplet surface molecular oxygen.[2] The branching ratios of channel 1a and 1d have impact on the ignition delay in combustion systems.[137]

Colcket et al.[138] reported an indirect kinetic study based on the experiments of high temperature oxidation of acetaldehyde. The rate constant for channel 1a is evaluated based on the rate constant of the reference reaction of $H + HO_2 \rightarrow OH + OH$ as $k_{1a} = 3x10^{-11}$ $cm^3molecule^{-1}$ s^{-1} with an uncertainty of an order of magnitude.

Scire et al.[139] employed a variable pressure flow reactor combined with final product analysis technique. Reaction 1 was studied using the methane perturbed moist carbon monoxide oxidation at 1000 K. They reported the rate constant of reaction 1 as $k_1 = 3x10^{-11}$ $cm^3molecule^{-1}sec^{-1}$ at 1000 K with a significant uncertainty (a factor of 2.5).

Zhu and Lin[4] used ab initio molecular orbital theory and variational RRKM calculations to predict the individual rate constants for channel 1a and channel 1d. Large values were reported for the individual channels $k_{1a}= 1.38x10^{-10}$ $cm^3molecule^{-1}$ s^{-1} and $k_{1d}= 8.34x10^{-12}$ $cm^3molecule^{-1}$ s^{-1} at 300 K. These values are ca. 2.3 times larger than the rate constant recommended by Scire et al.[139]

Hong et al.[140] used shock tube to study reaction 1 between 1054 and 1249 K temperature range at about 3.5 atm. $H_2O_2/CH_4/Ar$ mixtures were used to produce the hydroperoxy and methyl radicals in the shock tube. The decay profiles of H_2O, OH and HO_2 were recorded using laser absorption spectroscopy behind reflected shock waves. The determined rate constant of reaction 1a is $k_{1a} = 1.13x\ 10^{-11}$ cm^3 $molecule^{-1}$ s^{-1} with an uncertainty factor of 1.4, the rate constant of channel 1d is $k_{1d} = 7.31x\ 10^{-12}$ cm^3 $molecule^{-1}$ s^{-1} with an uncertainty factor of 2.1 in the temperature range 1072 - 1139 K.

Sangwan et al.[1] used photolysis of $N_2O/H_2O/CH_4/H_2O_2$/He mixtures at 193.3 nm coupled with UV absorption spectroscopy. The room temperature value is reported as $k_1 = (3.7 \pm 1.2)x10^{-11}$ $cm^3molecule^{-1}s^{-1}$ (295 K, 1 bar, He) (± 1 st. dev.). Due to the decomposition of one of the precursors (H_2O_2) at elevated temperatures, the experiments were limited to ambient temperature.

Even though significant efforts have been made, the direct measurements of reaction 1 are still insufficient. Due to the lack of direct photolysis sources of HO_2 radicals, kinetic studies of CH_3 and HO_2 radicals are difficult. Only very limited experimental studies are available, especially over extended temperature range. This is the motivation to determine the rate constant as well as the branching ratios of reaction 1.

6.2 Experimental Approach

The experimental set-up is described in detail in Chapter 2, therefore only brief description critical for the current experiment is given here. The approach is based on the excimer laser pulsed photolysis coupled to UV-vis transient absorption spectroscopy and to a high-pressure flow system. Both "old" heatable high-pressure reactor and "new" heatable high-pressure were used in this study. Helium is used as a bath gas in all experiments. The measurements are performed over 296 – 500 K temperature range limited by the thermal stability of the precursors.

Acetone, methanol and oxalyl chloride were carefully degassed for gas mixtures preparation in the high-pressure vessels. The concentrations of the precursors used: $(0.49 – 1.15)\times10^{16}$ molecule cm^{-3} for CH_3OH, $(0.44 – 3.32)\times10^{15}$ for CH_3COCH_3, $(1.82 – 4.13)\times10^{15}$ for O_2 and $(1.24 – 6.54)\times10^{15}$ for $(COCl)_2$. The laser photon fluence inside the

reactor is varied in the range $(5.2 – 11.9)\times10^{15}$ photons cm^{-2} $pulse^{-1}$. The temperature range is 295 – 500 K. The highest temperature is limited by the thermal stability of the precursors which is discussed in Chapter 2. The experimental conditions are listed in Table 6.1.

In situ actinometry. The *in situ* actinometery is based on the ozone formation in the photolysis of $N_2O/O_2/N_2$ mixtures at 1 bar and 298 K. The details are discussed in Chapter 2.

Hydroperoxy radicals (HO_2) were produced in a sequence of very fast reactions initiated by chlorine atoms, produced in photolysis of oxalyl chloride. In the initial experiments, HO_2 radicals were produced through the reaction of $O(^1D)$ formed in photodissociation of N_2O with H_2O_2. However, H_2O_2 has a weak oxygen-oxygen bond that is easily broken at elevated temperatures. Therefore, to extend the temperature range, much more stable precursor oxalyl chloride, $(COCl)_2$, was used to initilize the reaction.

Methyl (CH_3) radicals were generated by excimer laser pulse photolysis of acetone. Detail of the radicals generation and monitoring can be found in Chapter 2.

Reagents. Helium used in the experiments is BIP®Helium from Airgas with 99.9999% purity with reduced oxygen content (<10 ppb). UHP oxygen is obtained from Matheson TriGas (99.98% purity). Acetone (Fisher Scientific 99.7%), methanol (Fisher Scientific >99.5 %) and oxalyl chloride (Sigma-Aldrich, >99%) were degassed through three freeze-pump-thaw cycles. Nitrogen for purging the window is obtained from Matheson Tri-Gas with 99.998% purity.

Table 6.1 Experimental Conditions and the Rate Constants of Reaction 1 at 296 – 500 K Temperature Range and Pressure 1 bar

T / K	P / bar	$[(CH_3)_2CO]$ / 10^{15} molecule cm^{-3}	$[(COCl)_2]$ / 10^{15} molecule cm^{-3}	$[CH_3OH]$ / 10^{16} molecule cm^{-3}	$[O_2]$ / 10^{15} molecule cm^{-3}	Photonfluence / 10^{15} photon cm^{-2} $pulse^{-1}$	k_1 / 10^{-11} $cm^3 molecule^{-1} s^{-1}$
297	1.01	1.69	3.77	1.15	2.69	5.74	5.27
297	1.01	1.82	2.06	1.24	2.90	5.74	3.86
297	1.01	1.48	6.54	1.00	2.35	5.74	5.59
296	1.02	3.18	3.63	0.53	3.05	5.20	5.16
296	1.02	3.32	1.98	0.55	3.30	5.20	6.07
296	1.02	2.94	6.27	0.49	2.65	5.20	5.41
414	1.02	0.53	4.72	0.75	2.21	11.9	3.28
414	1.02	0.61	2.74	0.86	2.54	11.8	3.22
414	1.02	0.66	1.51	0.93	2.74	11.7	3.27
500	1.02	0.51	2.26	0.71	2.09	10.3	3.99
500	1.02	1.00	2.18	0.68	4.13	10.3	2.67
500	1.02	0.55	1.24	0.77	2.26	10.3	3.46
500	1.02	0.44	3.89	0.62	1.82	10.3	3.18

6.3 Results and Discussion

Transient absorption profiles of CH_3 radicals were measured at temperature range 292 – 558 K. Examples of measured temporal profiles of absorption at 216.36 nm and 222 nm are shown in Figure 6.1. To determine the rate constant of reaction 1, a reaction mechanism described below (Table 6.2) was used to model and fit the experimental profiles. The absorption profiles were fitted by a numerical solution of a system of differential equations corresponding to the reaction mechanism using MicroMath SCIENTST software. The parasitic absorption by ozone formed outside the reactor is completely suppressed by purging the overlapping areas of the photolysis and the monitoring beams with nitrogen. Small “baseline shift” caused by the mirrors reflectivity

change after a laser pulse, is accurately measured in the absence of the reactants and taken into account in the profiles processing.

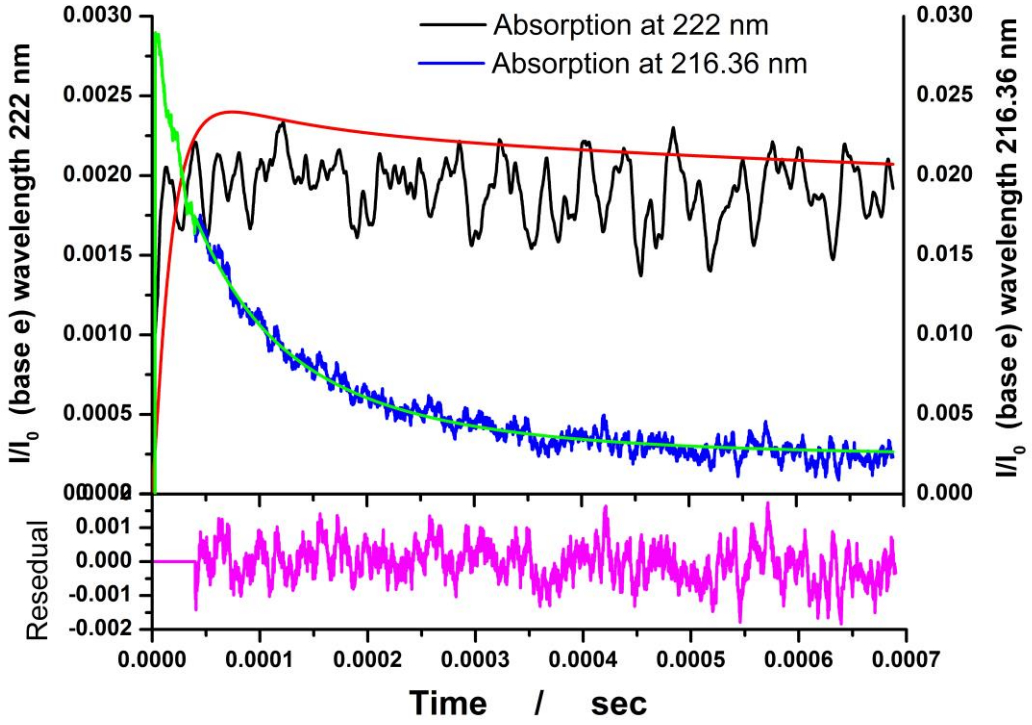

Figure 6.1 Sample temporal profiles of CH_3 decay at 216.36 and HO_2 decay at 222 nm. Solid line: fit by the reaction mechanism (see text), 1 bar (He), 500 K, $[(CH_3)_2CO]$ = 9.96×10^{14}, $[(COCl)_2]$ = 2.18×10^{15}, $[CH_3OH]$=6.84×10^{15}, $[O_2]$= 4.13×10^{15} molecules cm^{-3} and Photon fluence = 10.3×10^{15} photons cm^{-2} $pulse^{-1}$.

The UV absorption cross-section and the rate constants are either measured in previous work[22; 39; 40; 43] (absorption cross section of CH_3, acetone and $(COCl)_2$ and the rate constants of the reactions OH + OH, CH_3 + OH, CH_3 + CH_3 and CH_3O_2 + OH) or are taken from the literature. The determination of the rate constants was performed based on the CH_3 radical decay and branching ratios of channel 1a and channel 1d as determined from the OH radical decay curves. Based on the literature[2] channel 1a and channel 1d are

the important channels compared with the other channels. The reported branching ratios[2] are α_{1a} = 0.7 and α_{1d} = 0.3 these values were used in the profiles fitting. In the profiles simulation, these parameters were varied.

The transient species in the kinetic modeling are OH, HO_2, CH_3, O, H, H_2O_2, O_3, Cl, CH_2, Cl_2 and CH_3O. The concentrations of acetone, $(COCl)_2$, and CH_3OH, which are present in large excess of the transient species, are considered to be constant during the course of the reaction after the laser pulse.

Rate constant. The rate constants of reaction 1 are determined form the experimental methyl transient absorption profiles fitted by the reaction mechanism. The concentrations of HO_2 radicals measured directly at 222 nm wavelength are used for determination of the initial concentrations of HO_2. The lifetime of Cl atoms is much shorter than the lifetime of HO_2 radicals due to the fast reaction of Cl atoms with CH_3OH. Therefore, the decay profiles of CH_3 radicals are sensitive to the reaction 1 after the initial stage of the decay shown in Figure 6.1. The reported rate constants are summarized in Table 6.1 and shown in Figure 6.2.

$$k_1 = (5.10 \pm 0.95) \times 10^{-11} (T / 298\ K)^{-1.01} \qquad (292 – 500\ K, 1\ bar) \quad (E6.1)$$

The final value of the overall rate constant of reaction 1 is shown in (E1). Figure 6.2 shows comparison of the reported result in this study with the previous data. The rate constant of reaction 1 measured in this study is ca. 40% higher than the most recent experimental result[1] and the theoretical determination by Jasper et al.[2] The rate constant

of reaction 1 is a factor of 2.7 lower than that predicted in theoretical study by Zhu and Lin.[4]

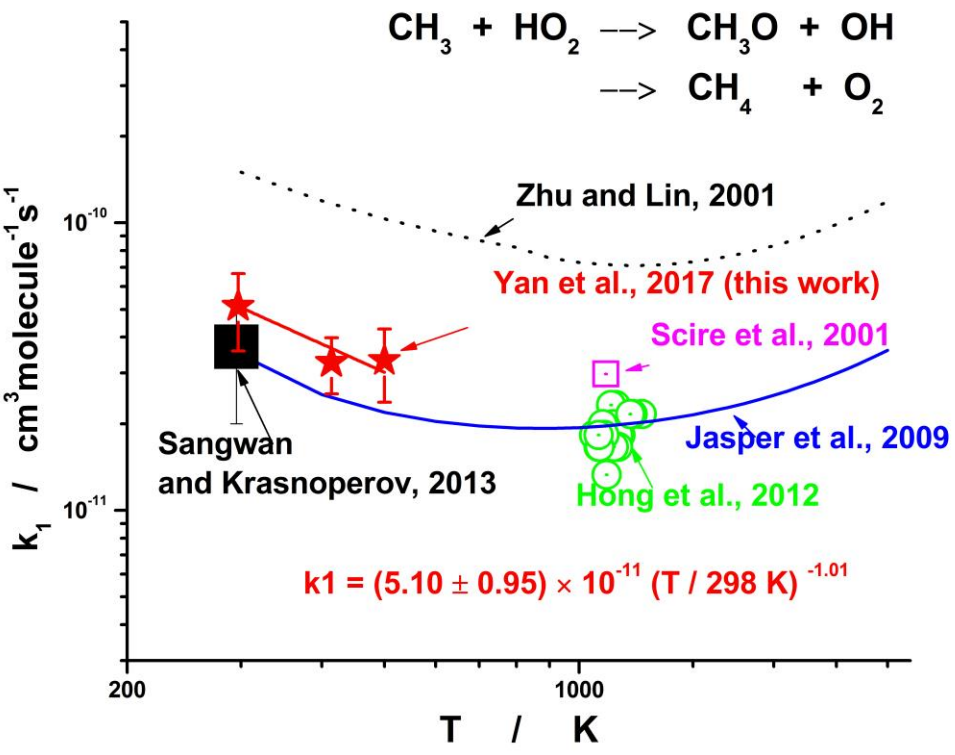

Figure 6.2 The rate constant of the reaction $CH_3 + HO_2$ → products. Red star: this work; black block: Sangwan et al.;[1] green dotted circle: Hong et al.;[140] blue line: Jasper et al., (Theory);[2] dotted line: Zhu and Lin (Theory)[4] and magenta dotted square: Scire et al.[138]

Branching Ratios. The experimental hydroxyl transient absorption profiles are compared with the simulation of the reaction mechanism with different branching ratios. Channel (1a) produces two radicals (CH_3O and OH), whereas the channel 1d does not produce OH. Therefore, the branching ratio can be measured using the absorption profiles of OH radicals (Figure 6.3).

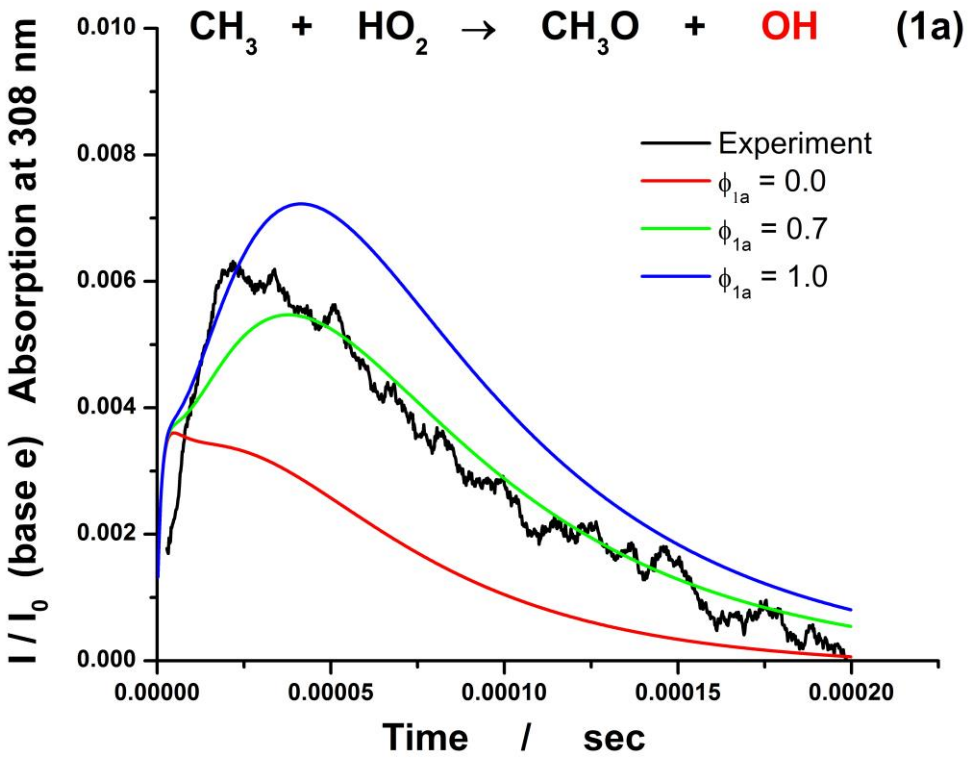

Figure 6.3 Comparison of the experimentally observed absorption profile at 308 nm with the simulated by the mechanism with different branching ratios of channel 1a. Black line – experimental profile; red line – simulation with $\alpha_{1a} = 0.0$; green line – simulation with $\alpha_{1a} = 0.7$; blue line – simulation with $\alpha_{1a} = 1.0$.

The branching ratio of the channel leading to OH radicals (channel 1a) is ca. 0.7 at ambient temperature. This result is consistent with the theoretical study by Jasper et al.[2]

Table 6.2 Reaction Mechanism Used to Simulate and Fit the Experimental Profiles

Reactants	Products	Rate constant[a]	Reference	Comment
CH_3+HO_2	CH3O+OH	To be determined		α_{1a}=0.7
	CH2O+H2O	To be determined		
	CH3OOH	To be determined		
	CH4+O2	To be determined		α_{1a}=0.3
	CH4+O2(1 delta)	To be determined		
$OH+CH_3$	$H_2O+{}^1CH_2$		Ref.[40]	
	CH_3OH			
OH+OH	H_2O+O	$7.1\times10^{13}\exp(210K/T)$	Ref.[72]	Literature for T<415 K, Troe fit above 414 K Ref.[73]
	H_2O_2	$k_{5b,\infty}=(2.4\pm0.6)\times10^{-11}$ $(T/300)^{-0.5}$ $k_{5b,0}=$ [He] $(9.0\pm2.2)\times10^{-31}$ $(T/300)^{-3.5\pm0.5}$ $F_{c=0.37}$.	Ref.[73]	
CH_3+CH_3	C_2H_6	$k_{9}=5.66\times10^{-11}(T/298)^{-0.37}$	Ref[22]	
$OH+CH_4$	H_2O+CH_3	$4.16\times10^{-13}(T/298)^{2.18}\exp(-1232/T)$	Ref.[74]	
OH+O	O_2+H	$2.4\times10^{-11}\exp(110/T)$	Ref.[67]	
OH+H	H_2+O	$6.86\times10^{-14}(T/298)^{2.8}\exp(-1950/T)$	Ref.[75]	
	H_2O	[M] $1.6\times10^{-31}(T/298)^{-2.6}$	Ref.[76]	
CH_3+O	H_2CO+H	1.4×10^{-10}	Ref.[45]	
CH_3+H	CH_4	$6.2\times10^{-29}(T/298)^{-1.8}$	Ref.[78]	
$OH+CH_2$	CH_2O+H	3×10^{-11}	Ref.[79]	
$OH+(CH_3)_2CO$	$CH_3CH_2CO+H_2O$	$3.15\times10^{-14}\times$ $(T/300)^4\exp(453/T)$	Ref.[80]	
$OH+H_2O_2$	H_2O+HO_2	$2.9\times10^{-12}\exp(109/T)$	Ref.[81]	
$OH+HO_2$	H_2O+O_2	$4.8\times10^{-11}\exp(250/T)$	Ref.[82]	
$CH_3+H_2O_2$	CH_4+HO_2	$2\times10^{-14}\exp(300/T)$	Ref.[79]	
$O+HO_2$	O_2+OH	$2.7\times10^{-11}\exp(224/T)$	Ref.[67]	
$O+H_2O_2$	$OH+HO_2$	$1.4\times10^{-12}\exp(-2000/T)$	Ref.[67]	
$H+HO_2$	H_2+O_2	$7.11\times10^{-11}\exp(-710/T)$	Ref.[141]	
	$O(^1D)+H_2O$	$3.29\times10^{12}(T/298)^{1.55}\exp(81/T)$	Ref.[142]	
	2OH	$2.8\times10^{-10}\exp(-440/T)$	Ref.[141]	
	H_2O+O	$5.00\times10^{-11}\exp(-433/T)$	Ref.[141]	
$H+O_2$	OH + O	$1.62\times10^{-10}\exp(-62110/8.31447/T)$	Ref.[104]	
	HO_2	[He] $5.4\times10^{-32}(T/298)^{-1.80}$	Ref.[105]	
CH_3+O	H_2CO+H	1.4×10^{-10}	Ref.[45]	
$O+O_2$	O_3	[He] $3.4\times10^{-34}(T/300)^{-1.2}$ $K_{eq}=4.00\times10^{-9}(T/298)^{-1.373}$ $\exp(14123/T)$	Ref.[106-108]	Equilibrium constant from $\Delta H_f298(O_3)$ = 141.746 $kJmol^{-1}$ from active thermochemical data[108] and O, O_2 fro GRI from NIST WebBook[109]

Table 6.2 Reaction Mechanism Used to Simulate and Fit the Experimental Profiles (Continued)

Reactants	Products	Rate constant[a]	Reference	Comment
$O+O_3$	O_2+O_2	$8\times10^{-12}\exp(-2060/T)$	Ref.[98]	
$H+O_3$	$OH+O_2$	$1.4\times10^{-10}\exp(-480/T)$	Ref.[143]	
HO_2+O_3	$OH+O_2+O_2$	$1.97\times10^{-16}(T/298)^{4.57}\exp(693/T)$	Ref.[67]	
HO_2+HO_2	$H_2O_2+O_2$	$2.2\times10^{-13}\exp(-600/T)$	Ref.[67]	
$CH_3O + CH_3$	$CH_2O + CH_4$	4×10^{-11}	Ref.[95]	
	$(CH_3)_2O$	5.5×10^{-11}	Ref.[114]	
$CH_3O + CH_3O$	$CH_3OH + CH_2O$	3.85×10^{-11}	Ref.[114]	
$CH_3O + CH_3O$	$(CH_3O)_2$	3×10^{-12}	Ref.[95]	
$CH_3O + OH$	$CH_2O + H_2O$	3×10^{-12}	Ref.[95]	
$CH_3O + O_2$	$CH_2O + HO_2$	$7.82 \times10^{-14}\exp(-9560/8.31447/T)$	Ref.[115]	
$CH_3O + HO_2$	$CH_2O + H_2O_2$	5×10^{-13}	Ref.[95]	
$CH_3O + O$	$CH_2O + OH$	1×10^{-11}	Ref.[95]	
	$CH_3 + O_2$	2.5×10^{-11}	Ref.[120]	
$CH_3O + H$	$CH_2O + H$	3.3×10^{-11}	Ref.[121]	
CH_3O	CH_2OH	$1\times10^{13}\exp(-109000/8.31447/T)$	Ref.[144]	
CH_3O	CH_2O+H	$9\times10^{-11}\exp(-56460/8.31447/T)$	Ref.[104]	
$CH_3 + Cl$	CH_3Cl	$(2.72 \pm0.35) \times10^{-35}(T/298)^{(5.0 \pm0.9)} / \exp(-4.0 \times10^3/T)$		
	$HCl + CH_2$	Neglected	Ref.[129]	
CH_3OH+Cl	$HCl+CH_2OH$	5.5×10^{-11}	Ref.[98]	
	$HCl+CH_3O$	5.5×10^{-13}	Ref.[145]	
CH_2OH+O_2	HO_2+CH_2O	0.95×10^{-11}	Ref.[98]	
$CH_3O + O_2$	$CH_2O + HO_2$	$7.82 \times10^{-14}\exp(-9560/8.31447/T)$	Ref.[115]	
$Cl + Cl$	Cl_2	$[He]\ 4.69 \times10^{-33}$	Ref.[130]	
$Cl+HO_2$	$HCl+O_2$	$1.8e \times10^{-11}\exp(1413/8.31447/T)$	Ref.[115]	
$Cl+O_2$	ClO_2	$[He]1.44 \times10^{-33}$	Ref.[98]	
Cl+acetone	products	2.08×10^{-12}	Ref.[135]	
$Cl+CH_3O$	$HCl+CH_2O$	1×10^{-10}	Ref.[146]	
$OH+CH_3OH$	products	$4.8\times10^{-12}\exp(-3990/8.31447/T)$	Ref.[147]	
$CH_3O_2 + CH_3$	$CH_3O + CH_3O$	4.5×10^{-11}	Ref.[116]	
$CH_3O_2 + O$	$CH_3O + O_2$	4.3×10^{-11}	Ref.[117]	
$CH_3O_2 + H$	$CH_3O + OH$	1.6×10^{-10}	Ref.[95]	
$CH_3O_2 + HO_2$	$CH_3OOH + O_2$	$3.8 \times10^{-13}\exp(6650/8.31447/T)$	Ref.[98]	
$CH_3O_2 + CH_3O_2$	$CH_3O + CH_3O + O_2$	$7.4 \times10^{-13}\exp(-4320/8.31447/T)$	Ref.[98]	
	$CH_2O + CH_3OH + O_2$	$k_{30b} = k_{30}/(1+25\exp(-9730/8.31447/T))$ $k_{30} = 1.0 \times10^{-13}\exp(3030/8.31447/T)$	Ref.[98]	
	$(CH_3O)_2 + O_2$	3×10^{-14}	Ref.[118]	

Table 6.2 Reaction Mechanism Used to Simulate and Fit the Experimental Profiles (Continued)

Reactants	Products	Rate constant[a]	Reference	Comment
$CH_3O_2 + CH_3O$	$CH_3OOH + CH_2O$	1.82×10^{-11}	Ref.[95]	The upper limit of reaction 12 was mesured at 296 K and 558 K separately.
$CH_3O_2 + OH$	$CH_3O + HO_2$	$(8.4 \pm 1.7) \times 10^{-11}_{0.81}(T/298\ K)^{-}$	Ref.[43]	
	$CH_2OO + H_2O$			
	TRIOX			
$CH_3Cl + Cl$	$CH_2Cl + HCl$	$1.7 \times 10^{-11}\exp(-8647/8.31447/T)$	Ref.[131]	
$C_2H_6 + Cl$	$C_2H_5 + HCl$	$8.3 \times 10^{-11}\exp(-830/8.31447/T)$	Ref.[98]	
$CH_3 + Cl_2$	CH_3Cl+Cl	1.55×10^{-12}	Ref.[148]	

6.4 Conclusions

The rate constant of reaction 1 was measured over an extended temperature range (296 – 500 K) and pressure of 1 bar. The branching ratios of channel 1a and 1d were measured. The measured branching ratios are in excellent agreement with the recent theoretical study by Jasper et al.[2]

CHAPTER 7

CONCLUSIONS

All the four projects described in this thesis aimed the same goal, which is a systematic fundamental study of the kinetics and mechanisms of free radical-radical reactions of combustion importance over extended temperature and pressure ranges.

For the work in the Chapter 3, where the self-reaction of methyl radicals is studied close to the high-pressure limit conditions, the rate constant in the high pressure limit exhibits negative temperature dependence in accord with the previous studies. The low temperature data are in good agreement with the literature.

In Chapter 4 and Chapter 6, the free radical-radical reactions (CH_3O_2 + OH) and (HO_2 + CH_3) were studied. The overall rate constants and branching ratios are reported over extended temperature and pressure ranges. The first experimental observation of the pressure dependent yield of TRIOX in the reaction (CH_3O_2 + OH) over 1 – 100 bar is reported.

The reaction of CH_3 with Cl is described in Chapter 5. The experiments were performed near the high pressure conditions. The low-pressure limit, high-pressure limit rate constants and the pressure falloff central pressure p_c are determined. Comparing with the CH_3 – Br system, lower pressure falloff central pressure is observed, which is rationalized based on the stronger C-Cl bond compared to the C-Br bond.

APPENDIX A

THE SCIENTIST MODELS

Radicals concentration traces were normally averaged for 500 to 5000 times by oscilloscope and transferred to a PC for processing. The profiles transferred from PC were fitted using a smooth function with sufficient number of parameters to provide adequate fitting flexibility. SCIENTIST software (MicroMath, Inc.) was used to perform the nonlinear least squares fitting by numerical solutions of the ODE system which corresponds to the reaction mechanism. Four models were constructed in SCIENTIST software and they are in A.1 – A.4.

A.1. This model produces the rate constant CH3+CH3 and SigmaCH3

```
// Time should be in the 1-st column, signal (light intensity) - in 2-nd and 3-rd

IndVars: TIME,SIGNAL1
DepVars: SIGNAL
Params: k6, SigmaCH3, shift

//Only information between the two dashed lines may be changed
// from experiment to experiment
//_____________________________________________________
//Time Window (all in sec)

t1=10e-6
t2=7e-4

//Exp 01/29/15 Exp5He 100.8bar
//Conditions:
T=714
M=9.97E+20
N2O=0
CH4=0
Acetone=1.289E+15
OHini=0
```

```
CH3ini=3.308E+14
Oini=0
NOini=0
Hini=0
CH2ini=0
HONOini=0
H2O2ini=0
HO2ini=0
OH=0

//Rate constant of CH3 recombination: depends upon pressure and temperature

//k6:    CH3 + CH3 --> C2H6          (6)
//T=298
//1 bar 6.29e-11
//10 bar 6.42e-11
//100 bar 6.47e-11
//Pass length (cm)
L=10

// Cross-sections at 216 nm
// Cross-section of CH3 is pressure dependent! (Temperature too!)
//From Krasnoperov, Mehta for Sigma(216.51), correction for triangular slit function
//0.6 nm as x1.019 (Grebenkin, Krasnoperov), and p-dependence as in Mehta, et al.

//for T=298K
//pHe=1 bar SigmaCH3 = 3.59e-17
//pHe= 3 bar SigmaCH3 = 3.51e-17
//pHe=10 bar SigmaCH3 = 3.27e-17
//pHe=30 bar SigmaCH3 = 2.73e-17
//pHe=100 bar SigmaCH3=1.74e-17
// Pilling temperature dependance corrected /1.33 1bar     /1.8 100bar

//SigmaCH3=1e-17*(7.58-1.29e-2*T+7.28e-6*T*T)/1.8

SigmaH2O2=2.96e-19
SigmaHONO=1.79e-18

//_____________________________________________________________
//Reaction Mechanism  based on Macdonald J.Phys.Chem. A 2007, 111, 3850-3861

// N2O + hv -->O(1D) + N2                (0)
// O(1D)+N2O -->  2 NO                   (1a)
// O(1D)+N2O -->  N2 +O2                 (1b)
//O(1D)+H2O -->  2 OH                    (2)
//O(1D)+CH4 -->  OH + CH3                (3)
```

// OH + OH --> H2O+O (4a)
// OH + OH --> H2O2 (4b)
// OH + CH3 --> H2O + CH2 (Xa) ka
// OH + CH3 --> CH3OH (Xb) kb **ka+kb=k**
//OH + CH4 --> H2O + CH3 (5)
//CH3 + CH3 --> C2H6 (6)
//OH + O --> O2 +H (7)
//OH + H --> H2O (8)
//OH + H --> H2 + O (8b)
// CH3 + O --> H2CO + H (9)
// OH + NO --> HONO (10)
// CH3 + H --> CH4 (11)
// OH + CH2 --> CH2O + H (12)
// OH + (CH3)2CO -->(CH3)(CH2)CO+H2O (13)
// OH + H2O2 --> H2O + HO2 (14)
// OH + HO2 --> H2O + O2 (15)
// HO2 + NO --> OH + NO2 (16)
//CH3 + NO -->CH3NO (17)
//CH3 + H2O2 --> CH4 + HO2 (18)

//Rate constants:

ka=alpha*k
kb=(1-alpha)*k

//k4b obtained from OH profile fits
k4b=3.9e-12
//k4a: OH+OH --> H2O + O (4)

//2007McDon
// k4a decrese with temperature. 1/T dependence arbitrary introdused
k4a=2.6e-12*(298/T)
//k4b: OH+OH --> H2O2 (4b)

//OH + CH4 --> H2O + CH3 (5)
k5 =4.16e-13*(T/298)^2.18*exp(-1232/T)

//OH + O --> O2 +H (7)
// 2004 ATK/BAU
k7=2.4e-11*exp(109/T)

//OH + H --> H2O (8)
//77 ZEL/ERL
k8=M*1.6e-31*(T/298)^(-2.6)

//OH + H --> H2 + O (8b)

```
//86TSA/HAM
k8b = 6.86e-14*(T/298)^2.8*exp(-1950/T)

// CH3 + O --> H2CO    +  H                    (9)
//1992ATK
k9= 1.4e-10

// OH   + NO  --> HONO                        (10)

k010=3.9e-31*(T/298)^(-2.6)
kinf10=3.3e-11
Fcent10=1.23*exp(-T/815)
x10=k010*M/kinf10
c10=-0.4-0.67*Log10(Fcent10)
N10=0.75-1.27*Log10(Fcent10)
d=0.14
y10=Log10(x10)+c10
LF10=Log10(Fcent10)/(1+(y10/(N10-d*y10))^2)
F10=10^LF10
k10=kinf10*F10*x10/(1+x10)

// CH3 + H  --> CH4                           (11)
//Pilling1997
k011=6.2e-29*(T/298)^(-1.8)
kinf11=3.5e-10
Fcent11=0.638*exp(-T/3231)
x11=k011*M/kinf11
c11=-0.4-0.67*Log10(Fcent11)
N11=0.75-1.27*Log10(Fcent11)
d=0.14
y11=Log10(x11)+c11
LF11=Log10(Fcent11)/(1+(y11/(N11-d*y11))^2)
F11=10^LF11
k11=kinf11*F11*x11/(1+x11)

// OH  +  CH2  -->  CH2O + H                  (12)
//1986TSA/HAM
k12=3e-11

// OH  +  (CH3)2CO  -->(CH3)(CH2)CO+H2O       (13)
//2003YAM/TAY
k13=3.15e-14*(T/300)^4*exp(453/T)

// OH + H2O2 --> H2O + HO2                    (14)
//2004JIM/GIE
k14=2.9e-12*exp(-109/T)
```

```
// OH + HO2 -->  H2O + O2                    (15)
//1988KEY
k15=4.8e-11*exp(250/T)

// HO2 + NO --> OH + NO2                     (16)
//2003BAR/BAC
k16=4e-12*exp(223/T)

//CH3 + NO -->CH3NO                         (17)
//1991 Pilling Ar
//A.H.Langer,A.M.Bass.Int.J.Chem.Kin.V.7,639-648(1975) kHe=kAr
k017=6.9e-32*exp(1430/T)
kinf17=1.5e-11*exp(-60/T)
Fcent17=5*exp(-T/120)
x17=k017*M/kinf17
c17=-0.4-0.67*Log10(Fcent17)
N17=0.75-1.27*Log10(Fcent17)
d=0.14
y17=Log10(x17)+c17
LF17=Log10(Fcent17)/(1+(y17/(N17-d*y17))^2)
F17=10^LF17
k17=kinf17*F17*x17/(1+x17)

//CH3 + H2O2 -->   CH4 + HO2                (18)
//1986TSA
k18=2e-14*exp(300/T)
alpha=0.1
k=1.2e-10


//Species transient:  OH,  CH3, O,  H, NO, CH2, HONO, H2O2,HO2
//Species stable: N2O, ACETONE,CH4
//Equations:


r4a=k4a*OH*OH
r4b=k4b*OH*OH
r5=k5*OH*CH4
ra=ka*OH*CH3
rb=kb*OH*CH3
r6=k6*CH3*CH3
r7=k7*OH*O
r8=k8*OH*H
r8b=k8b*OH*H
r9=k9*CH3*O
```

```
r10=k10*OH*NO
r11=k11*CH3*H
r12=k12*OH*CH2
r13=k13*OH*ACETONE
r14=k14*OH*H2O2
r15=k15*OH*HO2
r16=k16*HO2*NO
r17=k17*CH3*NO
r18=k18*CH3*H2O2

//OH'=-2*r4a-2*r4b-r5-ra-rb-r7-r8-r8b-r10-r12-r13-r14-r15+r16
CH3'=r5-ra-rb-2*r6-r9-r11-r17-r18
O'=r4a-r7+r8b-r9
H'=r7-r8-r8b+r9-r11+r12
NO'=-r10-r16-r17
CH2'=ra-r12
HONO'=r10
H2O2'=r4b-r14-r18
HO2'=r14-r15-r16

Absorption = L*(SigmaCH3*CH3+SigmaHONO*HONO+SigmaH2O2*H2O2)+shift

F1=SIGNAL1
F2=Absorption
gate=UNIT(TIME-t1)*UNIT(t2-TIME)
SIGNAL=(1-gate)*F1+gate*F2
***
//Initial Conditions

TIME=0
CH3=CH3ini
O=Oini
NO=NOini
H=Hini
CH2=CH2ini
HONO=HONOini
H2O2=H2O2ini
HO2=HO2ini

//Initial Parameters and Constraints

k6=7e-11
SigmaCH3=3e-17
shift=0
```

A.2. This model produces the rate constant CH3O2+OH and branching ratio

// **Chao Yan Modified August 19 to incorporate possible T dependence of the reactions and relaxation of O(1D)**
//Modeling CH3O2+OH
// Reaction OH + CH3O2 --> CH3O + HO2 (77) main channel k77 = 2.3e-10 according to Christa Fittschen ICCK 2015
// Reaction CH3+ HO2, rate constant as well as the branching ratio
//Photolysis of N2O/Acetone/O2/He at 193.3 nm
//Absorptions of CH3O2 are taken into account
// Reactions of CH3O2 included
//_____
//Troe Formalizm Functions Definitions:
// It looks like that User Defined Functions do not work properly!!!!!!!!!!!!!
//This is for the reference only:
//c(y)=-0.4-0.67*Log10(y)
//N(y)=0.75-1.27*Log10(y)
//d=0.14
//LF(x,y)=Log10(y)/(1+((Log10(x)+c(y))/(N(y)-d*(Log10(y)+c(y))))^2)
//F(x,y)=10^LF(x,y)
//_____
// Time should be in the 1-st column, signal (absorbance) - in 2-nd and 3-rd

IndVars: TIME,A308_1
DepVars: A308
Params: k77, PhotonFluenceFactor

//Fitting Interval (sec)
t1=25e-6
t2=150e-6

//_____
//Cross-sections and O(1D) reactions

// Photolysis of water at 193.3 nm (1.51e-21, our measurements, 03/22/11)
// Photolysis of O2 at 193.3 nm (ca. 3e-22, our rough estimate)
// Photolysis of N2O at 193.3 at 1 bar, 298 K 8.77e-20
//O(1D)+H2--> OH(all)+H 1.35e-10 (Vranckx et al, PCCP, 2010, 9213)
// The following rate constants for O(1D)+N2O are averages of three recent
//determinations, as discussed by
//Macdonald
//Shaun Avondale Carl, PCCP,2005,7,4051-4053, E.J.Dunlea,Ravishankra PCCP,2004,6,2152-2161,
// K. Takahashi,Yukari Takeuchi, Yutaka Matsumi Chem. Phys. Lett. //410(2005),196-200.
// However, these recent study do not distinguish between the two channels,

```
// and it is accepted the branching ratios as 7.2/11.6=0.62 for 2 NO and //4.4/11.6 = 0.38
for N2+O2
// Accepting total as 1.35e-10, this results in
// O(1D)+N2O--> 2 NO 8.37e-11   (1)
// O(1D)+N2O-->N2 +O2 5.13e-11 (2)
// Quenching on N2O is kq/k=0.056 (Carl, 2005) => kq(N2O)=0.756e-11 (3)
//O(1D)+H2O--> 2 OH (1)  1.7e-10exp(36/T) (Vranckx et al.PCCP, 2010
//O(1D)+H2O--> H2 +O2 (2) 2.2 e -12
// Quenching on water is < 0.003 of the total (Carl, 2005), and is neglected.
//O(1D)+O2 -->O(3P) + O2  3.3e-11?xp(55/T)  k298 =  3.95e-11   JPL 2011
//O(1D)+CH4 --> OH + CH3 1.0e-10 (IUPAC online) (1)
// O(1D)+CH4 -->CH2O+H2  7.5 e-12 (IUPAC online) (2)
// O(1D)+CH4-->CH3O or CH2OH + H 3.4e-11 (IUPAC online) (3)
//O(1D)+H2--> OH(all)+H  1.35e-10 (Vranckx et al.PCCP, 2010, 12)
// O(1D)+Acetone--> OH + CH3COCH2 Rate constant???? Arbitrarily set to
// 5e-10 (typical for C-H bond)
// O(1D)+H2O2 --> OH + HO2 5.2e-10 1976FLE/HUS
kN2Och1=8.37e-11
kN2Och2=5.13e-11
kN2Och3=0.756e-11
kH2Och1=1.7e-10*exp(36/T)
kH2Och2=2.2e-12
kO2=3.30e-11*exp(55/T)
kCH4ch1=1.0e-10
kCH4ch2=7.5e-12
kCH4ch3=3.4e-11
kH2=1.35e-10
kAcetone=5e-10
kH2O2=5.2e-10

//Cross-sections: 193=193.3 nm, 216=216.4 nm, 230=230 nm, 254=253.6

//Cross-sections of H2O2 at 1 bar, 298 K (JPL-15)
sH2O2at193=60.1e-20
sH2O2at216=29.3e-20
sH2O2at224=22.5e-20
sH2O2at230=18.2e-20
sH2O2at254=7.1e-20

//Cross-sections of HO2, at 1 bar, 298 K (JPL-15)
sHO2at193=390e-20
sHO2at216=373e-20
sHO2at224=299e-20
sHO2at230=230e-20
sHO2at254=32.4e-20
```

```
//Cross-sections of N2O, at 1 bar, 298 K (JPL-15)
// Manuvesh 1 bar
sN2Oat193=8.15e-20+2.74e-22*(T-298)
//sN2Oat193=8.70e-20
sN2Oat216=0.205e-20
sN2Oat224=0.0375e-20
sN2Oat230=0.00955e-20
sN2Oat254=0

// Cross-sections of H2O
// Our measurement, 02/16/12/ exp 11
// sH2Oat193=1.51e-21
// Chao, Stefani measurement 454 K 1bar, 11/03/15
//sH2Oat193=1.33e-21
// Chao, Stefani measurement 500 K 1bar, 11/03/15
sH2Oat193=1.286e-21

// Cross-sections of O2
sO2at193=1.72e-22

// Cross-section of O3 (JPL-15, actually - narrow bands, see JPL-15)
sO3at193=42.9e-20
sO3at216=118e-20
sO3at224=255e-20
sO3at230=490e-20
sO3at254=1148e-20*(T/298)^(-0.2303)

// Cross-section of HONO at 1 bar, 298 K (JPL-15)
sHONOat193=155e-20
sHONOat216=176e-20
sHONOat224=121e-20
sHONOat230=84.5e-20
sHONOat254=15.0e-20

// Cross-sections of acetone at 1 bar, 298 K
// Our measurements
// Acetone cross section 526 K
sAcetoneat193=5.00e-18
//old our measurement (paper with Kashyap Mehta):0.18e-20
// Gierczak et al., 1998
sAcetoneat216=0.186e-20
sAcetoneat224=0.346e-20
sAcetoneat230=0.584e-20
sAcetoneat254=2.82e-20

// Cross-sections of CH3 at 1 bar, 298 K
```

```
// Our measurements
sCH3at216=3550e-20
sCH3at224=0
sCH3at230=0
sCH3at254=0

// Cross-sections of Oxalyl Chloride, 1 bar, 298 K
// Baklanov, Krasnoperov
sOxClat193=383e-20
sOxClat216=130e-20
sOxClat224=85e-20
sOxClat230=63e-20
sOxClat240=39e-20
sOxClat254=23e-20
sOxClat308=7.2e-20

// Cross-sections of OH, 1 bar, 298 K
// Sangwan et al.
sOHat308=4.23e-17

//Cross-sections CH3O2, 1 bar, 298 K

//JPL-2006, at 308 -short extrapolation based on the Gaussian fitted to the tail
sCH3O2at216=291e-20
sCH3O2at224=367e-20
sCH3O2at230=408e-20
sCH3O2at254=348e-20
sCH3O2at308 = 20e-20

//Cross-sections of Methanol
sCH3OHat193=30.5e-20
sCH3OHat216=2.5e-22
//absorbtion at 216 nm is neglected

// CONDITIONS
//--------------------------------------------------------------------------------

// Date 12/15/15   04
// (COCl)2/CH3OH/H2O/O2/CH4/He 1 bar
// Pressure in bar

//Old reactor
L=10.13
//New reactor
//L=10
```

```
p=1.006
T=500
M=2.429e19*(298.15/T)*p

H2O2_0=0
H2O_0=10.87e17
H2_0=0
CH3_0=0
OxCl_0=0
CH3OH_0=0
CH4_0=0
O2_0=3.01e17
N2O_0=1.975e16
Acetone_0=1.597e15
Cl2_0=0
PhotonFluence_0 = 6.33e15*PhotonFluenceFactor

// Linear approximation for A193 < 0.2
PhotonFluence = PhotonFluence_0*(1- L*sOxClat193*OxCl_0/2-
L*sCH3OHat193*CH3OH_0/2)

ZeroShift308=0
ZeroShift254=0

//_____________________________________________________________
//Initial Conditions Calculations

QuenchN2O = (kN2Och1+kN2Och2+kN2Och3)*N2O_0
QuenchH2O = (kH2Och1+kH2Och2)*H2O_0
QuenchH2O2=kH2O2*H2O2_0
QuenchO2=kO2*O2_0
QuenchH2=kH2*H2_0
QuenchCH4=(kCH4ch1+kCH4ch2+kCH4ch3)*CH4_0
QuenchAcetone=kAcetone*Acetone_0
Quench1 = QuenchN2O+QuenchH2O+QuenchO2+QuenchH2O2
Quench2=QuenchH2+QuenchCH4+QuenchAcetone
TotalQuench=Quench1+Quench2
fN2Och1=kN2Och1*N2O_0/TotalQuench
fN2Och2=kN2Och2*N2O_0/TotalQuench
fN2Och3=kN2Och3*N2O_0/TotalQuench
fH2Och1=kH2Och1*H2O_0/TotalQuench
fH2Och2=kH2Och2*H2O_0/TotalQuench
fO2=kO2*O2_0/TotalQuench
fH2=kH2*H2_0/TotalQuench
fCH4ch1=kCH4ch1*CH4_0/TotalQuench
fCH4ch2=kCH4ch2*CH4_0/TotalQuench
```

```
fCH4ch3=kCH4ch3*CH4_0/TotalQuench
fH2O2=kH2O2*H2O2_0/TotalQuench
fAcetone=kAcetone*Acetone_0/TotalQuench
fTotal1= fN2Och1+fN2Och2+fN2Och3+fH2Och1+fH2Och2+fO2+fH2+fCH4ch1
fTotal2=fCH4ch2+fCH4ch3+fH2O2+fAcetone
fTotal=fTotal1+fTotal2

//_____________________________________________________
//Quantum Yields
//Photolysis of N2O at 193, quantum yield O(1D)=1
//Photolysis of H2O2 at 193. Quantum yield of OH =1.5 (JPL-15)
//Quantum yield of O-atoms is 0.16 (JPL-15)
// H2O2 +hnu(193) --> 2 OH   Fi(OH)=1.5 (JPL-15)
//                    --> H2O + O (Okabe), Fi(O) =0.16 (JPL-15)
//Photolysis of acetone at 193 nm, Fi(CH3)=0.95x2
// Photolysis of water at 193 nm, Fi(H)=1, Fi(OH)=1,(JPL-15)
//Photolysis of oxygen at 193 nm. Both atoms are ground state O-atoms.
//(Okabe). Fi(O)=2.
// Methane, of course, does not absorb anywhere close
// Photolysis of OxCl at 193.3 nm. Fi(Cl)=2.

O1Dini=PhotonFluence*sN2Oat193*N2O_0
Clini=PhotonFluence*sOxClat193*OxCl_0*2
delN2O=-PhotonFluence*sN2Oat193*N2O_0-O1Dini*(fN2Och1+fN2Och2)
delOxCl=-PhotonFluence*sOxClat193*OxCl_0
delH2O=-PhotonFluence*sH2Oat193*H2O_0-O1Dini*(fH2Och1+fH2Och2)
delH2O2=-PhotonFluence*sH2O2at193*H2O2_0-O1Dini*fH2O2
delO2=-PhotonFluence*sO2at193*O2_0
delAcetone=-PhotonFluence*sAcetoneat193*Acetone_0-O1Dini*fAcetone
delCH4=-O1Dini*(fCH4ch1+fCH4ch2+fCH4ch3)
delCH3OH=-PhotonFluence*sCH3OHat193*CH3OH

OHfromH2O2=PhotonFluence*sH2O2at193*H2O2_0*1.5
OHfromH2O = PhotonFluence*sH2Oat193*H2O_0
HfromH2O=OHfromH2O
OfromH2O2=PhotonFluence*sH2O2at193*H2O2_0*0.16
OfromO2 = PhotonFluence*sO2at193*O2_0*2
CH3fromAcetone=PhotonFluence*sAcetoneat193*Acetone_0*2*0.95
CH3OfromCH3OH=PhotonFluence*sCH3OHat193*CH3OH
HfromCH3OH=PhotonFluence*sCH3OHat193*CH3OH

N2O=N2O_0+delN2O
H2O=H2O_0+delH2O
O2=O2_0+delO2
CH4=CH4_0+delCH4
CH3OH=CH3OH_0+delCH3OH
```

```
Cl2=Cl2_0
OHini1=O1Dini*(2*fH2Och1+fCH4ch1+fH2+fAcetone+fH2O2)
OHini2=OHfromH2O+OHfromH2O2
OHini=OHini1+OHini2
Hini= O1Dini*(fCH4ch3+fH2)+HfromH2O+HfromCH3OH
//Oini= O1Dini*(fN2Och3+fO2)+OfromO2+OfromH2O2
Oini=O1Dini*fO2+OfromO2
CH3ini=O1Dini*fCH4ch1+CH3fromAcetone
HO2ini=O1Dini*fH2O2
NOini=O1Dini*2*fN2Och1
HONOini=0
CH2ini=0
H2O2ini=H2O2_0+delH2O2
Acetoneini=Acetone_0-delAcetone
O3ini=0
CH3Oini=CH3OfromCH3OH
CH2OHini=0
CH3O2ini=0
ClOini=0
CH2OOini=0

//_____________________________________________________________
//Wall Reactions

// Diffusion coefficient 0.88 bar cm2 s-1 according to Ivanov et al at 296
// Temperature dependence T^1.6 is ASSUMED
// 0.146 is R^2 (R =0.76 cm/2)

kwOH = (5.748/0.146)*(0.88/p)*(T/296)^1.6
kwO=0
kwH=0
kwHO2=0

//_____________________________________________________________
// Reaction Mechanism


//CH3 + HO2 --> CH3O + OH          (1a)
//CH3 + HO2 --> CH2O + H2O         (1b)
//CH3 + HO2 --> CH3OOH             (1c)
//CH3 + HO2 --> CH4 + O2           (1d)
//CH3 + HO2 --> CH4 + O2(1 Delta)  (1e)
// OH + CH3 --> H2O + CH2          (3a)
// OH + CH3  --> CH3OH             (3b)
// OH+OH --> H2O + O               (4a)
// OH+OH --> H2O2                  (4b)
```

// OH + CH4 --> H2O + CH3 (5)
// CH3 + CH3 --> C2H6 (6)
// OH + O --> O2 +H (7a)
// OH + O --> HO2 (7b)
// OH + H --> H2 + O (8a)
// OH + H --> H2O (8b)
// CH3 + O --> H2CO + H (9)
// OH + NO --> HONO (10)
// CH3 + H --> CH4 (11)
// OH + CH2 --> CH2O + H (12)
// OH + (CH3)2CO -->(CH3)(CH2)CO+H2O (13)
// OH + H2O2 --> H2O + HO2 (14)
// OH + HO2 --> H2O + O2 (15)
// HO2 + NO --> OH + NO2 (16)
// CH3 + NO -->CH3NO (17)
// CH3 + H2O2 --> CH4 + HO2 (18)
// O + HO2-->O2+OH (19)
// O + H2O2--> OH + HO2 (20)
// H + HO2 --> H2 +O2 (21a)
// H + HO2 --> 2 OH (21b)
// H + HO2 --> H2O + O (21c)
// H + HO2 --> O(1D) +H2O (21d)

// O + O2 <-> O3 (30) reversible
// H + O2 --> OH + O (31a)
// H + O2 --> HO2 (31b)
// HO2 + O2 --> OH + O3 (32)
// OH +O3 --> HO2 + O2 (35)
// O + O3 --> O2 + O2 (36)
// H + O3 --> OH + O2 (37)
// HO2 + O3 --> OH + O2 + O2 (38)
// HO2 + HO2 -->H2O2+O2 (39)
// O3 + NO --> NO2 + O2 (40)

//CH3 + CH3COCH3 --> CH4 + CH3COCH2 (50)

//Reactions of Methoxy Radical, CH3O
// CH3O --> CH2OH (60a)
// CH3O --> CH2O + H (60b)
// CH3O + N2O --> products (61)
// CH3O + H2O2 --> products (62)
// CH3O + CH4 --> CH3OH + CH3 (63)
// CH3O + HO2 --> CH2O + H2O2 (64)
// CH3O + CH3 --> CH2O + CH4 (65a)
// CH3O + CH3 --> (CH3)2O (65b)
// CH3O + CH3O --> CH3OH + CH2O (66a)

// CH3O + CH3O --> (CH3O)2 (66b)
// CH3O + OH --> CH2O + H2O (67a)
// CH3O + OH --> CH3OOH (67b)
// CH3O + O --> CH2O + OH (68a)
// CH3O + O --> CH3 + O2 (68b)
// CH3O + O --> CH3OO (68c)
// CH3O + H --> CH2O + H2 (69a)
// CH3O + H --> CH3OH (69b)
// Cl + CH3OH --> HCl + CH2OH (70a)
// Cl + CH3OH --> HCl + CH3O (70b)
// CH2OH + O2 --> CH2O + HO2 (71)
// CH3O + O2 --> CH2O + HO2 (72)
// CH3 + O2 --> CH3O2 (73)
// Cl + CH4 --> HCl+CH3 (74)
// Cl + CH3 --> CH3Cl (75)

// Reactions of Methyl peroxy radical, CH3O2
// * labeles reactions important in the CH3O2 concentration profiles

// CH3 + CH3O2 --> CH3O + CH3O (76) *
// OH + CH3O2 --> CH3OH + O2 (77) *
// O + CH3O2 -->CH3O+O2 (78)
// H + CH3O2 -->CH3O + OH (79a)
// H + CH3O2 --> CH4 + O2 (79b)
// HO2 + CH3O2 -->CH3OOH + O2 (80) *
//CH3O2 + CH3O2 --> products (81)
// CH3O2 + CH3O2 --> CH3O+CH3O + O2 (81a)
// CH3O2 + CH3O2 --> CH2O+CH3OH + O2 (81b)
//CH3O2+CH3O2 --> (CH3O)2 + O2 (81c)
// Cl + CH3O2 --> CH3O + ClO (82a) marginal importance at early stages
// Cl+CH3O2 -> HCl + CH2OO (82b) marginal importance at early stages
// CH3O2 + CH3O -->CH3OOH+CH2O (83)
//HO2+(COCl)2 --> products (90)
//CH2OH+Cl-->HCl+CH2O (91)
//CH2OH+CH3-->CH4+CH2O (92)
// Cl + Cl --> Cl2 (100)
// CH3 + Cl2 --> CH3Cl + Cl (101)
//_____

//Rate Constants

//CH3 + HO2 --> CH3O + OH (1a)
//CH3 + HO2 --> CH2O + H2O (1b)
//CH3 + HO2 --> CH3OOH (1c)
//CH3 + HO2 --> CH4 + O2 (1d)
//CH3 + HO2 --> CH4 + O2(1 Delta) (1e)

```
// According to Jasper et al., 2009, the only important channels are
// channel 1a, 1c and 1d.
// This is reaction under study. k1=k1a+k1b+k1c+k1d+k1e
// According to Jasper et al., 2009, the branching ratio between 1a and 1d
// is k1a/(k1a+k1d)=0.7 at 300 K (obtained approximately from Figures).
// for now we will leave only these two channels, 1a and 1d
alpha1a=0.7
k1ad=3.7e-11
k1a=k1ad*alpha1a
k1b=0
k1c=0
k1d=k1ad*(1-alpha1a)
k1e=0
k1=k1a+k1b+k1c+k1d+k1e

// OH + CH3 --> H2O + CH2                    (3a) ***
// OH + CH3  --> CH3OH                       (3b)***
// Our work 2012, pressure independent 1 - 100 bar
k3=1.2e-10*(T/300)^(-0.49)

// OH+OH --> H2O + O                         (4a)
// Low T <420K 1999 Bedjanian et al, high T>550K  - our data 2011
// fit of the data that were submitted in the final version
//k4a=1.07e-12*(1+1.0e-4*((T-483)^2))^0.2

// Our study, 2012. 296 - 414 K, 1 bar - 100 bar
k4a=1.39e-12*(T/298)^(-0.76)

// OH+OH --> H2O2                            (4b)
// 2011 Sangwan et al.
k04b=9.0e-31*(T/300)^(-3.5)
kinf4b=2.4e-11*(T/300)^(-0.5)
Fcent4b=0.37
x4b=k04b*M/kinf4b
c4b=-0.4-0.67*Log10(Fcent4b)
N4b=0.75-1.27*Log10(Fcent4b)
d=0.14
y4b=Log10(x4b)+c4b
LF4b=Log10(Fcent4b)/(1+(y4b/(N4b-d*y4b))^2)
F4b=10^LF4b
k4b=kinf4b*F4b*x4b/(1+x4b)
//This generates k4b=4.4e-12 at 1 bar 1nd 298 K
// Our direct value is (6.2-1.4)e-12

// Our study, 2012. 296-834 K, 1bar -100 bar
//k4b=M*9.21e-31*(T/298)^(-0.35)
```

```
// OH + CH4 --> H2O + CH3                    (5)
// 2005SRI/SU
k5=4.16e-13*(T/298)^2.18*exp(-1232/T)

// CH3 + CH3 = C2H6                         (6) ***
// Our study 2012, for 1 bar
k6=5.66e-11*(T/298)^(-0.37)

//OH + O -->  O2   +H                       (7a) *
// 2004 ATK/BAU
k7a=2.4e-11*exp(109/T)

// OH + O --> HO2                           (7b) *
// No data, set as OH+H
k7b=M*1.6e-31*(T/298)^(-2.6)

//OH + H --> H2   +    O                    (8a)
//86TSA/HAM
//k8a = 6.86e-14*(T/298)^2.8*exp(-1950/T)
k8a=0

//OH + H --> H2O                           (8b)
//77 ZEL/ERL
k8b=M*1.6e-31*(T/298)^(-2.6)

// CH3 + O --> H2CO    +  H                 (9) ***
//1992ATK
k9= 1.4e-10

// OH   + NO  --> HONO                      (10)

k010=3.9e-31*(T/298)^(-2.6)
kinf10=3.3e-11
Fcent10=1.23*exp(-T/815)
x10=k010*M/kinf10
c10=-0.4-0.67*Log10(Fcent10)
N10=0.75-1.27*Log10(Fcent10)
d=0.14
y10=Log10(x10)+c10
LF10=Log10(Fcent10)/(1+(y10/(N10-d*y10))^2)
F10=10^LF10
k10=kinf10*F10*x10/(1+x10)

// CH3 + H  --> CH4                         (11) **
//Pilling1997
```

```
k011=6.2e-29*(T/298)^(-1.8)
kinf11=3.5e-10
Fcent11=0.638*exp(-T/3231)
x11=k011*M/kinf11
c11=-0.4-0.67*Log10(Fcent11)
N11=0.75-1.27*Log10(Fcent11)
d=0.14
y11=Log10(x11)+c11
LF11=Log10(Fcent11)/(1+(y11/(N11-d*y11))^2)
F11=10^LF11
k11=kinf11*F11*x11/(1+x11)

// OH  +  CH2  -->  CH2O + H                    (12)
//1986TSA/HAM
k12=3e-11

// OH  +  (CH3)2CO  -->(CH3)(CH2)CO+H2O        (13) *
//2003YAM/TAY
k13=3.15e-14*(T/300)^4*exp(453/T)

// OH + H2O2 --> H2O + HO2                     (14)
//2004JIM/GIE
k14=2.9e-12*exp(-109/T)

// OH + HO2 -->  H2O + O2                      (15) *
//1988KEY
k15=4.8e-11*exp(250/T)

// HO2 + NO --> OH + NO2                       (16)
//2003BAR/BAC
k16=4e-12*exp(223/T)

//CH3 + NO -->CH3NO                            (17)
//1991 Pilling Ar
//A.H.Langer,A.M.Bass.Int.J.Chem.Kin.V.7,639-648(1975) kHe=kAr
k017=6.9e-32*exp(1430/T)
kinf17=1.5e-11*exp(-60/T)
Fcent17=5*exp(-T/120)
x17=k017*M/kinf17
c17=-0.4-0.67*Log10(Fcent17)
N17=0.75-1.27*Log10(Fcent17)
d=0.14
y17=Log10(x17)+c17
LF17=Log10(Fcent17)/(1+(y17/(N17-d*y17))^2)
F17=10^LF17
k17=kinf17*F17*x17/(1+x17)
```

```
//CH3 + H2O2 -->   CH4 + HO2                (18)
//1986TSA
k18=2e-14*exp(300/T)

//O + HO2-->O2+OH                           (19) *
//2004ATK/BAU
k19= 2.70E-11*exp(1860/8.31447/T)

//O + H2O2--> OH + HO2                      (20)
//2004ATK/BAU
k20 =1.40E-12*exp(-16630/8.31447/T)

//H + HO2 --> H2 +O2                        (21a)
//1992 BOU/COB
k21a=7.11E-11*exp(-5900/8.31447/T)

//H + HO2 --> 2 OH                          (21b)
//1992Bau/COB
k21b=2.81E-10*exp(-3660/8.31447/T)

//H + HO2 --> H2O + O                       (21c)
//1992 BAU/COB
k21c=5.00E-11*exp(-7200/8.31447/T)

//H + HO2 --> O(1D) +H2O                    (21d)
//2007MOU/SAH1901-1913
// A theoretical paper - important reaction, thou!
// Will be used as H + HO2 --> 2OH +H2O
k21d=3.29E-12*(T/298)^1.55*exp(670/8.31447/T)

// O + O2 --> O3                            (30) ***
// Hippler, Rahn, Troe 1990 (on He)
k30 = M*3.4e-34*(T/300)^(-1.2)

//Equilibrium constant from dHf298(O3)=141.746 kJmol-1
//(from Active Thermo Tables), O and O2 fro GRI, and
// the rest for ozone from NIST WebBook.
Keq30=4.0007e-9*(T/298)^(-1.37313)*exp(14123.53/T)
kfkr30=Keq30*10*8.31451*T/6.022e23

// H + O2 --> OH + O                         (31a)
//1994 Bau/Cob
//Plays role only at high T
k31a = 1.62E-10*exp(-62110/8.31447/T)
```

```
// H + O2 --> HO2                          (31b) ****
// 1997ATK/BAU (for N2):
k31b = M*5.4E-32*(T/298)^(-1.80)

// HO2 + O2 --> OH + O3                    (32)
// This reaction is ENDOTHERMIC by ca. 180 kJ mol-1
// Plays absolutely no role
k32=0

// OH +O3 --> HO2 + O2                     (35)
// 2004 ATK/BAU
k35 = 1.7E-12*exp(-7820/8.31447/T)

// O + O3 --> O2 + O2                      (36)
// 2001 ATK/BAU
k36=8.0E-12*exp(-17130/8.31447/T)

// H + O3 --> OH + O2                      (37)
// 1989 ATK/BAU
k37=1.4E-10*exp(-3990/8.31447/T)

// HO2 + O3 --> OH + O2 + O2               (38)
// 2004 ATK/BAU
k38 =1.97E-16 *(T/298)^4.57*exp(5760/8.31447/T)

// HO2 + HO2 -->H2O2+O2                    (39)
//2004 ATK/BAU
k39=2.2e-13*exp(4990/8.31447/T)+5.2e-32*M

// O3 + NO --> O2 + NO2                    (40)
// 2004 Atk/Bau  k40 at  298 = 1.80E-14
// Does not play any role at 298
// Not taken into account
k40=0

//CH3 + CH3COCH3 --> CH4 + CH3COCH2        (50)
// my fit from NIST database
k50= 1.06e-12*exp(-42720/8.31447/T)

// CH3O --> CH2OH                          (60a)
// 1981 BAT/BUR
k60a = 1e13*exp(-109000/8.31447/T)

// CH3O --> CH2O + H                       (60b)
// 1994 BAU/COB
k60b = 9e-11*exp(-56460/8.31447/T)
```

```
// CH3O + N2O --> products                    (61)
//1980 SUN/BUT k61 < 1.66e-14 at 298 K
//k61=1.66e-14
k61=0

// CH3O + H2O2 --> CH3OH + HO2                (62)
// 1987 TSA k62 = 5e-15*exp(-10810/8.31447/T)
k62 = 5e-15*exp(-10810/8.31447/T)

// CH3O + CH4 --> CH3OH + CH3                 (63)
// 1989 WAN/OLD
k63 = 2.2e-10*exp(-63020/8.31447/T)

// CH3O + HO2 --> CH2O + H2O2                 (64)
// 1986 TSA
k64=5e-13

// CH3O + CH3 --> CH2O + CH4                  (65a)
// 1986 TSA/HAM
k65a=4e-11

// CH3O + CH3 --> (CH3)2O                     (65b)
// 1979 HAS/KOS
k65b=5.5e-11

// CH3O + CH3O --> CH3OH + CH2O               (66a) *
// 1979 HAS/KOS
k66a=3.85e-11

// CH3O + CH3O --> (CH3O)2                    (66b)
// 1986 TSA/HAM
k66b=3e-12

// CH3O + OH --> CH2O + H2O                   (67a)
// 1986 TSA
k67a=3e-11

// CH3O + OH --> CH3OOH                       (67b)
// not known
k67b=0

// CH3O + O --> CH2O + OH                     (68a)
// 1987 TSA
k68a=1e-11
```

```
// CH3O + O --> CH3 + O2                (68b) *
//1987 ZEL
k68b=2.5e-11

// CH3O + O --> CH3OO                   (68c)
// not known
k68c=0

// CH3O + H --> CH2O + H2               (69a)
//1991 DOB/BER
k69a=3.3e-11

// CH3O + H --> CH3OH                   (69b)
// not known
k69b=0

// Cl + CH3OH --> HCl + CH2OH           (70a)
// 2001 Atk/Bau k70a = 5.5e-11 temperature independent
k70a = 5.5e-11

// Cl + CH3OH --> HCl + CH3O            (70b)
// 1994 DOB/BER k70b=0.01*k70a
k70b=0.01*k70a
// CH2OH + O2 --> CH2O + HO2            (71)
// 2001 ATK/BAU k71 = 0.95e-11
k71=0.95e-11

// CH3O + O2 --> CH2O + HO2             (72) **
// 2003ORL/TYN
k72=7.82e-14*exp(-9560/8.31447/T)

// CH3 + O2 --> CH3O2                   (73) *****
// 1992ATK/BAU1125-1568
k073=1.0e-30*(T/300)^(-3.30)
kinf73=1.21e-12*(T/300)^1.20
// Fc from Fernandes RX, Luther K, Troe J. 2006
Fcent73=0.33
x73=k073*M/kinf73
c73=-0.4-0.67*Log10(Fcent73)
N73=0.75-1.27*Log10(Fcent73)
d=0.14
y73=Log10(x73)+c73
LF73=Log10(Fcent73)/(1+(y73/(N73-d*y73))^2)
F73=10^LF73
k73=kinf73*F73*x73/(1+x73)
```

```
//Equilibrium constant from fitting Gutman's data (1985)
// at P0=1 atm
lKeq73 = -15.5144+15.97615e3/T
Keq73=exp(lKeq73)

kfkr73=Keq73*10*8.31451*T/6.022e23/1.01325

// Cl + CH4 --> HCl + CH3                    (74)
// 2002BRY/SLA
k74 =8.24E-13*(T/298)^2.49*exp(-5060/8.31447/T)

// Cl + CH3 --> CH3Cl                        (75)
//2007PAR/PAY
k75=6.11e-11
//1986TIM/KOS
//k75=2.56e-10

//Reactions of CH3O2

// CH3 + CH3O2 --> CH3O + CH3O               (76) ***
//1985PIL/SMI4713
k76=4.5e-11
// OH + CH3O2 --> CH3OH + O2                 (77) ***
//1986TSA/HAM1087
//k77=1.0e-10
//According the Christa Fittschen talk on ICCK 2015
// The main channel is OH + CH3O2 --> CH3O + HO2, k77 = 2.3e-10
//k77=2.3e-10

// O + CH3O2 -->CH3O+O2                      (78) *
//1987ZEL403-407
//k78=6.0e-12
//1988ZEL
k78=4.3e-11

// H + CH3O2 -->CH3O + OH                    (79a) *
//1986TSA/HAM1087
k79a=1.6e-10

// H + CH3O2 --> CH4 + O2                    (79b)
// 2004BOG/BAK486-490
//k79b=7.83E-24 activation energy 69 kJ mol-1, NEGLECTED

// HO2 + CH3O2 -->CH3OOH + O2                (80) *
//2001ATK/BAU1-56
k80=3.80E-13*exp(6650/8.31447/T
```

```
//CH3O2 + CH3O2 --> products                (81) *
//2001ATK/BAU1-56 total rate constant
k81=1.00E-13*exp(3030/8.31447/T)

// CH3O2 + CH3O2 --> CH3O+CH3O + O2 (81a)
//2001ATK/BAU1-56
k81a=7.40E-13*exp(-4320/8.31447/T)

// CH3O2 + CH3O2 --> CH2O+CH3OH + O2        (81b)
//1994BAU/COB847-1033
k81b=k81/(1+25*exp(-9730/8.31447/T))

//CH3O2+CH3O2 --> (CH3O)2 + O2          (81c)
//1989ATK/BAU881-1097
//k81c < 1e-14 NEGLECTED

// Cl + CH3O2 --> CH3O + ClO                (82a)
//1994DEM/SAN
k82a=7.7e-11
// Cl+CH3O2 -> HCl + CH2OO                  (82b)
// 1995 JUN/KUK
k82b=5.6e-11

// CH3O2 + CH3O -->CH3OOH+CH2O       (83)
//1986TSA/HAM1087, estimate
// our measurment
k83=1.82e-11

// HO2+(COCl)2 --> products                 (90)
//unknown
k90=0

//CH3+Cl2 -->CH3Cl + Cl                    (101)
//Timonen 2008
k101=1.55e-12

//Important Reactions : * >1% of r77 max, **>5%, *** comparable with r77 Max, and
***** exceeds at least several times

//        Max rate, 1/(cm3 sec) Relative to r77 max
//R3CALC      1.82788724E17         0.6379570762 ***
//R6CALC      7.74159206E17         2.7019190943 ***
//R7ACALC     7.47607636E15         0.0260925057 *
//R9CALC      2.7114581E17 0.9463351152 ***
//R11CALC     2.80850688E16         0.0980206436 **
```

```
//R13CALC    3.20364926E15       0.0111811641 *
//R15CALC    5.60099183E15       0.0195482101 *
//R19CALC    5.90241596E15       0.0206002206 *
//R30CALC    1.41874235E17       0.4951600415 ***
//R31BCALC   1.80513874E18       6.300175457          ****
//R66ACALC   4.51950862E15       0.0157736891 *
//R68BCALC   2.30629149E15       0.0080492655 *
//R72CALC    1.60867406E16       0.0561448747 **
//R73CALC    7.68752604E19       268.3049330746       *****
//R76CALC    1.48655354E17       0.5188270531 ***
//R77CALC    2.86521979E17       1.0000000000 ***
//R78CALC    1.01322123E16       0.0353627751 *
//R79ACALC   3.87344526E15       0.0135188416 *
//R80CALC    8.32897046E15       0.0290692201 *
//R81CALC    4.30397381E15       0.0150214438 *
//R81BCALC   2.95932298E15       0.0103284327 *

//_____________________________________________________________
//System of Ordinary Differential Equations


//Species "transient":  CH3, HO2, OH,O, H,O3,NO,HONO,CH2, H2O2,CH3O, CH3O2
// Acetone, N2O
//Species initially present: N2O, H2O, CH4, H2O2, Acetone
//Reaction Rates:

r1a=k1a*CH3*HO2
r1b=k1b*CH3*HO2
r1c=k1c*CH3*HO2
r1d=k1d*CH3*HO2
r1e=k1e*CH3*HO2
r1=k1*CH3*HO2
r3=k3*OH*CH3
r4a=k4a*OH*OH
r4b=k4b*OH*OH
r5=k5*OH*CH4
r6=k6*CH3*CH3
r7a=k7a*OH*O
r7b=k7b*OH*O
r8a=k8a*OH*H
r8b=k8b*OH*H
r9=k9*CH3*O
r10=k10*OH*NO
r11=k11*CH3*H
r12=k12*OH*CH2
r13=k13*OH*Acetone
```

r14=k14*OH*H2O2
r15=k15*OH*HO2
r16=k16*HO2*NO
r17=k17*CH3*NO
r18=k18*CH3*H2O2
r19=k19*O*HO2
r20=k20*O*H2O2
r21a=k21a*H*HO2
r21b=k21b*H*HO2
r21c=k21c*H*HO2
r21d=k21d*H*HO2
r30=k30*(O*O2-O3/kfkr30)
r31a=k31a*H*O2
r31b=k31b*H*O2
r32=k32*HO2*O2
r35=k35*OH*O3
r36=k36*O*O3
r37=k37*H*O3
r38=k38*HO2*O3
r39=k39*HO2*HO2
r40=k40*O3*NO
r50=k50*CH3*Acetone
r60a=k60a*CH3O
r60b=k60b*CH3O
r61=k61*CH3O*N2O
r62=k62*CH3O*H2O2
r63=k63*CH3O*CH4
r64=k64*CH3O*HO2
r65a=k65a*CH3O*CH3
r65b=k65b*CH3O*CH3
r66a=k66a*CH3O*CH3O
r66b=k66b*CH3O*CH3O
r67a=k67a*CH3O*OH
r67b=k67b*CH3O*OH
r68a=k68a*CH3O*O
r68b=k68b*CH3O*O
r68c=k68c*CH3O*O
r69a=k69a*CH3O*H
r69b=k69b*CH3O*H
r70a=k70a*Cl*CH3OH
r70b=k70b*Cl*CH3OH
r71=k71*CH2OH*O2
r72=k72*CH3O*O2
r73=k73*(CH3*O2-CH3O2/kfkr73)
r74=k74*Cl*CH4
r75=k75*Cl*CH3

```
r76=k76*CH3O2*CH3
r77=k77*CH3O2*OH
r78=k78*CH3O2*O
r79a=k79a*CH3O2*H
r80=k80*CH3O2*HO2
r81=k81*CH3O2*CH3O2
r81a=k81a*CH3O2*CH3O2
r81b=k81b*CH3O2*CH3O2
r82a=k82a*CH3O2*Cl
r82b=k82b*CH3O2*Cl
r83=k83*CH3O2*CH3O
r90=k90*HO2*OxCl
r101=k101*CH3*Cl2
rOH1=r1a-r3-2*r4a-2*r4b-r5-r7a-r7b-r8a-r8b-r10-r12-r13-r14-r15
rOH2=r16+r19+r20+2*r21b+r31a+r32-r35+r37+r38-r67a-r67b+r68a-r77+r79a

// ODE System

OH'=rOH1+rOH2-kwOH*OH
CH3'=-r1-r3+r5-2*r6-r9-r11-r17-r18-r50+r63-r65a-r65b+r68b-r73+r74-r75-r76-r101
rHO21=-r1+r7b+r14-r15-r16+r18-r19+r20-r21a-r21b-r21c-r21d+r31b-r32+r35-r38-
2*r39-r64
rHO22=r71+r72+r77-r80-r90
HO2'=rHO21+rHO22
O'=r4a-r7a-r7b+r8a-r9-r19-r20+r21c-r30 +r31a-r36-r68a-r68b-r68c-r78-kwO*O
H'=r7a-r8a-r8b+r9-r11+r12-r21a-r21b-r21c-r21d-r31a-r31b-r37+r60b-r69a-r69b-r79a-
kwH*H
H2O2'=r4b-r14-r18-r20+r39-r62+r64
Acetone'=-r13-r50
O3'=r30+r32-r35-r36-r37-r38-r40
NO'=-r10-r16-r17
HONO'=r10
//for CH2 it is assumed that reaction 3 produces CH2 ONLY
CH2'=r3-r12
Cl'=-r70a-r70b-r74-r75 -r82a-r82b+r101
CH3O2'=r73-r76-r77-r78-r79a-r80-2*r81a-2*r81b-r82a-r82b-r83
rCH3O1=r1a-r60a-r60b-r61-r62-r63-r64-r65a-r65b-2*r66a-2*r66b
rCH3O2=-r67a-r67b-r68a-r68b-r68c-r69a-r69b+r70b-
r72+2*r76+r77+r78+r79a+2*r81a+r82a
CH3O'=rCH3O1+rCH3O2
CH2OH'=r60a+r70a-r71
ClO'=r82a
CH2OO'=r82b
O2=O2_0
CH3OH=CH3OH_0
N2O=N2O_0
```

```
Acetone=Acetone_0
H2O=H2O_0
H2=H2_0
CH4=CH4_0
OxCl=OxCl_0+delOxCl

//_____________________________________________________________
// Transient Absorptions

N2Otrans= delN2O
OxCltrans=delOxCl
H2O2trans=H2O2-H2O2_0
Acetonetrans=Acetone-Acetone_0

Abs216c1=L*(sCH3at216*CH3+sHO2at216*HO2+sH2O2at216*H2O2trans+sCH3O2at
216*CH3O2)
Abs216c2=L*(sHONOat216*HONO+sN2Oat216*N2Otrans+sO3at216*O3)
Abs216c3=L*(sAcetoneat216*Acetonetrans)
Abs216c4=L*(sOxClat216*OxCltrans)
Abs216=Abs216c1+Abs216c2+Abs216c3+Abs216c4
Abs216fromHO2=L*sHO2at216*HO2

Abs224c1=L*(sCH3at224*CH3+sHO2at224*HO2+sH2O2at224*H2O2trans+sCH3O2at
224*CH3O2)
Abs224c2=L*(sHONOat224*HONO+sN2Oat224*N2Otrans+sO3at224*O3)
Abs224c3=L*(sAcetoneat224*Acetonetrans)
Abs224c4=L*sOxClat224*OxCltrans
Abs224=Abs224c1+Abs224c2+Abs224c3+Abs224c4

Abs230c1=L*(sCH3at230*CH3+sHO2at230*HO2+sH2O2at230*H2O2trans+sCH3O2at
230*CH3O2)
Abs230c2=L*(sHONOat230*HONO+sN2Oat230*N2Otrans+sO3at230*O3)
Abs230c3=L*(sAcetoneat230*Acetonetrans)
Abs230c4=L*sOxClat230*OxCltrans
Abs230=Abs230c1+Abs230c2+Abs230c3+Abs230c4

Abs254c1=L*(sCH3at254*CH3+sHO2at254*HO2+sH2O2at254*H2O2trans+sCH3O2at
254*CH3O2)
Abs254c2=L*(sHONOat254*HONO+sN2Oat254*N2Otrans+sO3at254*O3)
Abs254c3=L*(sAcetoneat254*Acetonetrans)
Abs254c4=L*sOxClat254*OxCltrans
Abs254=Abs254c1+Abs254c2+Abs254c3

Abs308c1=L*(sOHat308*OH+sCH3O2at308*CH3O2)
Abs308c2=L*sOxClat308*OxCltrans
Abs308=Abs308c1+Abs308c2
```

```
//_____________________________________________________________________

//F216_1=A216_1
//F216=Abs216+ZeroShift216

//F224_1=A224_1
//F224=Abs224+ZeroShift224

F308=Abs308+ZeroShift308

//F254=Abs254+ZeroShift254
gate=UNIT(TIME-t1)*UNIT(t2-TIME)
//A216=(1-gate)*F216_1+gate*F216
A308=(1-gate)*A308_1+gate*F308
//A254=(1-gate)*A254_1+gate*F254

//Initial Conditions

TIME=0

CH3=CH3ini
HO2=HO2ini
OH=OHini
O=Oini
H=Hini
H2O2=H2O2ini
O3=O3ini
NO=NOini
HONO=HONOini
CH2=CH2ini
Acetone=Acetoneini
CH2OH=CH2OHini
CH3O=CH3Oini
Cl=Clini
CH3O2=CH3O2ini
ClO=ClOini
CH2OO=CH2OOini

//Initial Parameters and Constraints

k77=8e-11
//k77=8.21e-11
ZeroShift308=0
PhotonFluenceFactor=1
```

A.3. This model produces the rate constant CH3+Cl

```
// CH3_Cl.eqn.  v.2. Chao Y, 11/30/16
// Reaction CH3+Cl
// Photolysis of (COCl)2/Acetone/He at 193.3 nm
// Observation at 216.4

// Time should be in the 1-st column, signal (absorbance) - in 2-nd and 3-rd

IndVars: TIME, SIGNAL1
DepVars: SIGNAL, Cl
Params:   PhotonFluenceFactor, k75b
//_____

//Only information between the two dashed lines may be changed
// from experiment to experiment

//Cross-sections: 193=193.3 nm, 216=216.4 nm, 230=230 nm, 254=253.6

// Cross-sections of CH3 at 1 bar, 298 K
// Our measurements
//sCH3at216=3860e-20
sCH3at224=0
sCH3at230=0
sCH3at254=0
// At 555 K
sCH3at216=2550e-20

// Cross-sections of Oxalyl Chloride, 1 bar, 298 K
// Baklanov, Krasnoperov
//sOxClat193=383e-20
// At 558K
sOxClat193 = 478e-20
sOxClat216=130e-20
sOxClat224=85e-20
sOxClat240=39e-20

// Cross-sections of C2H5, 1 bar, 298 K
// Khamaganov(2007)
sC2H5at216=3e-18

// Cross-section of Acetone, 1 bar, 298 K
// Our measurements
//sAcetoneat193=334e-20
// at 414 K
//sAcetoneat193=447e-20
```

// At 555 K
sAcetoneat193=534e-20
//old our measurement (paper with Kashyap Mehta):3.23e-16 at 1 bar He 298K
// Gierczak et al., 1998
sAcetoneat216=0.186e-20
sAcetoneat224=0.346e-20
sAcetoneat230=0.584e-20
sAcetoneat254=2.82e-20
//sAcetoneat222 come from sAcetoneat216 and Acetoneat224
sAcetoneat222=0.306e-20

//_____
// Conditions//Time Window for fit (all in sec)

t1=30e-6
t2=200e-6

//Path length (cm)
L=10.00

// Conditions:
// Date 01/16/17 Exp 9
// (COCl)2/Acetone/O2/He 1 bar

p=1.026
T=558
M=2.429e19*(298.15/T)*p

H2O2_0=0
H2_0=0
CH3_0=0
OxCl_0=2.96e15
CH3OH_0=0
Acetone_0=2.32e15
H2O_0=0
CH4_0=0
O2_0=0
PhotonFluence_0 =2.19e15

TotalAbsorbance193=L*sOxClat193*OxCl_0+L*sAcetoneat193*Acetone_0

//Linear approximation for A193 < 0.2
PhotonFluence = PhotonFluence_0*exp(-TotalAbsorbance193)*PhotonFluenceFactor

ZeroShift216=0

```
//_____________________________________________________________
//Initial Conditions Calculations

//_____________________________________________________
//Quantum Yields

// Photolysis of OxCl at 193.3 nm. Fi(Cl)=2.
// Photolysis of Acetone at 193.3. Fi(CH3)=0.95*2

Clini=PhotonFluence*sOxClat193*OxCl_0*2
delAcetone=-PhotonFluence*sAcetoneat193*Acetone_0
delCH4=0
delOxCl=-PhotonFluence*sOxClat193*OxCl_0
CH3fromAcetone=2*PhotonFluence*sAcetoneat193*Acetone_0*0.95
CH4=CH4_0+delCH4
CH3ini=CH3fromAcetone
CH3Clini=0
C2H6ini=0
Cl2ini=0
COini=PhotonFluence*sOxClat193*OxCl_0*2
COClini=0
C2H5ini=0
OxClini=OxCl_0+delOxCl
Acetoneini=Acetone_0+delAcetone

//_____________________________________________________________
// Reaction Mechanism


// CH3 + CH3 --> C2H6                (6)
// Cl + CH3 --> CH2 + HCl            (75a)
// Cl + CH3 --> CH3Cl                (75b)
// Cl + Cl --> Cl2                   (79)
// CH3Cl + Cl --> CH2Cl + HCl        (82)
// C2H6 + Cl --> C2H5 + HCl          (83)
// CH3 + Cl2 --> CH3Cl + Cl          (97)
// CO + Cl --> COCl                  (99)
// COCl --> CO + Cl                  (100)
// COCl + Cl --> CO + Cl2            (101)
// C2H5+Cl-->C2H4+HCl                (102)
// C2H5+Cl-->C2H5Cl                  (103)
// C2H5+CH3-->C3H8                   (104)
// OxCl+CH3 --> p                    (105)
// Acetone+Cl --> Products           (106)
```

```
//_____________________________________________________
//Rate Constants

// CH3 + CH3 = C2H6                    (6)
// at 298 K k6 = 5.9e-11 assuming pressure independence
k6=5.66e-11*(T/298)^(-0.37)

// Cl + CH3 --> HCl + CH2              (75a)
// 1990GOL/TEM1367-1371
// k75a = 3.27E-17 at 298
// neglected

// Cl + CH3 --> CH3Cl                  (75b)
//  2007PAR/PAY1015-1023
//k75b=6.11e-11
//k75b=1.13e-10
// Our measurement 30bar and 100 bar
//k75b=2.9e-11

// Cl + Cl --> Cl2                     (79)
// HIP/TRO 1976
k79 = 4.69e-33*M

// CH3Cl + Cl --> CH2Cl + HCl          (82)
// 2009SAR/GOL
k82=1.7e-11*exp(-8647/8.31447/T)

// C2H6 + Cl --> C2H5 + HCl            (83)
// ATK/BAU 2001
k83=8.3e-11*exp(-830/8.31447/T)

//CH3+Cl2 -->CH3Cl + Cl               (97)
// Seetula, J.A. 1998
k97=2.93e-13*(T/298)^1.45*exp(-350/8.31447/T)

// CO+Cl --> COCl                      (99)
// ATK/BAU 2007
k99=M*1.33e-33

// COCl --> CO + Cl                    (100)
// ATK/BAU 2007
k100=4.1e-10*exp(-24610/8.31447/T)

// COCl+Cl-->CO+Cl2                    (101)
// BAU/DUX 1981
k101=2.16e-9*exp(-13891/8.31447/T)
```

// C2H5+Cl-->C2H4+HCl (102)
// SEA/WOO 1993
k102=3.01e-10

// C2H5+Cl-->C2H5Cl (103)
// TIM/KAL 1986
k103=4.55e-10

// C2H5+CH3-->C3H8 (104)
// BAU/COB 1994
k104=5.6e-11

// OxCl+CH3 --> p (105)
//estimate
//k105=1.67e-13

// Acetone+Cl --> p (106)
// 2008ZHA/HUS 259-267
k106=1.53e-11*exp(-4940/8.31447/T)

//_____
//System of Ordinary Differential Equations

//Species "transient": CH3, CH3Cl, C2H6, COCl, CO, Cl2, C2H5
//Species initially present: OxCl, Acetone

//Reaction Rates:

r6=k6*CH3*CH3
r75b=k75b*CH3*Cl
r79=k79*Cl*Cl
r82=k82*Cl*CH3Cl
r83=k83*Cl*C2H6
r97=k97*CH3*Cl2
r99=k99*CO*Cl
r100=k100*COCl*COCl
r101=k101*COCl*Cl
r102=k102*C2H5*Cl
r103=k103*C2H5*Cl
r104=k104*C2H5*CH3
r105=k105*OxCl*CH3
r106=k106*Acetone*Cl

// ODE System

```
CH3'=-2*r6-r75b-r97-r104-r105
Cl'=-r75b-2*r79-r82-r83+r97-r99+r100-r101-r102-r103
CH3Cl'=r75b-r82+r97
C2H6'=2*r6-r83
Cl2'=r79-r97+r101
CO'=-r99+r100+r101
COCl'=r99-r100-r101
C2H5'=r83-r102-r103-r104
Acetone'=-r106

//_____________________________________________________________
// Transient Absorptions


OxCltrans=delOxCl

A216=L*(sCH3at216*CH3+sOxClat216*OxCltrans+sC2H5at216*C2H5)
F216=A216+ZeroShift216

F1=SIGNAL1
F2=F216
gate=UNIT(TIME-t1)*UNIT(t2-TIME)
SIGNAL=(1-gate)*F1+gate*F2


//Initial Conditions

TIME=0

CH3=CH3ini
Cl=Clini
CH3Cl=CH3Clini
C2H6=C2H6ini
Cl2=Cl2ini
CO=COini
COCl=COClini
C2H5=C2H5ini
OxCl=OxClini
Acetone=Acetoneini

//Initial Parameters and Constraints
PhotonFluenceFactor=1.00
k75b=4.64e-11
k105=0
```

A.4. This model produces the rate constant CH3+HO2 and branching ratio

```
//CH3HO2_5.eqn.  v.5. C. Yan, 01/27/17
// Reaction CH3+ HO2
// Photolysis of (COCl)2/CH3OH/O2/CH4/He at 193.3 nm
// Observation at 216.4, 308nm and 224 nm

//Explicit HO2 concentration profiles

// Time should be in the 1-st column, signal (absorbance) - in 2-nd and 3-rd

IndVars: TIME, SIGNAL1
DepVars: SIGNAL
Params:  k1ad, PhotonFluenceFactor
//A216c1=L*(sCH3at216*CH3+sHO2at216*HO2+sH2O2at216*H2O2trans)
//A216c2=L*sO3at216*O3+L*sCH3O2at216*CH3O2
A1=L*sCH3at216*CH3
A2=L*sHO2at216*HO2
A3=L*sH2O2at216*H2O2trans
A4=L*sO3at216*O3
A5=L*sCH3O2at216*CH3O2
//_____________________________________________________________

//Only information between the two dashed lines may be changed
// from experiment to experiment

//Cross-sections: 193=193.3 nm, 216=216.4 nm, 230=230 nm, 254=253.6

//Cross-sections of H2O2 at 1 bar, 298 K (JPL-15)
sH2O2at193=60.1e-20
sH2O2at216=29.3e-20
sH2O2at224=22.5e-20
sH2O2at230=18.2e-20
sH2O2at254=7.1e-20
//sH2O2at222 come from sH2O2at216 and sH2O2at224
sH2O2at222=24.2e-20

//Cross-sections of HO2, at 1 bar, 298 K (JPL-15)
sHO2at193=390e-20
sHO2at216=373e-20
sHO2at224=299e-20
sHO2at230=230e-20
sHO2at254=32.4e-20
//sHO2at222 come from sHO2at216 and sHO2at224
sHO2at222=318e-20
```

```
//Cross-sections of N2O, at 1 bar, 298 K (JPL-15)
sN2Oat193=8.70e-20
sN2Oat216=0.205e-20
sN2Oat224=0.0375e-20
sN2Oat230=0.00955e-20
sN2Oat254=0
//sN2Oat222 come from sN2Oat216 and sN2Oat224
sN2Oat222=0.0794e-20

// Cross-sections of H2O
//Our measurement, 02/16/12/ exp 11
sH2Oat193=1.51e-21

// Cross-sections of O2
sO2at193=1.72e-22
sO2at222=3.4e-24

// Cross-section of O3 (JPL-15, actually - narrow bands, see JPL-15)
sO3at193=42.9e-20
sO3at216=118e-20
sO3at224=255e-20
sO3at230=490e-20
sO3at254=1148e-20*(T/298)^(-0.2303)
//sO3at222 come from sO3at216 and sO3at224
sO3at222=221e-20

// Cross-section of HONO at 1 bar, 298 K (JPL-15)
sHONOat193=155e-20
sHONOat216=176e-20
sHONOat224=121e-20
sHONOat230=84.5e-20
sHONOat254=15.0e-20

// Cross-sections of acetone at 1 bar, 298 K
// Our measurements
//sAcetoneat193=334e-20
//at 414 K
//sAcetoneat193=447e-20
// at 357 K
//sAcetoneat193=396e-20
// at 458
//sAcetoneat193=420e-20
// at 500 K
sAcetoneat193=500e-20
//old our measurement (paper with Kashyap Mehta):3.23e-16 at 1 bar He 298K
// Gierczak et al., 1998
```

```
sAcetoneat216=0.186e-20
sAcetoneat224=0.346e-20
sAcetoneat230=0.584e-20
sAcetoneat254=2.82e-20
//sAcetoneat222 come from sAcetoneat216 and Acetoneat224
sAcetoneat222=0.306e-20

// Cross-sections of CH3 at 1 bar, 298 K
// Our measurements
//sCH3at216=3860e-20
sCH3at224=0
sCH3at230=0
sCH3at254=0
// at 414 K
//sCH3at216=3220e-20
// at 357 K
//sCH3at216=3510e-20
// at 458 K
//sCH3at216=3020e-20
// at 500 K
sCH3at216=2810e-20

// Cross-sections of Oxalyl Chloride, 1 bar, 298 K
// Baklanov, Krasnoperov
//sOxClat193=383e-20
//sOxClat216=130e-20
sOxClat224=85e-20
//sOxClat240=39e-20
sOxClat254=23e-20
sOxClat308=7.2e-20
//sOxClat222 come from sOxClat216 and sOxClat224
//sOxClat222=96e-20

//at 414 K
//sOxClat193=455e-20
sOxClat216=78.4e-20
// at 357 K
//sOxClat193=431e-20
sOxClat222=0
//sOxClat216=104e-20
// at 458 K
//sOxClat193=463e-20
// at 500 K
sOxClat193=472e-20

// Cross-sections of Methanol, 1 bar, 298 K
```

```
// B.M. Cheng et al., 2002, see MPI-Mainz UV/Vis Spectral Atlas
sCH3OHat193=30.9e-20
sCH3OHat216=2.8e-22

//Cross-sections CH3O2, 1 bar, 298 K

//JPL-2006, at 308 -short extrapolation based on the Gaussian fitted to the tail
sCH3O2at216=291e-20
sCH3O2at224=367e-20
sCH3O2at230=408e-20
sCH3O2at254=348e-20
sCH3O2at308 = 20e-20
//sOxClat222 come from sOxClat216 and sOxClat224
sCH3O2at222=348e-20

// Cross-sections of OH, 1 bar, 298 K
// Sangwan et al.
sOHat308=4.23e-17

//_____
// Conditions//Time Window for fit (all in sec)
t1=40e-6
t2=150e-6

//Path length (cm)
L=10.00

// Conditions:
// Date 04/12/17 Exp 08
// (COCl)2/acetone/CH3OH/O2/He 1 bar

p=1.018
T=500
M=2.429e19*(298.15/T)*p

OxCl_0=2.18e15
CH3OH_0=6.84e15
Acetone_0=9.96e14
O2_0=4.13e15
PhotonFluence_0 =10.3e15

TotalAbsorbance193_1=L*(sOxClat193*OxCl_0+sAcetoneat193*Acetone_0)
TotalAbsorbance193_2=L*(sCH3OHat193*CH3OH_0+sO2at193*O2_0)
TotalAbsorbance193=TotalAbsorbance193_1+TotalAbsorbance193_2

PhotonFluenceFactor=1
```

```
// Exact calculation of average fluence along the reactor
FractionAbsorbed = 1-exp(-TotalAbsorbance193)
PhotonFluence_x=PhotonFluence_0*FractionAbsorbed/TotalAbsorbance193
PhotonFluence=PhotonFluence_x*PhotonFluenceFactor

ZeroShift216=0

//_____________________________________________________________
//Initial Conditions Calculations

//_____________________________________________________
//Quantum Yields

// Photolysis of water at 193 nm, Fi(H)=1, Fi(OH)=1,(JPL-15)
//Photolysis of oxygen at 193 nm. Both atoms are ground state O-atoms.
//(Okabe). Fi(O)=2
// Photolysis of OxCl at 193.3 nm. Fi(Cl)=2.
// Photolysis  of CH3OH at 193.3. Fi(CH3O+H)=0.98
// Chao: Fi(CH3+OH)= 0.02
Clini=PhotonFluence*sOxClat193*OxCl_0*2
delCH4=0
delOxCl=-PhotonFluence*sOxClat193*OxCl_0
delO2=-PhotonFluence*sO2at193*O2_0
delCH3OH=-PhotonFluence*sCH3OHat193*CH3OH_0
OfromO2 = PhotonFluence*sO2at193*O2_0*2
Factor=0.95
CH3OfromCH3OH=PhotonFluence*sCH3OHat193*CH3OH_0*Factor
HfromCH3OH=PhotonFluence*sCH3OHat193*CH3OH_0*Factor
CH3fromCH3OH=PhotonFluence*sCH3OHat193*CH3OH_0*(1-Factor)
OHfromCH3OH=PhotonFluence*sCH3OHat193*CH3OH_0*(1-Factor)
CH3fromAcetone=2*PhotonFluence*sAcetoneat193*Acetone_0*0.95
O2=O2_0+delO2
CH3OH=CH3OH_0+delCH3OH

OHini=OHfromCH3OH
Hini=HfromCH3OH
Oini=OfromO2
CH3ini=CH3fromAcetone+CH3fromCH3OH
HO2ini=0
CH2ini=0
O3ini=0
CH3Oini=CH3OfromCH3OH
CH2OHini=0
H2O2ini=0
CH3O2ini=0
Cl2ini=0
```

```
CH3Clini=0
C2H6ini=0

//_____________________________________________________________
//Wall Reactions

// Diffusion coefficient 0.88 bar cm2 s-1 according to Ivanov et al at 296
// Temperature dependence T^1.6 is ASSUMED
// 0.146 is R^2 (R =0.76 cm/2)

kwOH = (5.748/0.146)*(0.88/p)*(T/296)^1.6
kwO=0
kwH=0
kwHO2=0

//_____________________________________________________________
// Reaction Mechanism


//CH3 + HO2 --> CH3O + OH                (1a)
//CH3 + HO2 --> CH2O + H2O               (1b)
//CH3 + HO2 --> CH3OOH                   (1c)
//CH3 + HO2 --> CH4 + O2                 (1d)
//CH3 + HO2 --> CH4 + O2(1 Delta)        (1e)
// OH + CH3 --> H2O + CH2                (3a)
// OH + CH3  --> CH3OH                   (3b)
// OH+OH --> H2O + O                     (4a)
// OH+OH --> H2O2                        (4b)
// OH + CH4 --> H2O + CH3                (5)
// CH3 + CH3 --> C2H6                    (6)
// OH + O -->  O2   +H                   (7a)
// OH + O --> HO2                        (7b)
// OH + H --> H2   +    O                (8a)
// OH + H --> H2O                        (8b)
// CH3 + O --> H2CO    +  H              (9)
// CH3 + H  --> CH4                      (11)
// OH  +  CH2  -->  CH2O + H             (12)
// OH + H2O2 --> H2O + HO2               (14)
// OH + HO2 -->  H2O + O2                (15)
// CH3 + H2O2 -->   CH4 + HO2            (18)
// O + HO2-->O2+OH                       (19)
// O + H2O2--> OH + HO2                  (20)
// H + HO2 --> H2 +O2                    (21a)
// H + HO2 --> 2 OH                      (21b)
// H + HO2 --> H2O + O                   (21c)
// H + HO2 --> O(1D) +H2O                (21d)
```

// O + O2 <-> O3	(30) reversible
// H + O2 --> OH + O	(31a)
// H + O2 --> HO2	(31b)
// HO2 + O2 --> OH + O3	(32)
// OH +O3 --> HO2 + O2	(35)
// O + O3 --> O2 + O2	(36)
// H + O3 --> OH + O2	(37)
// HO2 + O3 --> OH + O2 + O2	(38)
// HO2 + HO2 -->H2O2+O2	(39)

//Reactions of Methoxy Radical, CH3O

// CH3O --> CH2OH	(60a)
// CH3O --> CH2O + H	(60b)
// CH3O + H2O2 --> products	(62)
// CH3O + HO2 --> CH2O + H2O2	(64)
// CH3O + CH3 --> CH2O + CH4	(65a)
// CH3O + CH3 --> (CH3)2O	(65b)
// CH3O + CH3O --> CH3OH + CH2O	(66a)
// CH3O + CH3O --> (CH3O)2	(66b)
// CH3O + OH --> CH2O + H2O	(67a)
// CH3O + OH --> CH3OOH	(67b)
// CH3O + O --> CH2O + OH	(68a)
// CH3O + O --> CH3 + O2	(68b)
// CH3O + O --> CH3OO	(68c)
// CH3O + H --> CH2O + H2	(69a)
// CH3O + H --> CH3OH	(69b)
// Cl + CH3OH --> HCl + CH2OH	(70a)
// Cl + CH3OH --> HCl + CH3O	(70b)
// CH2OH + O2 --> CH2O + HO2	(71)
// CH3O + O2 --> CH2O + HO2	(72)
// CH3 + O2 --> CH3O2	(73)
// Cl + CH4 --> HCl+CH3	(74)
// Cl + CH3 --> CH2 + HCl	(75a)
// Cl + CH3 --> CH3Cl	(75b)
// Cl + HO2 --> HCl + O2	(76)
// Cl + O2 --> ClO2	(77)
// Cl + acetone--> products	(78)
// Cl+CH3O--> HCl + CH2O	(79)
// H + CH3OH --> H2+ CH2OH	(80)
// H + acetone --> products	(81)
// OH + CH3OH --> products	
// CH3O2	
// CH3 + CH3O2 --> CH3O + CH3O	(83)
// OH + CH3O2 --> CH3O + HO2	(84a)
// OH + CH3O2 --> CH2OO + H2O	(84b)
// O + CH3O2 -->CH3O+O2	(85)

// H + CH3O2 -->CH3O + OH (86a)
// H + CH3O2 --> CH4 + O2 (86b)
// HO2 + CH3O2 -->CH3OOH + O2 (88)
// CH3O2 + CH3O2 --> products (89)
// CH3O2 + CH3O2 --> CH3O+CH3O + O2 (89a)
// CH3O2 + CH3O2 --> CH2O+CH3OH + O2 (89b)
//CH3O2+CH3O2 --> (CH3O)2 + O2 (89c)
// Cl + CH3O2 --> CH3O + ClO (90a)
// Cl+CH3O2 -> HCl + CH2OO (90b)
// CH3O2 + CH3O -->CH3OOH+CH2O (91)
//HO2+(COCl)2 --> products (92)
//CH2OH+Cl-->HCl+CH2O (93)
//CH2OH+CH3-->CH4+CH2O (94)
// CH2OH+H-->Products (95)
// CH2OH+HO2-->CH2O+H2O2 (96)
// CH2OH+CH2OH-->CH2O +CH2OH (97)
// Cl + Cl --> Cl2 (100)
// CH3 + Cl2 --> CH3Cl + Cl (101)
// CH3Cl + Cl --> CH2Cl + HCl (102)
// C2H6 + Cl --> C2H5 + HCl (103)
// OxCl + CH3--> Product (104)

//_____
//Rate Constants

//CH3 + HO2 --> CH3O + OH (1a)
//CH3 + HO2 --> CH2O + H2O (1b)
//CH3 + HO2 --> CH3OOH (1c)
//CH3 + HO2 --> CH4 + O2 (1d)
//CH3 + HO2 --> CH4 + O2(1 Delta) (1e)
// According to Jasper et al., 2009, the only important channels are
// channel 1a, 1c and 1d.
// This is reaction under study. k1=k1a+k1b+k1c+k1d+k1e
// According to Jasper et al., 2009, the branching ratio between 1a and 1d
// is k1a/(k1a+k1d)=0.7 at 300 K (obtained approximately from Figures).
// for now we will leave only these two channels, 1a and 1d
//k1ad=3.4e-11
k1a=k1ad*0.7
k1b=0
k1c=0
k1d=k1ad*0.3
k1e=0
k1=k1a+k1b+k1c+k1d+k1e

// OH + CH3 --> H2O + CH2 (3a)
// OH + CH3 --> CH3OH (3b)

```
// Our work 2012, pressure independent 1 - 100 bar
k3=1.2e-10*(T/300)^(-0.49)

// OH+OH --> H2O + O                    (4a)
// Low T <420K 1999 Bedjanian et al, high T>550K  - our data 2011
// fit of the data that were submitted in the final version
//k4a=1.07e-12*(1+1.0e-4*((T-483)^2))^0.2

// Our study, 2012. For 298 k, 1 bar, He
k4a=1.44e-12

// OH+OH --> H2O2                       (4b)
// 2011 Sangwan et al.
//k04b=9.0e-31*(T/300)^(-3.5)
//kinf4b=2.4e-11*(T/300)^(-0.5)
//Fcent4b=0.37
//x4b=k04b*M/kinf4b
//c4b=-0.4-0.67*Log10(Fcent4b)
//N4b=0.75-1.27*Log10(Fcent4b)
//d=0.14
//y4b=Log10(x4b)+c4b
//LF4b=Log10(Fcent4b)/(1+(y4b/(N4b-d*y4b))^2)
//F4b=10^LF4b
//k4b=kinf4b*F4b*x4b/(1+x4b)
//This generates k4b=4.4e-12 at 1 bar 1nd 298 K
// Our direct value is (6.2-1.4)e-12

// Our study, 2012. For 298 k, 1 bar, He
k4b= 4.73e-12

// CH3 + CH3 = C2H6                     (6)
// Yan et al., 2015
k6=5.66e-11*(T/298)^(-0.37)

//OH + O -->  O2   +H                   (7a)
// 2004 ATK/BAU
k7a=2.4e-11*exp(109/T)

// OH + O --> HO2                       (7b)
// No data, set as OH+H
k7b=M*1.6e-31*(T/298)^(-2.6)

//OH + H --> H2   +    O               (8a)
//86TSA/HAM
k8a = 6.86e-14*(T/298)^2.8*exp(-1950/T)
```

```
//OH + H --> H2O                                (8b)
//77 ZEL/ERL
k8b=M*1.6e-31*(T/298)^(-2.6)

// CH3 + O --> H2CO    +  H                      (9)
//1992ATK
k9= 1.4e-10

// CH3 + H  --> CH4                              (11)
//Pilling1997
k011=6.2e-29*(T/298)^(-1.8)
kinf11=3.5e-10
Fcent11=0.638*exp(-T/3231)
x11=k011*M/kinf11
c11=-0.4-0.67*Log10(Fcent11)
N11=0.75-1.27*Log10(Fcent11)
d=0.14
y11=Log10(x11)+c11
LF11=Log10(Fcent11)/(1+(y11/(N11-d*y11))^2)
F11=10^LF11
k11=kinf11*F11*x11/(1+x11)

// OH  +  CH2  -->  CH2O + H                     (12)
//1986TSA/HAM
k12=3e-11

// OH + H2O2 --> H2O + HO2                       (14)
//2004JIM/GIE
k14=2.9e-12*exp(-109/T)

// OH + HO2 -->  H2O + O2                        (15)
//1988KEY
k15=4.8e-11*exp(250/T)

//CH3 + H2O2 -->   CH4 + HO2                     (18)
//1986TSA
k18=2e-14*exp(300/T)

//O + HO2-->O2+OH                               (19)
//2004ATK/BAU
k19= 2.70E-11*exp(1860/8.31447/T)

//O + H2O2--> OH + HO2                          (20)
//2004ATK/BAU
k20 =1.40E-12*exp(-16630/8.31447/T)
```

```
//H + HO2 --> H2 +O2                    (21a)
//1992 BOU/COB
k21a=7.11E-11*exp(-5900/8.31447/T)

//H + HO2 --> 2 OH                      (21b)
//1992Bau/COB
k21b=2.81E-10*exp(-3660/8.31447/T)

//H + HO2 --> H2O + O                   (21c)
//1992 BAU/COB
k21c=5.00E-11*exp(-7200/8.31447/T)

//H + HO2 --> O(1D) +H2O                (21d)
//2007MOU/SAH1901-1913
// A theoretical paper - important reaction, thou!
// Will be used as H + HO2 --> 2OH +H2O
k21d=3.29E-12*(T/298)^1.55*exp(670/8.31447/T)

// O + O2 --> O3                        (30)
// Hippler, Rahn, Troe 1990 (on He)
k30 = M*3.4e-34*(T/300)^(-1.2)

//Equilibrium constant from dHf298(O3)=141.746 kJmol-1
//(from Active Thermo Tables), O and O2 fro GRI, and
// the rest for ozone from NIST WebBook.
Keq30=4.0007e-9*(T/298)^(-1.37313)*exp(14123.53/T)
kfkr30=Keq30*10*8.31451*T/6.022e23


// H + O2 --> OH + O                    (31a)
//1994 Bau/Cob
//Plays role only at high T
k31a = 1.62E-10*exp(-62110/8.31447/T)

// H + O2 --> HO2                       (31b)
// 1997ATK/BAU (for N2):
k31b = M*5.4E-32*(T/298)^(-1.80)

// HO2 + O2 --> OH + O3                 (32)
// This reaction is ENDOTHERMIC by ca. 180 kJ mol-1
// Plays absolutely no role
k32=0

// OH +O3 --> HO2 + O2                  (35)
// 2004 ATK/BAU
k35 = 1.7E-12*exp(-7820/8.31447/T)
```

```
// O + O3 --> O2 + O2                    (36)
// 2001 ATK/BAU
k36=8.0E-12*exp(-17130/8.31447/T)

// H + O3 --> OH + O2                    (37)
// 1989 ATK/BAU
k37=1.4E-10*exp(-3990/8.31447/T)

// HO2 + O3 --> OH + O2 + O2             (38)
// 2004 ATK/BAU
k38 =1.97E-16 *(T/298)^4.57*exp(5760/8.31447/T)

// HO2 + HO2 -->H2O2+O2                  (39)
//2005STO/ROW
k39=1.8e-14*exp(12472/8.31447/T)

// CH3O --> CH2OH                        (60a)
// 1981 BAT/BUR
k60a = 1e13*exp(-109000/8.31447/T)

// CH3O --> CH2O + H                     (60b)
// 1994 BAU/COB
k60b = 9e-11*exp(-56460/8.31447/T)

// CH3O + H2O2 --> CH3OH + HO2           (62)
// 1987 TSA k62 = 5e-15*exp(-10810/8.31447/T)
k62 = 5e-15*exp(-10810/8.31447/T)

// CH3O + HO2 --> CH2O + H2O2            (64)
// 1986 TSA
k64=5e-13

// CH3O + CH3 --> CH2O + CH4             (65a)
// 1986 TSA/HAM
k65a=4e-11
// I suspect 65a and 65b is the same channel
//k65a=0

// CH3O + CH3 --> (CH3)2O                (65b)
// 1979 HAS/KOS
k65b=5.5e-11

// CH3O + CH3O --> CH3OH + CH2O          (66a)
// 1979 HAS/KOS
k66a=3.85e-11
```

```
// CH3O + CH3O --> (CH3O)2                (66b)
// 1986 TSA/HAM
k66b=3e-12

// CH3O + OH --> CH2O + H2O               (67a)
// 1986 TSA
//k67a=3e-11

// CH3O + OH --> CH3OOH                   (67b)
// not known
k67b=0

// CH3O + O --> CH2O + OH                 (68a)
// 1987 TSA
k68a=1e-11

// CH3O + O --> CH3 + O2                  (68b)
//1987 ZEL
k68b=2.5e-11

// CH3O + O --> CH3OO                     (68c)
// not known
k68c=0

// CH3O + H --> CH2O + H2                 (69a)
//1991 DOB/BER
k69a=3.3e-11
//k69a=0

// CH3O + H --> CH3OH                     (69b)
// not known
k69b=0
// arbitrarily set to 2e-10
//k69b=2e-10

// CH3O + H --> CH3 + OH                  (69c)
//not know
//k69c=3e-11

// Cl + CH3OH --> HCl + CH2OH             (70a)
// 2001 Atk/Bau k70a = 5.5e-11 temperature independent
k70a = 5.5e-11

// Cl + CH3OH --> HCl + CH3O              (70b)
// 1994 DOB/BER k70b=0.01*k70a
```

```
k70b=0.01*k70a

// CH2OH + O2 --> CH2O + HO2                (71)
// 2001 ATK/BAU k71 = 0.95e-11
k71=0.95e-11

// CH3O + O2 --> CH2O + HO2                 (72)
// 2003ORL/TYN
k72=7.82e-14*exp(-9560/8.31447/T)


// CH3 + O2 --> CH3O2                       (73)
// 1992ATK/BAU1125-1568
k073=1.0e-30*(T/300)^(-3.30)
kinf73=1.21e-12*(T/300)^1.20
// Fc from Fernandes RX, Luther K, Troe J. 2006
Fcent73=0.33
x73=k073*M/kinf73
c73=-0.4-0.67*Log10(Fcent73)
N73=0.75-1.27*Log10(Fcent73)
d=0.14
y73=Log10(x73)+c73
LF73=Log10(Fcent73)/(1+(y73/(N73-d*y73))^2)
F73=10^LF73
k73=kinf73*F73*x73/(1+x73)*k73Factor

// Cl + CH3 --> HCl + CH2                   (75a)
// 1990GOL/TEM1367-1371
// k75a = 3.27E-17 at 298
// neglected

// Cl + CH3 --> CH3Cl                       (75b)
// Yan et al., 2016
k75b=7.95e-11*(T/298)^(-1.48)

// Cl + HO2 --> HCl + O2                    (76)
// 2001 ATK/BAU
k76 = 1.8e-11*exp(1413/8.31447/T)

//Cl + O2 --> ClO2                          (77)
//2007ATK/BAU
k77=1.44e-33*M

//Cl + acetone --> products                 (78)
//2008ZHA/HUS at 298
k78=2.08e-12
```

// Cl+CH3O--> HCl + CH2O (79)
//1995JUN/KUK1057-1066
k79 = 1e-10

// H + CH3OH --> H2+ CH2OH (80)
// k298 is ca. 3e-15, Ea ca. 20 kJ mol-1, no role at room T

// H + acetone --> products (81)
// abstraction - slow ca. 1e-15
// attachment slow too, no role at room T

// OH + CH3OH --> products (82)
//1987WAL/KUR
k82=4.8e-12*exp(-3990/8.31447/T)

// CH3 + CH3O2 --> CH3O + CH3O (83)
//1985PIL/SMI4713
k83=4.5e-11

// OH + CH3O2 --> CH3O + HO2 (84a)
// Yan et al., 2016
k84a = 8.4e-11*(T/298)^(-0.81)

// OH + CH3O2 --> CH2OO + H2O (84b)
// Yan et al.,
// k84b less than 5% out of total rate constant

// O + CH3O2 -->CH3O+O2 (85)
//1987ZEL403-407
//k85=6.0e-12
//1988ZEL
k85=4.3e-11

// H + CH3O2 -->CH3O + OH (86a)
//1986TSA/HAM1087
k86a=1.6e-10

// H + CH3O2 --> CH4 + O2 (86b)
// 2004BOG/BAK486-490
//k86b=7.83E-24 activation energy 69 kJ mol-1, NEGLECTED

// HO2 + CH3O2 -->CH3OOH + O2 (88)
//2001ATK/BAU1-56
k88=3.80E-13*exp(6650/8.31447/T)

// CH3O2 + CH3O2 --> products (89)
//2001ATK/BAU1-56 total rate constant
k89=1.00E-13*exp(3030/8.31447/T)

// CH3O2 + CH3O2 --> CH3O+CH3O + O2 (89a)
//2001ATK/BAU1-56
k89a=7.40E-13*exp(-4320/8.31447/T)

// CH3O2 + CH3O2 --> CH2O+CH3OH + O2 (89b)
//1994BAU/COB847-1033
k89b=k89/(1+25*exp(-9730/8.31447/T))

//CH3O2+CH3O2 --> (CH3O)2 + O2 (89c)
//1989ATK/BAU881-1097
//k89c < 1e-14 NEGLECTED

// Cl + CH3O2 --> CH3O + ClO (90a)
//1994DEM/SAN
k90a=7.7e-11

// Cl+CH3O2 -> HCl + CH2OO (90b)
// 1995 JUN/KUK
k90b=5.6e-11

// CH3O2 + CH3O -->CH3OOH+CH2O (91)
//1986TSA/HAM1087, estimate
// our measurment
k91=1.82e-11

//HO2+(COCl)2 --> products (92)
//unknown
k92=0e-13

// CH2OH + Cl --> CH2O + HCl (93)
// 1988PAG/MUN k=6.64e-10
// I expect about k=5e-11
k93=5e-10
//k93=5e-11

// CH2OH + CH3 --> CH2O + CH4 (94)
// 1987TSA
k94=4e-12

// CH2OH + H --> Products (95)
//1994DOB/BER

```
k95=6.81e-11

// CH2OH + H --> CH3 + OH                    (95b)
// 1987TSA
//k95b=1.6e-10
k95b=0

// CH2OH+HO2 --> CH2O + H2O2                 (96)
// 2011MOU/HOM
k96=5.16e-12

// CH2OH + CH2OH --> CH2O + CH3OH            (97)
// 1987TSA
k97=1.5e-11

// Cl + Cl --> Cl2                           (100)
// HIP/TRO 1976
k100 = 4.69e-33*M

// CH3 + Cl2 --> CH3Cl + Cl                  (101)
//Timonen 2008
k101=1.55e-12

// CH3Cl + Cl --> CH2Cl + HCl                (102)
// 2009SAR/GOL
k102=1.7e-11*exp(-8647/8.31447/T)

// C2H6 + Cl --> C2H5 + HCl                  (103)
// ATK/BAU 2001
k103=8.3e-11*exp(-830/8.31447/T)

// OxCl + CH3 --> Product                    (104)
// guess
k104=3e-13

//_____________________________________________________________
//System of Ordinary Differential Equations


//Species "transient":  CH3, HO2, OH,O, H, O3, CH2, H2O2, CH3O
// Acetone, N2O
//Species initially present: OxCl, O2, CH3OH, H2O, CH4

//Reaction Rates:

r1a=k1a*CH3*HO2
```

r1b=k1b*CH3*HO2
r1c=k1c*CH3*HO2
r1d=k1d*CH3*HO2
r1e=k1e*CH3*HO2
r1=k1*CH3*HO2
r3=k3*OH*CH3
r4a=k4a*OH*OH
r4b=k4b*OH*OH
r6=k6*CH3*CH3
r7a=k7a*OH*O
r7b=k7b*OH*O
r8a=k8a*OH*H
r8b=k8b*OH*H
r9=k9*CH3*O
r11=k11*CH3*H
r12=k12*OH*CH2
r14=k14*OH*H2O2
r15=k15*OH*HO2
r18=k18*CH3*H2O2
r19=k19*O*HO2
r20=k20*O*H2O2
r21a=k21a*H*HO2
r21b=k21b*H*HO2
r21c=k21c*H*HO2
r21d=k21d*H*HO2
r30=k30*(O*O2-O3/kfkr30)
r31a=k31a*H*O2
r31b=k31b*H*O2
r32=k32*HO2*O2
r35=k35*OH*O3
r36=k36*O*O3
r37=k37*H*O3
r38=k38*HO2*O3
r39=k39*HO2*HO2
r60a=k60a*CH3O
r60b=k60b*CH3O
r62=k62*CH3O*H2O2
r64=k64*CH3O*HO2
r65a=k65a*CH3O*CH3
r65b=k65b*CH3O*CH3
r66a=k66a*CH3O*CH3O
r66b=k66b*CH3O*CH3O
r67a=k67a*CH3O*OH
r67b=k67b*CH3O*OH
r68a=k68a*CH3O*O
r68b=k68b*CH3O*O

```
r68c=k68c*CH3O*O
r69a=k69a*CH3O*H
r69b=k69b*CH3O*H
r69c=k69c*CH3O*H
r70a=k70a*Cl*CH3OH
r70b=k70b*Cl*CH3OH
r71=k71*CH2OH*O2
r72=k72*CH3O*O2
r73=k73*CH3*O2
r75b=k75b*CH3*Cl
r76=k76*Cl*HO2
r77=k77*Cl*O2
r78=k78*Cl*Acetone_0
r79=k79*Cl*CH3O
r82=k82*OH*CH3OH
r83=k83*CH3*CH3O2
r84a=k84a*OH*CH3O2
r85=k85*O*CH3O2
r86a=k86a*H*CH3O2
r88=k88*HO2*CH3O2
r89=k89*CH3O2*CH3O2
r89a=k89a*CH3O2*CH3O2
r89b=k89b*CH3O2*CH3O2
r90a=k90a*Cl*CH3O2
r90b=k90b*Cl*CH3O2
r91=k91*CH3O2*CH3O
r92=k92*(OxCl_0+delOxCl)*HO2
r93=k93*CH2OH*Cl
r94=k94*CH2OH*CH3
r95=k95*CH2OH*H
r95b=k95b*CH2OH*H
r96=k96*CH2OH*HO2
r97=k97*CH2OH*CH2OH
r100=k100*Cl*Cl
r101=k101*CH3*Cl2
r102=k102*CH3Cl*Cl
r103=k103*C2H6*Cl
r104=k104*OxCl_0*CH3

// ODE System

rOH1=r1a-r3-2*r4a-2*r4b-r7a-r7b-r8a-r8b-r12-r14-r15
rOH2=r19+r20+2*r21b+r31a+r32-r35+r37+r38
rOH3=-r67a-r67b+r68a+r69c-r84a+r86a+r95b-r82
OH'=rOH1+rOH2+rOH3-kwOH*OH
CH3'=-r1-r3-2*r6-r9-r11-r18-r65a-r65b+r68b-r73-r75b-r101-r104+r69c+r95b-r83
```

```
rHO21=-r1+r7b+r14-r15+r18-r19+r20-r21a-r21b-r21c-r21d+r31b-r32+r35-r38-2*r39-r64
rHO22=r71+r72-r76+r84a-r88-r96-r92
HO2'=(rHO21+rHO22)*HO2Factor
O'=r4a-r7a-r7b+r8a-r9-r19-r20+r21c-r30 +r31a-r36-r68a-r68b-r68c-kwO*O-r85
rH1=-r86a-r95-r69c-r95b
rH2=r7a-r8a-r8b+r9-r11+r12-r21a-r21b-r21c-r21d-r31a-r31b-r37+r60b-r69a-r69b-
kwH*H
H'=rH1+rH2
H2O2'=r4b-r14-r18-r20+r39-r62+r64
O3'=r30+r32-r35-r36-r37-r38

//for CH2 it is assumed that reaction 3 produces CH2 ONLY
CH2'=r3-r12
Cl'=-r70a-r70b-r75b-r76-r77-r78-r79-r90a-r90b-2*r100+r101-r102-r103-r93-r94
rCH3O1=r1a-r60a-r60b-r62-r64-r65a-r65b-2*r66a-2*r66b+2*r83+r84a+r85+r86a
rCH3O2=-r67a-r67b-r68a-r68b-r68c-r69a-r69b+r70b-r72-r79+r90a-r91
CH3O'=rCH3O1+rCH3O2+2*r89a-r69c
CH2OH'=r60a+r70a-r71-r93-r94-r95-r96-2*r97-r95b
CH3O2'=r73-r83-r84a-r85-r86a-r88-2*r89a-2*r89a-r90a-r90b-r91
Cl2'=r100-r101
CH3Cl'=r75b+r101-r102
C2H6'=r6-r103

//_____________________________________________________________
// Transient Absorptions


OxCltrans=delOxCl
H2O2trans=H2O2

AbsHO2at216=L*sHO2at216*HO2

A216c1=L*(sCH3at216*CH3+sHO2at216*HO2+sH2O2at216*H2O2trans)
A216c2=L*sO3at216*O3+L*sCH3O2at216*CH3O2
A216c4=L*(sOxClat216*OxCltrans)
A216=A216c1+A216c2+A216c4

A222c1=L*(sHO2at222*HO2+sO2at222*O2+sO3at222*O3+sH2O2at222*H2O2trans)
A222c2=L*(sAcetoneat222*Acetone_0+sOxClat222*OxCltrans+sCH3O2at222*CH3O2)
A222=A222c1+A222c2

A224c1=L*(sCH3at224*CH3+sHO2at224*HO2+sH2O2at224*H2O2trans)
A224c2=L*(sO3at224*O3+sOxClat224*OxCltrans)
A224=A224c1+A224c2

A230c1=L*(sCH3at230*CH3+sHO2at230*HO2+sH2O2at230*H2O2trans)
```

```
A230c2=L*sO3at230*O3
A230=A230c1+A230c2

A254c1=L*(sCH3at254*CH3+sHO2at254*HO2+sH2O2at254*H2O2trans)
A254c2=L*sO3at254*O3
A254=A254c1+A254c2

Abs308c1=L*(sOHat308*OH+sCH3O2at308*CH3O2)
Abs308c2=L*sOxClat308*OxCltrans
Abs308=Abs308c1+Abs308c2
//_____________________________________________________________

//F216_1=A216_1
F216=A216+ZeroShift216

//F224=A224
//F224_1=A224_1
//F224=A224+ZeroShift224
//F308=Abs308
F222=A222

//gate=UNIT(TIME-t1)*UNIT(t2-TIME)
//A216=(1-gate)*F216_1+gate*F216
//A224=(1-gate)*F224_1+gate*F224

F1=SIGNAL1
F2=F216
gate=UNIT(TIME-t1)*UNIT(t2-TIME)
SIGNAL=(1-gate)*F1+gate*F2

//Initial Conditions

TIME=0

CH3=CH3ini
HO2=HO2ini
OH=OHini
O=Oini
H=Hini
H2O2=H2O2ini
O3=O3ini
CH2=CH2ini
CH2OH=CH2OHini
CH3O=CH3Oini
Cl=Clini
CH3O2=CH3O2ini
```

```
Cl2=Cl2ini
CH3Cl=CH3Clini
C2H6=C2H6ini
CH3OH=CH3OH_0

//Initial Parameters and Constraints

PhotonFluenceFactor=1
k1ad=3.4e-11
//k1ad=0
k73Factor=1
```

APPENDIX B

CALIBRATIONS OF MASS FLOW CONTROLLERS

The mass flow controllers used in this study are Brooks model 5850E. Depending upon the flow rate requirement, different mass flow controllers have been used for the gases. The mass flow controllers have been routinely calibrated. The calibrations of the mass controllers with different gases are shown in Figures B.1 – B.6.

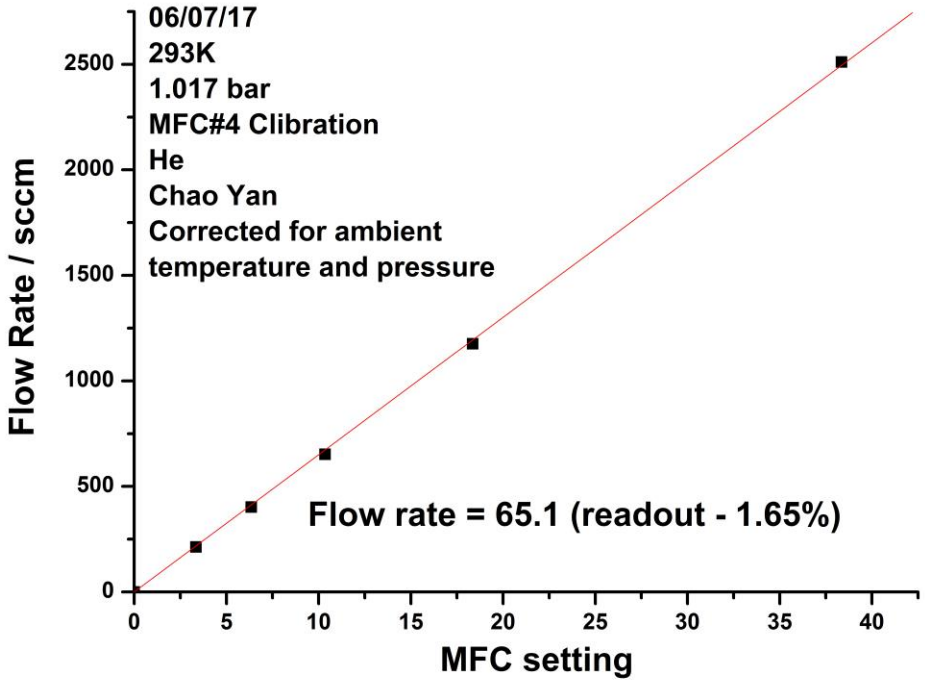

Figure B.1 Calibration of mass flow controller # 4 for He.

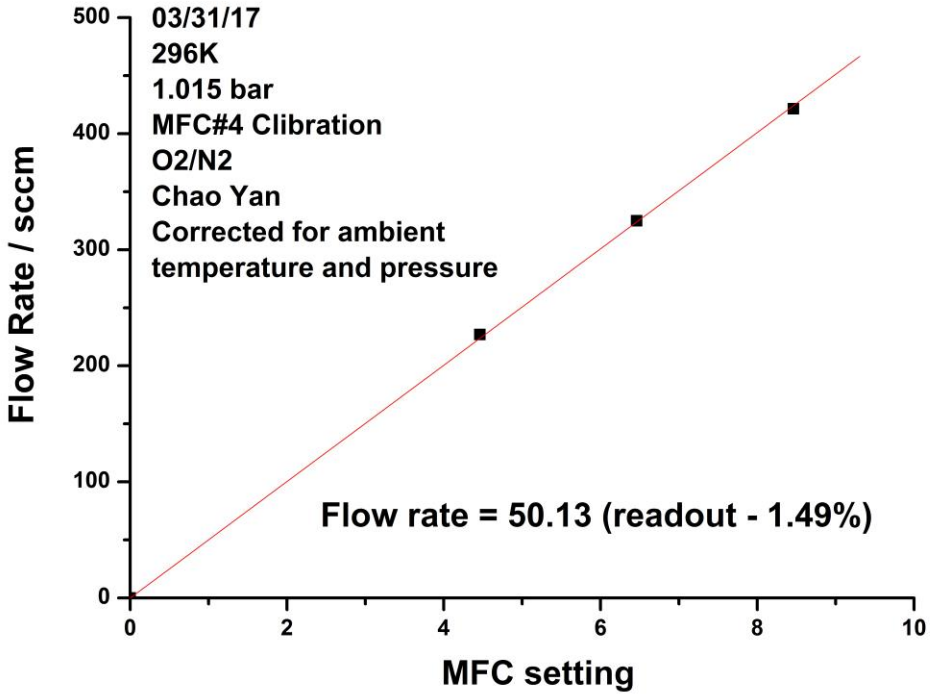

Figure B.2 Calibration of mass flow controller # 4 for O_2/N_2 mixture.

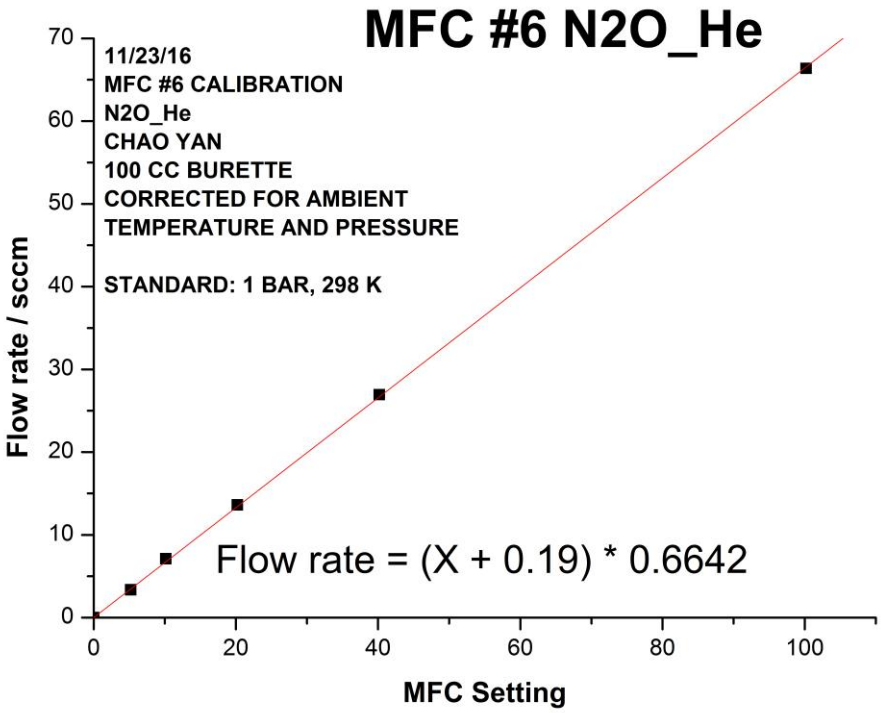

Figure B.3 Calibration of mass flow controller # 6 for O_2/N_2 mixture.

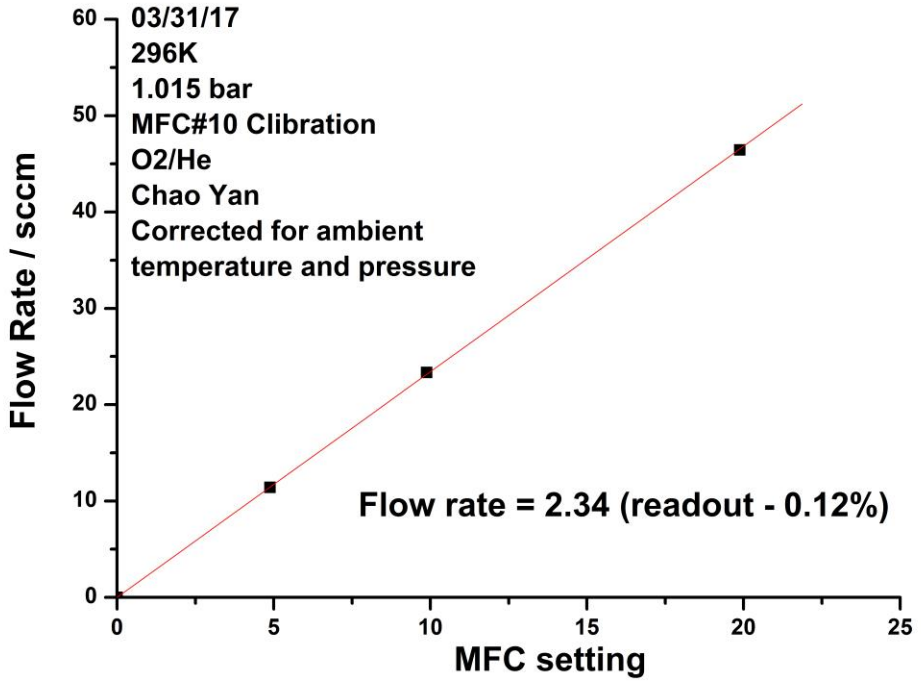

Figure B.4 Calibration of mass flow controller # 10 for O_2/He mixture.

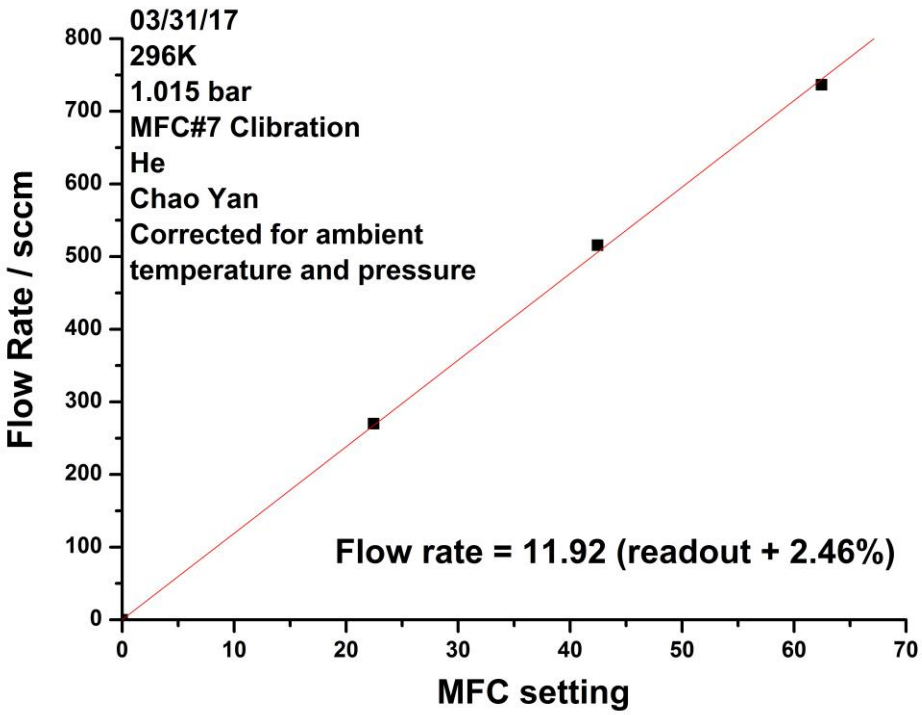

Figure B.5 Calibration of mass flow controller # 7 for He flush.

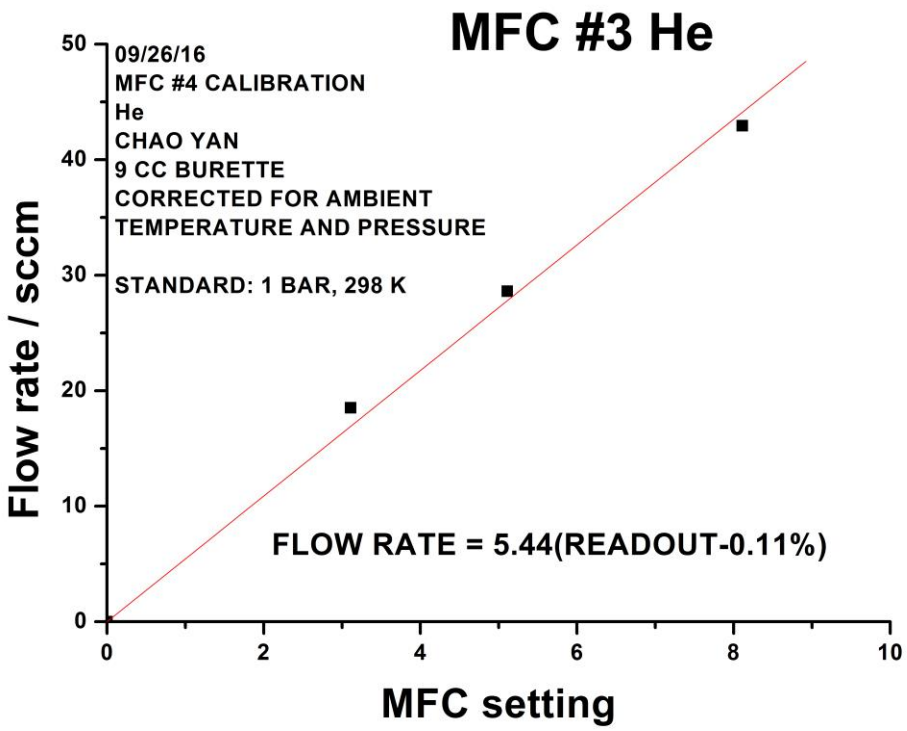

Figure B.6 Calibration of mass flow controller # 3 for gas mixture.

REFERENCES

1. Sangwan, M., Krasnoperov, L. N. (2013). Kinetics of the Gas Phase Reaction CH_3 + HO_2. *The Journal of Physical Chemistry A, 117*(14), 2916-2923.

2. Jasper, A. W., Klippenstein, S. J.,& Harding, L.B.(2009). Theoretical rate coefficients for the reaction of methyl radical with hydroperoxyl radical and for methylhydroperoxide decomposition. *Proceedings of the combustion institute, 32*(Pt. 1), 279-286. doi:10.1016/j.proci.2008.05.036.

3. Krasnoperov, L. N., & Mehta, K. (1999). Kinetic Study of CH_3+ HBr and CH_3+ Br Reactions by Laser Photolysis− Transient Absorption over 1− 100 Bar Pressure Range. *The Journal of Physical Chemistry A, 103*(40), 8008-8020.

4. Zhu, R., & Lin, M. C. (2001). The CH_3 + HO_2 Reaction: First-Principles Prediction of Its Rate Constant and Product Branching Probabilities. *Journal of Physical Chemistry A, 105*(25), 6243-6248. doi:10.1021/jp010698i

5. Wang, B., Hou, H., Yoder, L. M., Muckerman, J. T., & Fockenberg, C. (2003). Experimental and Theoretical Investigations on the Methyl−Methyl Recombination Reaction. *The Journal of Physical Chemistry A, 107*(51), 11414-11426. doi:10.1021/jp030657h

6. Ting, W. L., Chen, Y. H., Chao, W., Smith, M. C., & Lin, J. J. (2014). The UV absorption spectrum of the simplest Criegee intermediate CH_2OO. *Physical chemistry chemical physics : PCCP, 16*(22), 10438-10443. doi:10.1039/c4cp00877d

7. Parker, J. K., Payne, W. A., Cody, R. J., Nesbitt, F. L., Stief, L. J., Klippenstein, S. J., & Harding, L. B. (2007). Direct Measurement and Theoretical Calculation of the Rate Coefficient for Cl + CH_3 in the Range from T = 202−298 K. *The Journal of Physical Chemistry A, 111*(6), 1015-1023. doi:10.1021/jp066231v

8. Klippenstein, S. J., Georgievskii, Y., & Harding, L. B. (2006). Predictive theory for the combination kinetics of two alkyl radicals. *Physical Chemistry Chemical Physics, 8*(10), 1133-1147. doi:10.1039/B515914H

9. Sander, S. P., Golden, D. M., Kurylo, M. J., Moortgat, G. K., Wine, P. H., Ravishankara, A. R., Keller-Rudek, H. (2006). Chemical kinetics and photochemical data for use in atmospheric studies : evaluation number 15: Pasadena, CA : Jet Propulsion Laboratory, California Institute of Technology.

10. Blitz, M. A., N.J.B., G., Shannona, R. J., Pilling, M. J., Seakins, P. W., Western, C. M., & Robertson, S. H. (2015). Reanalysis of Rate Data for the Reaction

$CH_3+CH_3 \rightarrow C_2H_6$ using Revised Cross-Sections and a Linearised Second Order Master Equation. *Journal of Physical Chemistry A.*

11. Westbrook, C. K., & Dryer, F. L. (1981). Chemical Kinetics and Modeling of Combustion Processes. *Symposium (International) on Combustion, 18*(1), 749-767. doi:10.1016/s0082-0784(81)80079-3

12. Tsang, W. (1987). Chemical kinetic data base for combustion chemistry. Part 2. Methanol. *Journal of Physical and Chemical Reference Data, 16*, 471.

13. Miller, J. A., Kee, R. J., & Westbrook, C. K. (1990). Chemical Kinetics and Combustion Modeling. *Annual Review of Physical Chemistry, 41*, 345-387.

14. Baulch, D. L., Cobos, C. J., Cox, R. A., Frank, P., Hayman, G., Just, T., Warnatz, J. (1994). Evaluated kinetic data for combusion modelling. Supplement I. *Journal of Physical and Chemical Reference Data, 23*, 847-1033.

15. Du, H., Hessler, J. P., & Ogren, P. J. (1996). Recombination of Methyl Radicals. 1. New Data between 1175 and 1750 K in the Falloff Region. *Journal of Physical Chemistry, 100*(3), 974-983. doi:10.1021/jp951217w

16. Pilling, M. J. (1996). Radical-Radical Reactions. *Annual Review of Physical Chemistry, 47*, 81-108. doi:10.1146/annurev.physchem.47.1.81

17. Bowman, T., Hanson, R. K., Davidson, D. F., Gardiner, W. C. J., Lissianski, V., Smith, G. P., Goldenberg, M. (2002). GRI-Mech 2.11. Thermodynamic Data. http://www.me.berkeley.edu/gri_mech/data/thermo_table.html.

18. Smith, G. P., Golden, D. M., Frenklach, M., Moriarty, N. W., Eiteneer, B., Goldenberg, M., Qin, Z. (2002). GRI-Mech 3.0. http://www.me.berkeley.edu/gri_mech/.

19. Baulch, D. L., Bowman, C. T., Cobos, C. J., Cox, R. A., Just, T., Kerr, J. A., Warnatz, J. (2005). Evaluated Kinetic Data for Combustion Modeling: Supplement II. *Journal of Physical and Chemical Reference Data, 34*(3), 757-1397. doi:10.1063/1.1748524

20. Manion, J. A., Huie, R. E., Levin, R. D., Jr., D. R. B., Orkin, V. L., Tsang, W., Frizzell, D. H. (2008). *NIST Chemical Kinetics Database, NIST Standard Reference Database 17, Version 7.0 (Web Version), Release 1.4.3, Data version 2008.12, National Institute of Standards and Technology, Gaithersburg, Maryland, 20899-8320. Web address: http://kinetics.nist.gov/.*

21. Krasnoperov, L. N., & Michael, J. V. (2004). High-Temperature Shock Tube Studies Using Multipass Absorption: Rate Constant Results for OH + CH_3, OH + CH_2,

and the Dissociation of CH_3OH. *Journal of Physical Chemistry A, 108*(40), 8317-8323.

22. Sangwan, M., Yan, C., Chesnokov, E. N., & Krasnoperov, L. N. (2015). Reaction $CH_3 + CH_3 \rightarrow C_2H_6$ Studied over the 292–714 K Temperature and 1–100 bar Pressure Ranges. *The Journal of Physical Chemistry A, 119*(28), 7847-7857. doi:10.1021/acs.jpca.5b01276

23. Tsang, W., & Hampson, R. F. (1986). Chemical Kinetic Data Base for Combustion Chemistry. Part I. Methane and Related Compounds. *Journal of Physical and Chemical Reference Data, 15*(3), 1087-1279. Retrieved from http://link.aip.org/link/?JPR/15/1087/1

24. Archibald, A. T., Petit, A. S., Percival, C. J., Harvey, J. N., & Shallcross, D. E. (2009). On the importance of the reaction between OH and RO_2 radicals. *Atmospheric Science Letters, 10*(2), 102-108. doi:10.1002/asl.216

25. Bossolasco, A., Faragó, E. P., Schoemaecker, C., & Fittschen, C. (2014). Rate constant of the reaction between CH_3O_2 and OH radicals. *Chemical Physics Letters, 593*, 7-13. doi:10.1016/j.cplett.2013.12.052

26. Bian, H., Zhang, S., & Zhang, H. (2015). Theoretical study on the atmospheric reaction of CH_3O_2 with OH. *International Journal of Quantum Chemistry, 115*(17), 1181-1186. doi:10.1002/qua.24946

27. Müller, J.-F., Liu, Z., Nguyen, V. S., Stavrakou, T., Harvey, J. N., & Peeters, J. (2016). The reaction of methyl peroxy and hydroxyl radicals as a major source of atmospheric methanol. *Nature Communications, 7*, 13213. doi:10.1038/ncomms13213

28. Ravishankara, A. R. (2009). Are chlorine atoms significant tropospheric free radicals *Proceedings of the National Academy of Sciences*, *106*(33), 13639-13640. doi:10.1073/pnas.0907089106

29. Chang, C.-T., Liu, T.-H., & Jeng, F.-T. (2004). Atmospheric concentrations of the Cl atom, CIO radical, and HO radical in the coastal marine boundary layer. *Environmental Research, 94*(1), 67-74. doi:https://doi.org/10.1016/j.envres.2003.07.008

30. Rowland, F. S. (1991). Stratospheric ozone in the 21st century: the chlorofluorocarbon problem. *Environmental Science & Technology*, *25*(4), 622-628. doi:10.1021/es00016a005

31. Yokouchi, Y., Noijiri, Y., Barrie, L. A., Toom-Sauntry, D., Machida, T., Inuzuka, Y., Aoki, S. (2000). A strong source of methyl chloride to the atmosphere from tropical coastal land. *Nature, 403*, 295. doi:10.1038/35002049

32. Finlayson-Pitts, B. J., Ezell, M. J., & Pitts Jr, J. N. (1989). Formation of chemically active chlorine compounds by reactions of atmospheric NaCl particles with gaseous N_2O_5 and $ClONO_2$. *Nature, 337,* 241. doi:10.1038/337241a0

33. Dlugokencky, E. J., Steele, L. P., Lang, P. M., & Masarie, K. A. (1994). The growth rate and distribution of atmospheric methane. *Journal of Geophysical Research: Atmospheres, 99*(D8), 17021-17043. doi:doi:10.1029/94JD01245

34. Wang, J. J., & Keyser, L. F. (1999). Kinetics of the $Cl(^2PJ) + CH_4$ Reaction: Effects of Secondary Chemistry below 300 K. *The Journal of Physical Chemistry A, 103*(37), 7460-7469. doi:10.1021/jp9913259

35. Taatjes, C. A. (2006). Uncovering the Fundamental Chemistry of Alkyl + O_2 Reactions via Measurements of Product Formation. *The Journal of Physical Chemistry A, 110*(13), 4299-4312. doi:10.1021/jp056997f

36. Baklanov, A. V., & Krasnoperov, L. N. (2001). UV Absorption Spectrum and Rate Constant for Self-Reaction of Silyl Radicals. *The Journal of Physical Chemistry A, 105*(20), 4917-4922. doi:10.1021/jp004198l

37. Bryukov, M. G., Slagle, I. R., & Knyazev, V. D. (2002). Kinetics of Reactions of Cl Atoms with Methane and Chlorinated Methanes. *The Journal of Physical Chemistry A, 106*(44), 10532-10542. doi:10.1021/jp0257909

38. Sangwan, M. (2013). Study of elementary reactions of combustion importance at elevated temperatures and pressures. *Thesis*.

39. Sangwan, M., Chesnokov, E. N., & Krasnoperov, L. N. (2012). Reaction OH + OH Studied over the 298–834 K Temperature and 1 - 100 bar Pressure Ranges. *The Journal of Physical Chemistry A, 116*(24), 6282-6294. doi:10.1021/jp211805v

40. Sangwan, M., Chesnokov, E. N., & Krasnoperov, L. N. (2012). Reaction CH_3 + OH Studied over the 294 - 714 K Temperature and 1 - 100 Bar Pressure Ranges. *The Journal of Physical Chemistry A, 116*(34), 8661 - 8670. doi:10.1021/jp305070c

41. Sangwan, M., & Krasnoperov, L. N. (2012). Disproportionation Channel of Self-Reaction of Hydroxyl Radical, OH + OH → H_2O + O, Studied by Time-Resolved Oxygen Atom Trapping. *The Journal of Physical Chemistry A, 116*(48), 11817-11822. doi:10.1021/jp308885j

42. Sangwan, M., Chesnokov, E. N., & Krasnoperov, L. N. (2013). Recombination of CH_3 Radicals Studied over the 1 - 100 bar Pressure and 298 - 834 K Temperature Ranges. *The Journal of Physical Chemistry A, to be submitted*.

43.Yan, C., Kocevska, S., & Krasnoperov, L. N. (2016). Kinetics of the Reaction of CH_3O_2 Radicals with OH Studied over the 292–526 K Temperature Range. *The*

Journal of Physical Chemistry A, 120(31), 6111-6121. doi:10.1021/acs.jpca.6b04213

44. Lightfoot, P. D., Kirwan, S. P., & Pilling, M. J. (1988). Photolysis of Acetone at 193.3 nm. *Journal of Physical Chemistry, 92*(17), 4938-4946. doi:10.1021/j100328a024

45. Atkinson, R., Baulch, D. L., Cox, R. A., Hampson, R. F., Jr., Kerr, J. A., & Troe, J. (1992). Evaluated kinetic and photochemical data for atmospheric chemistry. Supplement IV. IUPAC Subcommittee on Gas Kinetic Data Evaluation for Atmospheric Chemistry. *Journal of Physical and Chemical Reference Data, 21*(6), 1125-1568. doi:10.1063/1.555918

46. Greenblatt, G. D., & Ravishankara, A. R. (1990). Laboratory Studies on the Stratospheric NOx Production Rate. *J. Geophys. Res., 95*(D4), 3539-3547. doi:10.1029/JD095iD04p03539

47. Butler, J. E., Talley, L. D., Smith, G. K., & Lin, M. C. (1981). Rotational and vibrational energy distributions of hydroxyl radical (oxygen-16)($X^2\Pi$) and hydroxyl radical (oxygen-18)($X^2\Pi$) produced in the reaction of atomic oxygen(^1D) with water and water(oxygen-18). *Journal of Chemical Physics, 74*(8), 4501-4508. doi:10.1063/1.441638

48. Sauder, D. G., Stephenson, J. C., King, D. S., & Casassa, M. P. (1992). Nascent product states in the photoinitiated reaction of ozone with water. *Journal of Chemical Physics, 97*(2), 952-961. doi:10.1063/1.463198

49. Tanaka, N., Takayanagi, M., & Hanazaki, I. (1996). Nascent rotational and vibrational distributions in ^{16}OH and ^{18}OH produced in the reaction of $O(^1D)$ with $H_2{}^{18}O$. *Chemical Physics Letters, 254*(1,2), 40-46. doi:10.1016/0009-2614(96)00296-5

50. Cleveland, C. B., & Wiesenfeld, J. R. (1992). Nascent product population distribution in the reaction excited atomic oxygen + water → hydroxyl + hydroxyl ($^{16}O(^1D_2) + H_2\ ^{18}O \rightarrow\ ^{16}OH + {}^{18}OH$). *Journal of Chemical Physics, 96*(1), 248-255.

51. Baklanov, A. V., & Krasnoperov, L. N. (2001). Oxalyl Chloride-A Clean Source of Chlorine Atoms for Kinetic Studies. *Journal of Physical Chemistry A, 105*(1), 97-103.

52. Krasnoperov, L. N., & Mehta, K. (1999). Kinetic Study of CH_3 + HBr and CH_3 + Br Reactions by Laser Photolysis-Transient Absorption over 1-100 Bar Pressure Range. *Journal of Physical Chemistry A, 103*(40), 8008-8020.

53. Grebenkin, S. Y., & Krasnoperov, L. N. (2004). Kinetics and Thermochemistry of the Hydroxycyclohexadienyl Radical Reaction with O_2: $C_6H_6OH + O_2 <=> C_6H_6(OH)O_2$. *Journal of Physical Chemistry A, 108*(11), 1953-1963.

54. Hahn, J., Krasnoperov, L., Luther, K., & Troe, J. (2004). Pressure Dependence of the Reaction $H + O_2$ (+Ar) --> HO_2 (+Ar) in the Range 1-900 bar and 300-700 K. *Physical Chemistry Chemical Physics, 6*(9), 1997-1999.

55. Krasnoperov, L. N., Chesnokov, E. N., Stark, H., & Ravishankara, A. R. (2004). Unimolecular Dissociation of Formyl Radical, HCO --> H + CO, Studied Over 1 - 100 bar Pressure Range. *Journal of Physical Chemistry A, 108*(52), 11526-11536. doi:10.1021/jp0403994

56. Johnson, D., Krasnoperov, L. N., Raoult, S., & Lesclaux, R. (2005). UV Absorption Spectra of Methyl-Substituted Hydroxy-Cyclohexadienyl Radicals in the Gas Phase. *Journal of Photochemistry and Photobiology, A: Chemistry, 176*, 98-106.

57. Luque, J., & Crosley, D. R. (1999). LIFBASE: Database and Spectral Simulation Program (Version 1.5). *SRI International Report MP 99-009*.

58. Carl, S. A. (2005). A highly sensitive method for time-resolved detection of $O(^1D)$ applied to precise determination of absolute $O(^1D)$ reaction rate constants and $O(^3P)$ yields. *Physical Chemistry Chemical Physics, 7*(24), 4051-4053. doi:10.1039/b513576c

59. Takahashi, K., Takeuchi, Y., & Matsumi, Y. (2005). Rate constants of the $O(^1D)$ reactions with N_2, O_2, N_2O, and H_2O at 295 K. *Chemical Physics Letters, 410*(4-6), 196-200. doi:10.1016/j.cplett.2005.05.062

60. Hippler, H., Luther, K., Ravishankara, A. R., & Troe, J. (1984). High-Pressure Effects in the Recombination Reaction $CH_3 + CH_3$ --> C_2H_6. *Zeitschrift fuer Physikalische Chemie Neue Folge, 142*, 1-12.

61. Macpherson, M. T., Pilling, M. J., & Smith, M. J. C. (1985). Determination of the absorption cross section for methyl at 216.36 nm and the absolute rate constant for methyl radical recombination over the temperature range 296-577 K. *The Journal of Physical Chemistry, 89*(11), 2268-2274. doi:10.1021/j100257a024

62. Mebel, A. M., & Lin, S.-H. (1997). Excited electronic states of the methyl radical. Ab initio molecular orbital study of geometries, excitation energies and vibronic spectra. *Chemical Physics, 215*(3), 329-341. doi:https://doi.org/10.1016/S0301-0104(96)00363-1

63. Oehlschlaeger, M. A., Davidson, D. F., & Hanson, R. K. (2005). High-temperature UV absorption of methyl radicals behind shock waves. *Journal of Quantitative*

Spectroscopy and Radiative Transfer, *92*(4), 393-402. doi:https://doi.org/10.1016/j.jqsrt.2004.08.006

64. Herzberg, G., & Shoosmith, J. (1956). ABSORPTION SPECTRUM OF FREE CH3 AND CD3 RADICALS. *Canadian Journal of Physics*, *34*(5), 523-525. doi:10.1139/p56-059

65. Callear, A. B., & Metcalfe, M. P. (1976). Oscillator strengths of the bands of the B̃2 A′1—X̃2 A″2 system of CD3 and a spectroscopic measurement of the recombination rate comparison with CH3. *Chemical Physics*, *14*(2), 275-284. doi:https://doi.org/10.1016/0301-0104(76)80045-6

66. Vranckx, S., Peeters, J., & Carl, S. (2010). Kinetics of $O(^1D) + H_2O$ and $O(^1D) + H_2$: absolute rate coefficients and $O(^3P)$ yields between 227 and 453 K. *Phys Chem Chem Phys*, *12*(32), 9213-9221.

67. Atkinson, R., Baulch, D. L., Cox, R. A., Crowley, J. N., Hampson, R. F., Hynes, R. G., Troe, J. (2004). Evaluated kinetic and photochemical data for atmospheric chemistry: Volume I - gas phase reactions of Ox, HO_x, NO_x and SO_x species. *Atmos. Chem. Phys.*, *4*(6), 1461-1738. doi:10.5194/acp-4-1461-2004

68. Nishida, S., Takahashi, K., Matsumi, Y., Taniguchi, N., & Hayashida, S. (2004). Formation of $O(^3P)$ Atoms in the Photolysis of N_2O at 193 nm and $O(^3P) + N_2O$ Product Channel in the Reaction of $O(^1D) + N_2O$. *Journal of Physical Chemistry A*, *108*(13), 2451-2456. doi:10.1021/jp037034o

69. Dunlea, E. J., & Ravishankara, A. R. (2004). Kinetic studies of the reactions of $O(^1D)$ with several atmospheric molecules. *Physical Chemistry Chemical Physics*, *6*(9), 2152-2161. doi:10.1039/b400247d

70. Bahng, M.-K., & Macdonald, R. G. (2007). Determination of the Rate Constant for the $OH(X^2\Pi) + OH(X^2\Pi) \rightarrow O(^3P) + H_2O$ Reaction over the Temperature Range 293-373 K. *Journal of Physical Chemistry A*, *111*(19), 3850-3861. doi:10.1021/jp066359c

71. IUPAC Subcommittee on Gas Kinetic Data Evaluation – Data Sheet HO_x. (2001). *Website: http://www.iupac-kinetic.ch.cam.ac.uk, IUPAC Subcommittee on Gas Kinetic Data Evaluation*(Data Sheet HOx9).

72. Bedjanian, Y., Le Bras, G., & Poulet, G. (1999). Kinetic Study of OH + OH and OD + OD Reactions. *Journal of Physical Chemistry A*, *103*(35), 7017-7025. doi:10.1021/jp991146r

73. Sangwan, M., Chesnokov, E. N., & Krasnoperov, L. N. (2012). Reaction OH + OH Studied over the 298–834 K Temperature and 1 - 100 bar Pressure Ranges. *The Journal of Physical Chemistry A*. doi:10.1021/jp211805v

74. Srinivasan, N. K., Su, M. C., Sutherland, J. W., & Michael, J. V. (2005). Reflected Shock Tube Studies of High-Temperature Rate Constants for OH + CH_4 → CH_3 + H_2O and CH_3 + NO_2 → CH_3O + NO. *J. Phys. Chem. A, 109*(9), 1857-1863. doi:10.1021/jp040679j

75. Tsang, W., & Hampson, R. F. (1986). Chemical Kinetic Data Base for Combustion Chemistry. Part I. Methane and Related Compounds. *J. Phys. Chem. Ref. Data, 15*(3), 1087-1279.

76. Zellner, R., Erler, K., & Field, D. (1977). Kinetics of the recombination reaction OH + H + M → H_2O + M at low temperatures. *Symposium (International) on Combustion, [Proceedings], 16*, 939-948. doi:10.1016/s0082-0784(77)80386-x

77. Fulle, D., Hamann, H. F., Hippler, H., & Troe, J. (1998). Temperature and pressure dependence of the addition reactions of HO to NO and to NO_2. IV. Saturated laser-induced fluorescence measurements up to 1400 bar. *Journal of Chemical Physics, 108*(13), 5391-5397. doi:10.1063/1.475971

78. Pereira, R. D. A., Baulch, D. L., Pilling, M. J., Robertson, S. H., & Zeng, G. (1997). Temperature and Pressure Dependence of the Multichannel Rate Coefficients for the CH_3 + OH System. *Journal of Physical Chemistry A, 101*(50), 9681-9693. doi:10.1021/jp972140+

79. Tsang, W., & Hampson, R. F. (1986). Chemical kinetic data base for combustion chemistry. Part I. methane and related compounds. *J. Phys. Chem. Ref. Data, 15*(3), 1087-1279. doi:10.1063/1.555759

80. Yamada, T., Taylor, P. H., Goumri, A., & Marshall, P. (2003). The reaction of OH with acetone and acetone-d[sub 6] from 298 to 832 K: Rate coefficients and mechanism. *Journal of Chemical Physics, 119*(20), 10600-10606. Retrieved from http://dx.doi.org/10.1063/1.1619950

81. Jiménez, E., Gierczak, T., Stark, H., Burkholder, J. B., & Ravishankara, A. R. (2004). Reaction of OH with HO_2NO_2 (Peroxynitric Acid): Rate Coefficients between 218 and 335 K and Product Yields at 298 K. *Journal of Physical Chemistry A, 108*(7), 1139-1149. doi:10.1021/jp0363489

82. Keyser, L. F. (1988). Kinetics of the reaction hydroxyl + hydroperoxo → water + oxygen from 254 to 382 K. *Journal of Physical Chemistry, 92*(5), 1193-1200. doi:10.1021/j100316a037

83. Bardwell, M. W., Bacak, A., Teresa Raventos, M., Percival, C. J., Sanchez-Reyna, G., & Shallcross, D. E. (2003). Kinetics of the HO_2 + NO reaction: A temperature and pressure dependence study using chemical ionisation mass spectrometry. *Physical Chemistry Chemical Physics, 5*(11), 2381-2385. Retrieved from http://dx.doi.org/10.1039/B300842H

84. Davies, J. W., Green, N. J. B., & Pilling, M. J. (1991). Association reaction of CH_3 and NO: evidence for the involvement of the triplet surface. *Journal of the Chemical Society, Faraday Transactions, 87*(15), 2317-2324. Retrieved from http://dx.doi.org/10.1039/FT9918702317

85. Alberty, R. A., & Hammes, G. G. (1958). Application of the Theory of Diffusion-controlled Reactions to Enzyme Kinetics. *The Journal of Physical Chemistry, 62*(2), 154-159. doi:10.1021/j150560a005

86. Franck, J., & Rabinowitsch, E. (1934). Some remarks about free radicals and the photochemistry of solutions. *Transactions of the Faraday Society, 30*(0), 120-130. doi:10.1039/TF9343000120

87. Hippler, H., Otto, B., Schroeder, J., Schubert, V., & Troe, J. (1985). Diffusion Controlled Atom Recombination and Photolytic Cage Effect of Halogens in Compressed Gases and Liquids. *Berichte der Bunsengesellschaft für physikalische Chemie, 89*(3), 240-242. doi:10.1002/bbpc.19850890308

88. Hippler, H., Schubert, V., & Troe, J. (1984). Photolysis quantum yields and atom recombination rates of bromine in compressed gases. Experiments up to 7 kbar. *The Journal of Chemical Physics, 81*(9), 3931-3941. doi:10.1063/1.448186

89. Noyes, R. M. (1954). A Treatment of Chemical Kinetics with Special Applicability to Diffusion Controlled Reactions. *The Journal of Chemical Physics, 22*(8), 1349-1359. doi:10.1063/1.1740394

90. Oum, K., Luther, K., & Troe, J. (2004). High-Pressure Studies of Radical−Solvent Molecule Interactions in the CCl_3 and Bromine Combination Reactions of CCl_3. *The Journal of Physical Chemistry A, 108*(14), 2690-2699.

91. Zhang, P., & Law, C. K. (2009). A fitting formula for the falloff curves of unimolecular reactions. *International Journal of Chemical Kinetics, 41*(11), 727-734. doi:10.1002/kin.20451

92. Troe, J., & Ushakov, V. G. (2011). Revisiting falloff curves of thermal unimolecular reactions. *The Journal of Chemical Physics, 135*(5), 054304. doi:10.1063/1.3615542

93. .Troe, J., & Ushakov Vladimir, G. (2014). Representation of "Broad" Falloff Curves for Dissociation and Recombination Reactions *Zeitschrift für Physikalische Chemie* (Vol. 228, pp. 1).

94. Lightfoot, P. D., Cox, R. A., Crowley, J. N., Destriau, M., Hayman, G. D., Jenkin, M. E., Zabel, F. (1992). Organic peroxy radicals: Kinetics, spectroscopy and tropospheric chemistry. *Atmospheric Environment, 26*(10), 1805-1961. doi:http://dx.doi.org/10.1016/0960-1686(92)90423-I

95. Tsang, W., & Hampson, R. F. (1986). Chemical Kinetic Data Base for Combustion Chemistry. Part I. Methane and Related Compounds. *Journal of Physical and Chemical Reference Data, 15*, 1087.

96. Fittschen, C., Whalley, L. K., & Heard, D. E. (2014). The reaction of CH_3O_2 radicals with OH radicals: a neglected sink for CH_3O_2 in the remote atmosphere. *Environmental Science and Technology, 48*(14), 7700-7701. doi:10.1021/es502481q

97. Assaf, E., Song, B., Tomas, A., Schoemaecker, C., & Fittschen, C. (2016). Rate Constant of the Reaction between CH_3O_2 Radicals and OH Radicals Revisited. *The Journal of Physical Chemistry A, 120*(45), 8923-8932. doi:10.1021/acs.jpca.6b07704

98. Atkinson, R., Baulch, D. L., Cox, R. A., Crowley, J. N., Hampson, R. F., Hynes, R. G., Troe, J. (2001). IUPAC Subcommittee on Gas Kinetic Data Evaluation for Atmospheric ChemistryWeb Version December 2001. *IUPAC Subcommittee on Gas Kinetic Data Evaluation for Atmospheric ChemistryWeb Version December 2001*, 1-56.

99. Criegee, R. (1975). Mechanism of Ozonolysis. *Angewandte Chemie International Edition in English, 14*(11), 745-752. doi:10.1002/anie.197507451

100. Beames, J. M., Liu, F., Lu, L., & Lester, M. I. (2012). Ultraviolet Spectrum and Photochemistry of the Simplest Criegee Intermediate CH_2OO. *Journal of the American Chemical Society, 134*(49), 20045-20048. doi:10.1021/ja310603j

101. Fernandes, R. X., Luther, K., & Troe, J. (2006). Falloff Curves for the Reaction $CH_3 + O_2 (+ M) \rightarrow CH_3O_2 (+ M)$ in the Pressure Range 2−1000 Bar and the Temperature Range 300−700 K. *The Journal of Physical Chemistry A, 110*(13), 4442-4449. doi:10.1021/jp056850o

102. Vranckx, S., Peeters, J., & Carl, S. (2010). Kinetics of $O(^1D) + H_2O$ and $O(^1D) + H_2$: absolute rate coefficients and $O(^3P)$ yields between 227 and 453 K. *Physical chemistry chemical physics : PCCP, 12*(32), 9213-9221. Retrieved from http://pubs.rsc.org/en/content/articlepdf/2010/cp/b923959f

103. DeMore, W. B., Sander, S. P., Golden, D. M., Hampson, R. F., Kurylo, M. J., Howard, C. J., Molina, M. J. (1997). Chemical Kinetics and Photochemical Data for Use in Stratospheric Modeling. *JPL Publication 97-4, Evaluation number 12*.

104. Baulch, D. L., Cobos, C. J., Cox, R. A., Frank, P., Hayman, G., Just, T., Warnatz, J. (1994). Evaluated Kinetic Data for Combusion Modelling. Supplement I. *Journal of Physical and Chemical Reference Data*, *23*, 847-1033.

105. Atkinson, R., Baulch, D. L., Cox, R. A., Hampson, J. R. F., Kerr, J. A., Rossi, M. J., & Troe, J. (1997). Evaluated Kinetic and Photochemical Data for Atmospheric Chemistry: Supplement VI. IUPAC Subcommittee on Gas Kinetic Data Evaluation for Atmospheric Chemistry. *Journal of Physical and Chemical Reference Data*, *26*(6), 1329-1499. Retrieved from http://dx.doi.org/10.1063/1.556010

106. Hippler, H., Rahn, R., & Troe, J. (1990). Temperature and pressure dependence of ozone formation rates in the range 1--1000 bar and 90--370 K. *Journal of Chemical Physics*, *93*(9), 6560-6569. Retrieved from http://dx.doi.org/10.1063/1.458972

107. Manion, J. A., Huie, R. E., Levin, R. D., Jr., D. R. B., Orkin, V. L., Tsang, W., Frizzell, D. H. (2015). *NIST Standard Reference Database 17, Version 7.0 (Web Version), Release 1.6.8*.

108. Active Thermochemical Tables, A. T. (2015). *Active Thermochemical Tables version 1.118*.

109. Linstrom, P. J., Mallard, W. G., & Eds. (2016). *NIST Chemistry WebBook*.

110. Yamada, T., Taylor, P. H., Goumri, A., & Marshall, P. (2003). The reaction of OH with acetone and acetone-d6 from 298 to 832 K: Rate coefficients and mechanism. *The Journal of Chemical Physics*, *119*(20), 10600-10606. doi:10.1063/1.1619950

111. Keyser, L. F. (1988). Kinetics of the reaction hydroxyl + hydroperoxo .fwdarw. water + oxygen from 254 to 382 K. *The Journal of Physical Chemistry*, *92*(5), 1193-1200. doi:10.1021/j100316a037

112. Davies, J. W., Green, N. J. B., & Pilling, M. J. (1991). Association reaction of CH_3 and NO: evidence for the involvement of the triplet surface. *Journal of the Chemical Society, Faraday Transactions*, *87*(15), 2317-2324. doi:10.1039/FT9918702317

113. Fulle, D., Hamann, H. F., Hippler, H., & Troe, J. (1998). Temperature and pressure dependence of the addition reactions of HO to NO and to NO_2. IV. Saturated

laser-induced fluorescence measurements up to 1400 bar. *The Journal of Chemical Physics, 108*(13), 5391-5397. doi:10.1063/1.475971

114. Hassinen, E., & Koskikallio, J. (1979). Flash Photolysis of Methyl Acetate in Gas Phase. Products and Rate Constants of Reactions between Methyl, Methoxy and Acetyl Radicals. *Acta Chem. Scand. Ser. A, 33*(8), 625-630.

115. Orlando, J. J., Tyndall, G. S., & Wallington, T. J. (2003). The Atmospheric Chemistry of Alkoxy Radicals. *Chemical Reviews, 103*(12), 4657-4690. doi:10.1021/cr020527p

116. Pilling, M. J., & Smith, M. J. C. (1985). A laser flash photolysis study of the reaction methyl + molecular oxygen .fwdarw. methylperoxy (CH_3O_2) at 298 K. *The Journal of Physical Chemistry, 89*(22), 4713-4720. doi:10.1021/j100268a014

117. Zellner, R., Hartmann, D., Karthauser, J., Rhasa, D., & Weibring, G. (1988). A laser photolysis/LIF study of the reactions of $O(^3P)$ atoms with CH_3 and CH_3O_2 radicals. *Journal of the Chemical Society Faraday Transactions 2, 84*(5), 549-568. doi:10.1039/F29888400549

118. Atkinson, R., Aschmann,S.M., Arey,J., Carter,W.P.L. (1989). Formation of ring-retaining products from the hydroxyl radical-initiated reactions of benzene and toluene. *International Journal of Chemical Kinetics, 21*, 801-827.

119. Baulch, D. L., Cobos, C. J., Cox, R. A., Esser, C., Frank, P., Just, T., Warnatz, J. (1992). Evaluated kinetic data for combustion modelling. *Journal of Physical and Chemical Reference Data, 21*, 411-429.

120. Zellner, R. (1987). Recent advances in free radical kinetics of oxygenated hydrocarbon radicals. *J. Chim. Phys., 84*, 403-407.

121. Dobe, S., Berces, T., & Szilagyi, I. (1991). Kinetics of the reaction between methoxyl radicals and hydrogen atoms. *Journal of the Chemical Society, Faraday Transactions, 87*(15), 2331-2336. Retrieved from http://dx.doi.org/10.1039/FT9918702331

122. Buras, Z. J., Elsamra, R. M. I., & Green, W. H. (2014). Direct Determination of the Simplest Criegee Intermediate (CH_2OO) Self Reaction Rate. *The Journal of Physical Chemistry Letters, 5*(13), 2224-2228. doi:10.1021/jz5008406

123. Faragó, E. P., Viskolcz, B., Schoemaecker, C., & Fittschen, C. (2013). Absorption Spectrum and Absolute Absorption Cross Sections of CH_3O_2 Radicals and CH_3I Molecules in the Wavelength Range 7473–7497 cm–1. *The Journal of Physical Chemistry A, 117*(48), 12802-12811. doi:10.1021/jp408686s

124. Sheps, L. (2013). Absolute Ultraviolet Absorption Spectrum of a Criegee Intermediate CH_2OO. *The Journal of Physical Chemistry Letters, 4*(24), 4201-4205. doi:10.1021/jz402191w

125. Schauffler, S. M., Atlas, E. L., Donnelly, S. G., Andrews, A., Montzka, S. A., Elkins, J. W., Stroud, V. (2003). Chlorine budget and partitioning during the Stratospheric Aerosol and Gas Experiment (SAGE) III Ozone Loss and Validation Experiment (SOLVE). *Journal of Geophysical Research: Atmospheres, 108*(D5). doi:doi:10.1029/2001JD002040

126. Parker, J. K., Payne, W. A., Cody, R. J., Nesbitt, F. L., Stief, L. J., Klippenstein, S. J., & Harding, L. B. (2007). Direct Measurement and Theoretical Calculation of the Rate Coefficient for Cl + CH_3 in the Range from T = 202−298 K. *Journal of Physical Chemistry A, 111*(6), 1015-1023. doi:10.1021/jp066231v

127. Timonen, R., Kalliorinne, K., & Koskikallio, J. (1986). *Kinetics of Reactions of Methyl and Ethyl Radicals with Chlorine in the Gas Phase Studied by Photochlorination of Methane* (Vol. 40a).

128. Shold, D. M., & Rebbert, R. E. (1978). The photochemistry of methyl chloride. *J. Photochem., 9*(5), 499-517. doi:https://doi.org/10.1016/0047-2670(78)85018-7

129. Goldbach, A., Temps, F., & Wagner, H. G. (1990). Kinetics of the Reactions of $CH_2(\tilde{X}^3B^1)$ with HCl and HBr. *Berichte der Bunsengesellschaft für physikalische Chemie, 94*(11), 1367-1371. doi:doi:10.1002/bbpc.199000034

130. Hippler, H., & Troe, J. (1976). Flash photolysis study of the recombination of chlorine atoms in the presence of various inert gases and NO. *International Journal of Chemical Kinetics, 8*(4), 501-510. doi:doi:10.1002/kin.550080404

131. Sarzyński, D., Gola, A. A., Dryś, A., & Jodkowski, J. T. (2009). Kinetic study of the reaction of chlorine atoms with chloromethane in the gas phase. *Chemical Physics Letters, 476*(4), 138-142. doi:https://doi.org/10.1016/j.cplett.2009.04.086

132. Seetula, J. A. (1998). R + Cl_2 reactions. *Journal of the Chemical Society, Faraday Transactions, 94*, 3561.

133. Baulch, D., Duxbury, J., Grant, S., & Montague, D. (1981). *Evaluated kinetic data for high temperature reactions. Volume 4. Homogeneous gas phase reactions of halogen-and cyanide-containing species*. Retrieved from

134. Seakins, P. W., Woodbridge, E. L., & Leone, S. R. (1993). A laser flash photolysis, time-resolved Fourier transform infrared emission study of the reaction monochlorine+ ethyl. fwdarw. hydrogen chloride (v)+ ethene. *The Journal of Physical Chemistry, 97*(21), 5633-5642.

135. Zhao, Z., Huskey, D. T., Nicovich, J. M., & Wine, P. H. (2008). Temperature-dependent kinetics study of the gas-phase reactions of atomic chlorine with acetone, 2-butanone, and 3-pentanone. *International Journal of Chemical Kinetics, 40*(5), 259-267. doi:doi:10.1002/kin.20321

136. Gilbert, R. G., Luther, K., & Troe, J. (1983). Theory of Thermal Unimolecular Reactions in the Fall-off Range. II. Weak Collision Rate Constants. *Berichte der Bunsen-Gesellschaft fuer Physikalische Chemie, 87*, 169-177.

137. Hong, Z., Davidson, D. F., Lam, K.-Y., & Hanson, R. K. (2012). A shock tube study of the rate constants of HO2 and CH3 reactions. *Combust. Flame, 159*(10), 3007-3013. doi:10.1016/j.combustflame.2012.04.009

138. Colket Iii, M. B., Naegeli, D. W., & Glassman, I. (1977). High temperature oxidation of acetaldehyde. *Symp. (Int.) Combust., 16*(1), 1023-1039. doi:http://dx.doi.org/10.1016/S0082-0784(77)80393-7

139. Scire, J. J., Jr., Yetter, R. A., & Dryer, F. L. (2001). Flow reactor studies of methyl radical oxidation reactions in methane-perturbed moist carbon monoxide oxidation at high pressure with model sensitivity analysis. *International Journal of Chemical Kinetics, 33*(Copyright (C) 2012 American Chemical Society (ACS). All Rights Reserved.), 75-100. doi:10.1002/1097-4601(200102)33:2<75::aid-kin1000>3.0.co;2-9

140. Hong, Z., Davidson, D. F., Lam, K.-Y., & Hanson, R. K. (2012). A shock tube study of the rate constants of HO2 and CH3 reactions. *Combustion and Flame, 159*(10), 3007-3013. doi:10.1016/j.combustflame.2012.04.009

141. Baulch, D. L., Cobos, C. J., Cox, R. A., Esser, C., Frank, P., Just, T., . . . et al. (1992). Evaluated kinetic data for combustion modeling. *J. Phys. Chem. Ref. Data, 21*(3), 411-734. doi:10.1063/1.555908

142. Mousavipour, S. H., & Saheb, V. (2007). Theoretical Study on the Kinetic and Mechanism of H+HO₂ Reaction. *Bulletin of the Chemical Society of Japan, 80*(10), 1901-1913.

143. Atkinson, R., Baulch, D. L., Cox, R. A., Hampson, R. F., Kerr, J. A., & Troe, J. (1989). Evaluated Kinetic and Photochemical Data for Atmospheric Chemistry: Supplement III. *Journal of Physical and Chemical Reference Data, 18*(3), 881-1097.

144. Batt, L., Burrows, J. P., & Robinson, G. N. (1981). On the isomerisation of the methoxy radical relevance to atmospheric chemistry and combustion. *Chemical Physics Letters, 78*(3), 467-470. doi:http://dx.doi.org/10.1016/0009-2614(81)85238-4

145. Dobbs, K. D., & Dixon, D. A. (1994). Cl + CH4 theory. *Journal of Physical Chemistry, 98,* 12584.

146. Liu, J., Chen, M.-W., Melnik, D., Yi, J. T., & Miller, T. A. (2009). The spectroscopic characterization of the methoxy radical. I. Rotationally resolved ~A 2A1-~X 2E electronic spectra of CH3O. *Journal of Chemical Physics, 130*(7), 074302/074301-074302/074319. doi:10.1063/1.3072104

147. Wallington, T. J., Neuman,D.M., Kurylo,M.J. (1987). Kinetics of the gas phase reaction of hydroxyl radical with ethane, benzene, and a series of halogenated benzenes over the temperature range 234-438 K. *J. Int. Chem. Kinet., 19*, 725-739.

148. Eskola, A. J., Timonen, R. S., Marshall, P., Chesnokov, E. N., & Krasnoperov, L. N. (2008). Rate Constants and Hydrogen Isotope Substitution Effect in CH3 + HCl and CH3 + Cl2 Reactions. *Journal of Physical Chemistry A, 112*(32), 7391-73401.